BRNO UNIVERSITY OF TECHNOLOGY
VYSOKÉ UČENÍ TECHNICKÉ V BRNĚ

FACULTY OF CHEMISTRY
FAKULTA CHEMICKÁ

INSTITUTE OF MATERIALS SCIENCE
ÚSTAV CHEMIE MATERIÁLŮ

POLYMER COMPOSITES WITH CONTROLLED INTERPHASE

POLYMERNÍ KOMPOZITY S ŘÍZENOU MEZIFÁZÍ

MASTER'S THESIS
DIPLOMOVÁ PRÁCE

AUTHOR — Milan Zvonek
AUTOR PRÁCE

SUPERVISOR — prof. RNDr. Vladimír Čech, Ph.D.
VEDOUCÍ PRÁCE

BRNO 2018

Zadání diplomové práce

Číslo práce:	FCH-DIP1201/2017
Ústav:	Ústav chemie materiálů
Student:	**Bc. Milan Zvonek**
Studijní program:	Chemie, technologie a vlastnosti materiálů
Studijní obor:	Chemie, technologie a vlastnosti materiálů
Vedoucí práce:	**prof. RNDr. Vladimír Čech, Ph.D.**
Akademický rok:	2017/18

Název diplomové práce:

Polymerní kompozity s řízenou mezifází

Zadání diplomové práce:

–Literární rešerše z oblasti plazmochemické depozice z plynné fáze, polymerních kompozitů a jejich smykových testů.

–Praktické zvládnutí technologie přípravy tenkých vrstev, výroby kompozitních vzorků a smykových zkoušek.

–Návrh depozičních podmínek, povrchová modifikace skleněných vláken a mechanická odezva vláken v polymerním kompozitu s polyesterovou matricí (smykový test).

–Příprava série kompozitních vzorků s proměnlivou smykovou pevností.

Termín odevzdání diplomové práce: 7.5.2018

Diplomová práce se odevzdává v děkanem stanoveném počtu exemplářů na sekretariát ústavu. Toto zadání je součástí diplomové práce.

Bc. Milan Zvonek student(ka)	prof. RNDr. Vladimír Čech, Ph.D. vedoucí práce	prof. RNDr. Josef Jančář, CSc. vedoucí ústavu

prof. Ing. Martin Weiter, Ph.D.
Děkan

V Brně dne 31.1.2018

ABSTRACT

The aim of the diploma thesis is preparation of glass fiber-reinforced polymer composites with controlled interphase using the method of plasma-enhanced chemical vapour deposition (PECVD) and tetravinylsilane as the monomer. The theoretical part focuses on literature recherché on plasma and plasma polymerization, thin films and composites. Experimental part deals with materials and equipment used for fiber surface modification and preparation of fiber-reinforced composites. The fiber surface modification was done using different deposition conditions. The chemical and mechanical analysis of formed interlayers was done using FTIR spectrometry and scratch test. The effect of surface modification was evaluated by acquired interlaminar shear strength using short beam shear test.

ABSTRAKT

Cieľom diplomovej práce je príprava polymerných kompozitov vyztužených sklenenými vláknami s riadenou medzifázou za použitia metódy plazmochemickej depozície z plynnej fáze a monomeru tetravinylsilanu. Teoretická časť je zameraná na literárnu rešerš o plazme, plazmovej polymerácií, tenkých vrstvách a kompozitoch. Experimentálna časť popisuje použité materiály a aparaturu použitú na povrchovú modifikáciu sklenených vlákien a prípravu vláknom vyztužených kompozitov. Povrchová úprava sklenených vlákien prebiehala za rôznych depozičných podmienok. Chemické a mechanické analýzy vytvorenej medzivrstvy prebiehali za použitia FTIR spektrometrie a vrypového testu. Vliv povrchovej úpravy bol zistený pomocou získanej interlaminárnej šmykovej sily použítím testu krátkych trámečkov.

KEYWORDS

Glass fiber, polymer composite, PECVD, tetravinylsilane, adhesion, interphase, interlaminar shear strength

KĽÚČOVÉ SLOVÁ

Sklenené vlákno, polymerný kompozit, PECVD, tetravinylsilan, adhézia, medzifáza, interlaminárna šmyková sila

ZVONEK, M. *Polymerní kompozity s řízenou mezifází.* Brno: Vysoké učení technické v Brně, Fakulta chemická, 2018. 80 s. Vedoucí diplomové práce prof. RNDr. Vladimír Čech, Ph.D..

DECLARATION

I declare that the bachelor thesis has been worked out by myself and that all the quotations from the used literary sources are accurate and complete. The content of the bachelor thesis is the property of the Faculty of Chemistry of Brno University of Technology and all commercial uses are allowed only if approved by both the supervisor and the dean of the Faculty of Chemistry, BUT.

…….

student's signature

ACKNOWLEDGEMENT

I would like to thank my supervisor prof. RNDr. Vladimír Čech, Ph.D. for technical leadership, provided consultations and literature during thesis solution. I would also like to thank Ing. Martin Branecký for the help and advice they provided during measurement, Ing. Tomáš Plichta for scratch test measurement and Bc. Veronika Širjovová for the help with composite preparation. Finally, I would like to thank my family and friends for the support during the study. This work was supported in part by the Technology Agency of the Czech Republic, grant no. TA01010796, and the Czech Science Foundation, grant no. 16-09161S.

CONTENTS

1 INTRODUCTION

Composites are hybrid materials consisting of multiple phases with different physical and chemical properties. Composites are good replacement for conventional materials and are widely used in construction, aviation and electrotechnical industry. Compared to conventional materials, composites have relatively high strength, low density and good chemical resistance. This thesis focuses on fiber-reinforced composites that consist of a polymer matrix and a fiber reinforcement. The most important parameter is the adhesion of the fiber-matrix interface. The adhesion has major effects on the mechanical properties of said composites. This can be done by introducing a thin layer that is compatible with fibers as well as matrix.

Plasma-enhanced chemical vapour deposition (PECVD) is a good method for creating such interlayer. This method uses non-thermal low temperature plasma in high vacuum. With good control over the deposition conditions, thin films with desired mechanical and chemical properties can be formed using various monomers.

The focus of this thesis is the preparation of unsaturated polyester resin-based polymer composites with controlled interphase using different deposition conditions. The effect of prepared interphases and change in the adhesion in the composite is evaluated using short beam shear test.

2 THEORETICAL PART

2.1 Polymer Composites

Composites can be defined as materials that consist of two or more chemically and physically different phases separated by a distinct interface. The different systems are combined to achieve a system with better structural or functional properties nonobtainable by any of the constituent alone. The individual constituents retain their separate identities. One acts as matrix and second one as reinforcement. Matrix phase is the primary phase having a continuous character. Matrix is usually more ductile and less hard compared to dispersed phase(reinforcement). Composites then can be classified based on the material used for matrix (metal, polymer, ceramics). The reinforcing constituent is embedded in a matrix. To achieve better mechanical properties, it is necessary to have a strong bond and good load transfer between matrix and reinforcement. [1]

2.1.1 Classification

2.1.1.1 Classification based on the geometry of reinforcement

Particulate-reinforced composites

Particulates used in composites are small particles of various shapes (hollow spheres, cubes, platelets, or carbon nanotubes) and sizes (< 0.25 μm). In each case, the particulates provide desirable material properties, and the matrix acts as a binding medium necessary for structural applications. Because of the usual randomness of particle distribution, these composites are regarded as quasi-homogeneous and quasi-isotropic on a scale larger than the particle size and spacing.. Particulate composites have improved strength, increased operating temperature, oxidation resistance, high creep resistance, and high strength to weight ratio. Typical examples of application are appliances, toys, cell phone casings, helmets, body panels of automotive cars, breaks, bumpers, and intake manifolds. [2]

Fiber-reinforced composites

Fiber-reinforced composites (FRC) use fibers of various lengths as a components of composite materials. They can be further divided into long fibers, whose aspect ratio length/diameter is usually very large (L/D > 100) and short fibers with L/D < 100. Short fiber reinforced composites display isotropic character, while long fiber reinforced composites have anisotropic character. The cross-section can be circular, square, or hexagonal. [2, 3]

Laminates

High-perfomance polymer components usually consist of layers of laminae stacked in a pre-determined manner. For the prediction of elastic properties of the component as a whole, each lamina may be regarded as homogenous in the sense that fiber arrangement and volume fraction are unvarying througout the lamina. The fibers in the laminae may be continuous or in short lengths and can be aligned in one or more directions or randomly distributed in two or three dimensions. An unidirectional lamina is called a ply and a stack of laminae is called a laminate. [3]

Whiskers

Whisker composites are composed of a matrix material and embedded reinforcing whisker materials (e.g., potassium titanate whisker, graphite, aluminum oxide, silicon oxide, silicon carbide, boron carbide, and beryllium oxide). A whisker is a nearly perfect, single-crystal material produced synthetically under controlled conditions. It is a very thin, short filament with high L/D ratio and is smaller than chopped fibers. Whiskers are almost free of internal defects and yields strength is close to the maximum theoretical value. [2]

2.1.1.2 Classification based on matrix characteristics

Thermosettic resins

The most commonly used resins are epoxy, unsaturated polyester and vinyl ester. They cover a wide range of physical and mechanical properties. During curing, the liquid resin is transformed into a hard rigid solid by chemical cross-linking, which leads to tightly bound three-dimensional network. The mechanical properties depend on the chemicals used and on the length and density of the cross-links, which is governed by the cross-linking processes in the cure. Curing can be achieved at room temperature, but often is used a curing schedule to one or more temperatures for predetermined times to achieve optimal cross-linking. The curing is accompanied by shrinkage, which can lead to residual stress in the composite. [3]

Thermoplastics

Thermoplastics derive their strength and stiffness from the inherent properties of the monomer units and the very high molecular weight. This ensures that in amorphous thermoplastics there is a high concentration of molecular entanglements, which act as cross-links and that in semicrystalline materials there is a high degree of molecular order and alignment. Heat transforms the thermoplastics into a viscous liquid. The fact that they are polymeric before the composite is made causes problems during fabrication due to their high viscosity and low wettability. Thermoplastics used as matrices are PP, PEEK, PMMA. Comparison of selected properties between thermoplastic matrices and thermosettic resins can be found in table 2.1. [3]

Table 2.1: Selected properties for different types of matrix [3]

Matrix	Density ρ [Mg m^{-3}]	Young's modulus E [GPa]	Tensile strength σ [GPa]	Failure strain ϵ_* [%]	Thermal expansivity α [10^{-6} K^{-1}]	Thermal conductivity K [W m^{-1} K^{-1}]
Epoxy resins	1,1–1,4	3–6	0,035–0,1	1–6	60	0,1
Polyesters	1,2–1,5	2,0–4,5	0,04–0,09	2	100–200	0,2
Nylon 6,6	1,14	1,4–2,8	0,06–0,07	40–80	90	0,2
Polypropylene	0,9	1,0–1,4	0,02–0,04	300	110	0,2
PEEK	1,26–1,32	3,6	0,17	50	47	0,2

2.1.2 Matrix

2.1.2.1 Unsaturated polyester resins (UP)

These resins consist of a viscous solution of linear unsaturated polyesters containing reactive double bond C=C dissolved in a reactive solvent (mostly styrene) where polymerization occurs. The chain length and its viscosity are regulated by the ratio of dicarboxylic acids and diols to saturated hydrocarbon chain. Viscosity can be also lowered by the abundance of the reactive solvent. The disadvantage of UP resin is in the volume contraction in percentages during the curing process, which limits the use of these resins to smaller parts. [4]

Synthesis

Common reactants for the UP synthesis are maleic anhydride, maleic acid (undergoing isomerization into fumaric acid) and polyhydric alcohols (propylene glycol, ethylene glycol). The isomerization of maleic acid is beneficial, because this leads to formation of linear chains during polymerization resulting in better mechanical properties of the cured resin.

Due to the high reactivity of UP with diols, maleic and fumaric acid, polyesters are modified by adding another acid into the polymer chain. This leads to a significant improvement of mechanical properties. Most common acids used for modification are isomers of phthalic acid (metaphthalic, paraphthalic) and phthalanhydride.

Synthesis of UP is done by melt esterification at 180 – 220°C in the presence of N_2 or CO_2. The resulting unsaturated polyester is shown in Figure 2.1.

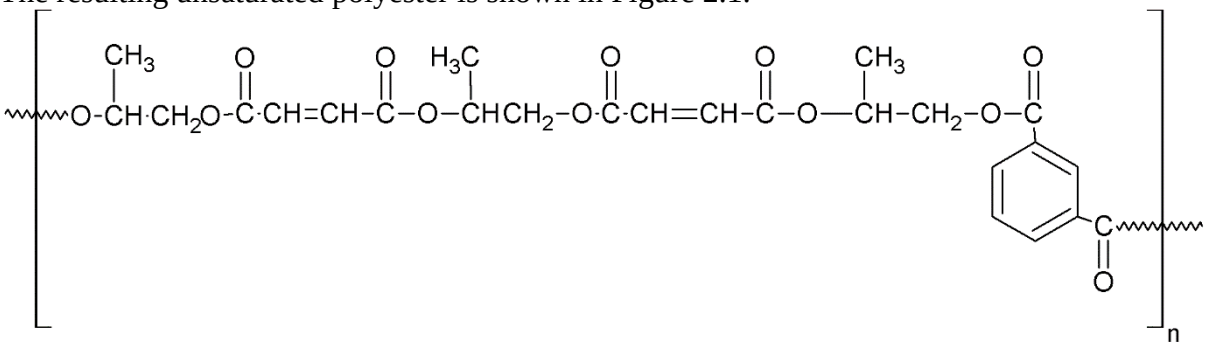

Fig. 2.1: Unsaturated polyester chain

Curing mechanism

Unsaturated polyester chains are linked with styrene during the curing process, undergoing radical cross-linking copolymerization. Vinyl groups -CH=CH- in monomer chains allow styrene to form a bond between two chains, forming a vinyl bridge between them (Fig. 2.2). The curing temperature is set based on the initiator used, forming cross-linked, insoluble product.

Initiator of the cross-linking reaction are peroxide radicals, which are formed by thermal fission of organic diperoxides (dibenzoyl peroxide). Metal salt reaction accelerators are used to regulate the reaction speed. These metal salts contain cations, which can exist in two different oxidation states:

$$ROOH + Co^{2+} \rightarrow RO\bullet + OH^{-} + Co^{3+} \text{ (fast reaction)}$$

$$ROOH + Co^{3+} \rightarrow ROO\bullet + H^{+} + Co^{2+} \text{ (slow reaction)}$$

In the next step the radical attacks the unstable double bond of polyester or styrene (M_1 – UP, M_2 – styrene):

$R\bullet + M_1 \rightarrow RM_1\bullet$

$R\bullet + M_2 \rightarrow RM_2\bullet$

The secondary radical reacts further with another monomer chain, forming a three-dimensional matrix. There are four addition reactions, which may occur:

$RM_1\bullet + M_1 \rightarrow RM_1M_1\bullet \quad [k_{11}]$

$RM_1\bullet + M_2 \rightarrow RM_1M_2\bullet \quad [k_{12}]$

$RM_2\bullet + M_1 \rightarrow RM_2M_1\bullet \quad [k_{21}]$

$RM_2\bullet + M_2 \rightarrow RM_2M_2\bullet \quad [k_{22}]$

Constants k_{ij} are reaction rate constants. The ratios $r_1 = \frac{k_{11}}{k_{12}}$ and $r_2 = \frac{k_{22}}{k_{21}}$ are copolymerization parameters characterized by the copolymerization. When the value of constants is $k_{11} >> k_{12}$ and $k_{22} >> k_{21}$ $(r_1, r_2 >> 1)$, only homopolymers of styrene and polyester are formed. If the ratio is $r_i < 1$, then a copolymer is formed, in case of $r_i << 1$, an alternating copolymer forms. When the ratio is around $r_i = 1$, a statistical copolymer is formed.

Termination is done by the reaction of two radicals, disproportionation or by chain transfer, where the growing radical is satiated and a new radical is formed. [4]

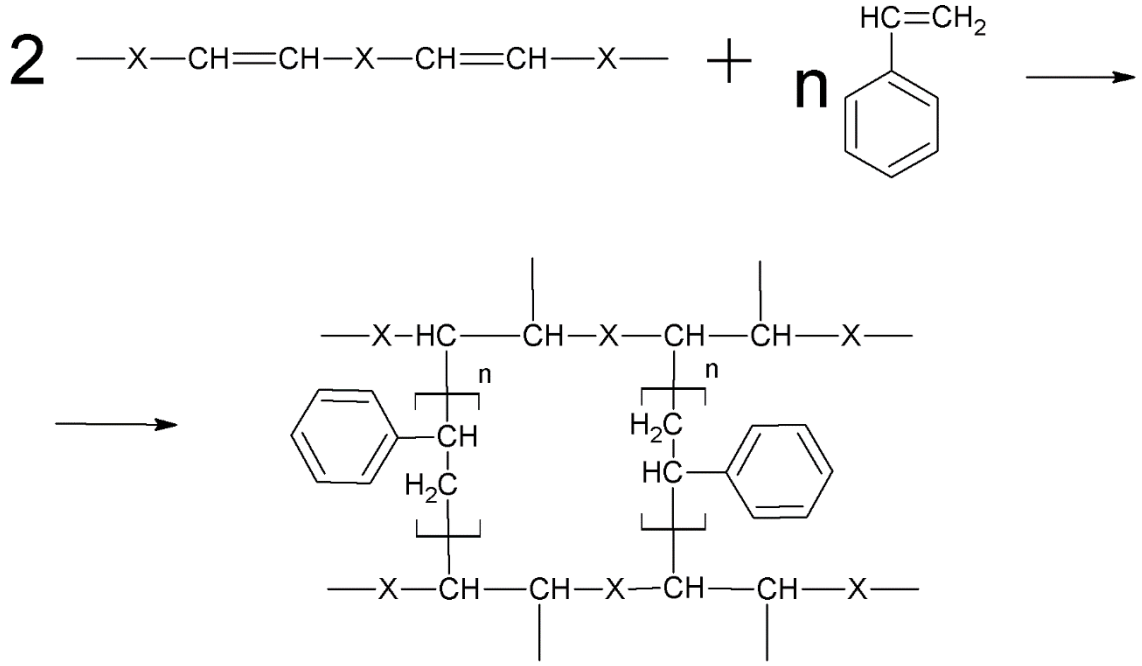

Fig. 2.2: Cured unsaturated polyesters

2.1.2.2 Vinyl ester resins (VE)

Basic reactants for vinyl eseter formation are acrylic acid, dian group(bisphenol A) and a compound with an epoxy bond (epichlorohydrin). The synthesis is based on alcalic condenzation followed by esterification of epoxy groups by acrylic acid.

Vinyl ester resins are cross-linked only at the ends of the monomer chains, because of the double bonds of the vinyl group, which leads to higher toughness of cured resin because of

the easier conformation changes during resin stress. Occurance of free hydrophillic hydroxyl groups improves adhesion to glass fibers.

The curing process is similar to UP with styrene as a reactive solvent and organic diperoxide as an initiator. During the curing process, the glass transition temperature (T_g) increases with increasing conversion rate and with decreasing transport rate. To achieve complete conversion, the temperature must be held over T_g at all times during the process. [4]

2.1.2.3 Epoxy resins (ER)

Epoxy resins can be divided into two basic groups. Resins containing glycidyl groups and glycidyl amine based resins. Epoxy resins have a wide range of use, thanks to different methods that can be used to open the epoxy ring. During the curing step, there is no side product and thus no curing contraction, which can be used to create high volume parts. Epoxy resins have good mechanical properties and high chemical resistance. Synthesis of ER is similar to vinyl ester resins, only difference is in the chlorohydrin ether groups, which remain present in the final product.

The curing of epoxy resins can be done many ways. The curing process used depends on the particular use of the resin and its processing technology. The most common type is polyaddition of epoxy groups or polycondensation of hydroxyl groups. [4]

2.1.2.4 Thermoplastic matrices

Compared to the thermosets, thermoplastics have higher viscosity during processing, which have negative effect on reinforcement impregnation. Another difference is that the thermoplastic matrix is not cross-linked. The need of pre-impregnation and work with the thermoplast melt vastly increases the cost of the technological processing. Advantages of thermoplastic matrices are high chemical resistance, thermal stability, low water absorbtion, low curing contraction, dielectric properties and the possibility to use injection moulding as one of the technologies in processing. The most common thermoplastic matrices are PP, nylon 66, PEEK and PMMA and are applied mostly in aircraft and automotive industries. Comparison between thermoplastic matrices and thermosettic resins can be found in table 2.2. [3, 4]

Table 2.2: Comparison between thermosets and thermoplastics, their dimensional and environmental stability [3]

Property	Thermosets		Thermoplastics		
	Epoxy resins	Polyester resins	Nylon 6,6	PP	PEEK
Melting temperature [°C]	–	–	265	164	334
Distortion temperature [°C]	50–200	50–110	120–150	80–120	150–200
Shrinkage on curing [%]	1–2	4–8	–	–	–
Water absorbtion (24h, 20°C) [%]	0,1–0,4	0,1–0,3	1,3	0,03	0,1
Chemical resistance	Good, attacked by strong acids	Attacked by strong acids and alkalis	Good, attacked by strong acids	Excellent	Excellent

2.1.3 Fiber reinforcements

Fiber-reinforced composites combine high strength of rigid reinforcements with high toughness of flexible matrix. The synergy between the two phases create mechanical properties of the composite material which could not be achieved with either of the constituents alone.

The load applied to the composite is transmitted from matrix to the fibers acting as a reinforcement and causes shear stress through the matrix-reinforcement region called interphase. Mechanical properties of a composite are influenced by the interphase, which reflects the matrix-fiber adhesion.

Basic types of fiber reinforcements are inorganic fibers (glass, carbon, metal), natural organic fibers (cellulose, flax, cotton) and synthetic organic fibers (aramid, PE, PP). The most commonly used fibers are glass fibers because of their good mechanical properties, high chemical resistance and low price [3, 5, 6].[5]

2.1.3.1 Glass fibers

Structure, composition and properties

Glass fibers are amorphous, based on silica (SiO_2) with the addition of other oxides (Ca, B, Na, Fe and Al). They form a three-dimensional network of Si-O bonds from the fundamental building-block of $[SiO_4]^{4-}$ tetrahedra. Two-dimensional model of the atomic structure of typical glass is depicted in figure 2.3 [6].

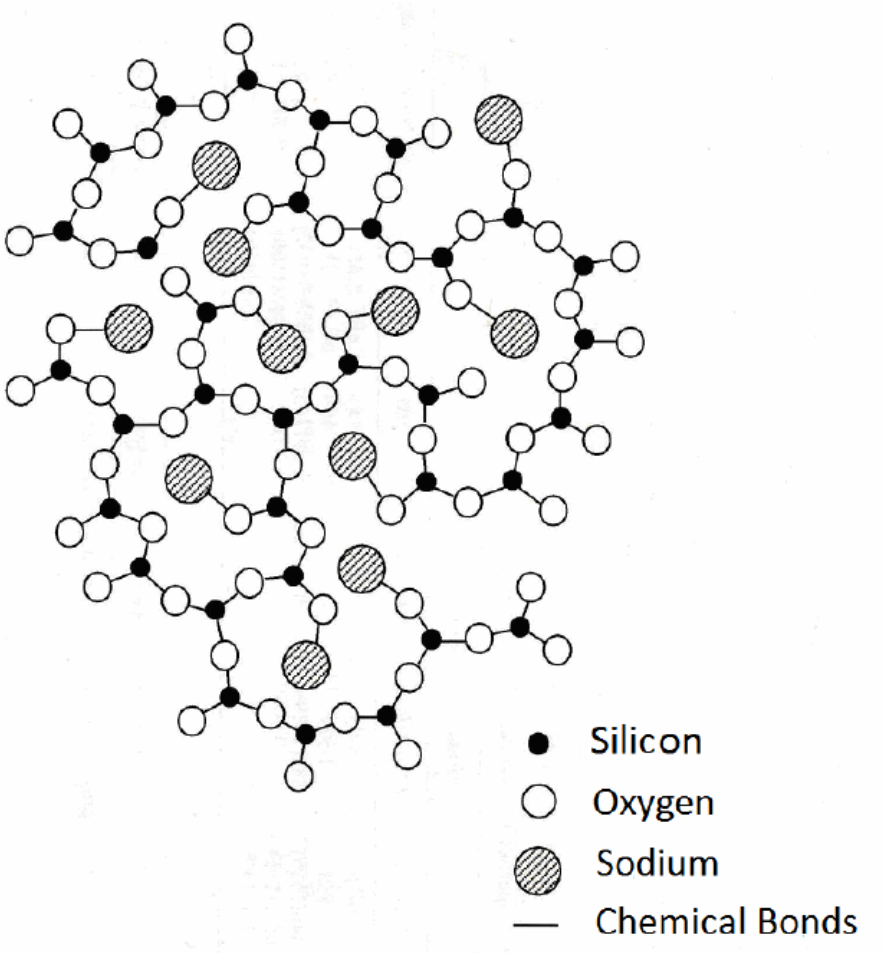

Fig. 2.3: Idealized model of isotropic amorphous atomic structure of a glass [6].

The most commonly used type of glass is E-glass with a maximum alkali content of 2% and no boron E-glass. It has good strength, stiffness, electrical and weathering properties. A-glass is a soda lime silicate glass that is less expensive to make (lower processing temperatures, zero boron content). D-glass is a borosilicate composition used for low dielectric constant in high-performance electrical applications. ECR-glass is a calcium aluminosilicate with maximum alkali content of 2%, with properties similar to E-glass, except it is more resistant to acidic environment. S-glass is a magnesium aluminosilicate glass that delivers the highest mechanical, thermal and chemical properties and is primarily used in aerospace and military applications. The composition of each type of glass is listed in table 2.6 [6].

Table 2.3: Typical composition of selected types of glass [6].

Oxide [%]	E-glass	No boron E-glass	A-glass	D-glass	ECR-glass	S-glass
SiO_2	52–56	52–56	63–72	72–75	54–62	64–66
Al_2O_3	12–16	12–16	0–6	0–1	9–15	24–25
B_2O_3	5–10	–	0–6	21–24	–	–
CaO	16–25	16–25	6–10	0–1	17–25	0–0,1
MgO	0–5	0–5	0–4	–	0–4	9,5–10
Na_2O+K_2O	0–2	0–2	14–16	0–4	0–2	0–0,2
Other	0–1	0–1	0–1	0–1	2–10	0–1

Other than silica, B_2O_3 is the only other network former, with a polyhedral structure that connects with the silica network. Other oxides (Al_2O_3, ZrO_2, TiO_2) provide cations that can substitute for silicon in a tetrahedral network, contributing to the network stability. Remaining oxides disrupt the network structure because they can form only one or two chemical bonds, effectively lowering the melting temperature of the glass, manipulating the viscosity-temperature behavior of the melt. [6]

The properties of glass fibers are isotropic. Typical E-glass fiber tensile strength is 3,5 GPa, Young's modulus is 70–80 GPa. Considering that 60–70% of the atoms in glass fibers are oxygen atoms, it is to be expected that the fiber surface will be oxygen rich and thus a high concentration of silanol groups (Si–OH) will be present due to hydrophillic character of the glass fibers. Water from air humidity adsorbs onto fiber surface, decreasing the adhesion and overall strength of the fibers. To improve the adhesion of the fiber surface, they are treated with appropriate sizing, which has better affinity to both matrix and fibers. Mechanical properties of particular types of glass fibers are listed in table 2.4 [3, 6].

Table 2.4: Mechanical properties of selected pristine glass fibers [6]

Physical properties	E-glass	No boron E-glass	A-glass	D-glass	ECR-glass	S-glass
Density [g cm^{-3}]	2,58	2,62	2,44	2,11	2,72	2,46
Tensile strength [MPa]	3445	3450	3310	2415	3445	4890
Young's modulus [GPa]	72,3	80,5	68,9	51,7	72,3	86,9
Elongation at break [%]	4,8	4,6	4,8	4,6	4,8	5,7

Glass fiber production

The most common raw materials used in production of glass fibers are glassmaking sand as the source of silica, china clay (aluminosilicate) with low alkali content as the source of alumina, magnesium is introduced with dolomite ($CaMg(CO_3)_2$) or burnt dolomite. Limestone is the source of calcium oxide and boric oxide is introduced with colemanite ($Ca_2B_6O_{11} \cdot 5 H_2O$) or boric acid. The glass is molten in a furnace(fig.) at 1400–1600 °C. Fibers are formed at the forehearth, where winders are located and the glass melt passes through Pt-Rh alloy plate called bushing.

Molten glass flows through 1–2 mm cylindrical tips, creating fibers with diameter of 3,5–20 µm. One bushing can have 10 000 tips. A rotating drum is located below the bushing and pulls the fibers at high speed (450–4500 m/min). Individual filaments are rapidly cooled by 10^4–10^5 °C per second. Fibers are elongated during this process and diameter is rapidly decreased, simultaneously modifying the fiber's density, refractive index, Young's modulus and chemical stability due to thermomechanical forming history. Lubricants are used during the fiber formation to decrease the number of damaged fibers during the process. This also decreases the adhesion of glass fibers to matrix and thus further surface modification is necessary. [6]

2.1.3.2 Other fiber types

Carbon fibers

In the graphite single crystal, the carbon atoms arranged in a sequence of hexagonal arrays. The atoms along the plane in the direction of fiber length (Fig. 2.4) are held together by strong covalent bonds, while only weak Van der Waals forces are applied between separate planes. These forces cause the carbon fibers to be highly anisotropic.

Carbon fibers have very good strength and Young's modulus, while maintaining low weight ratio. Typical diameter of carbon fibers is around 8 µm. They consist of small crystallites of turbostratic graphite, one of the allotropic forms of carbon. Turbostratic graphite closely resembles graphite single crystals, except that the layer planes are not are not regularly packed in z-axis. Carbon fibers can be produced by carbonization from polyacrylonitrile (PAN) fibers, from mesophase pitch or by pyrolytic deposition of hydrocarbons from the gas phase. [3]

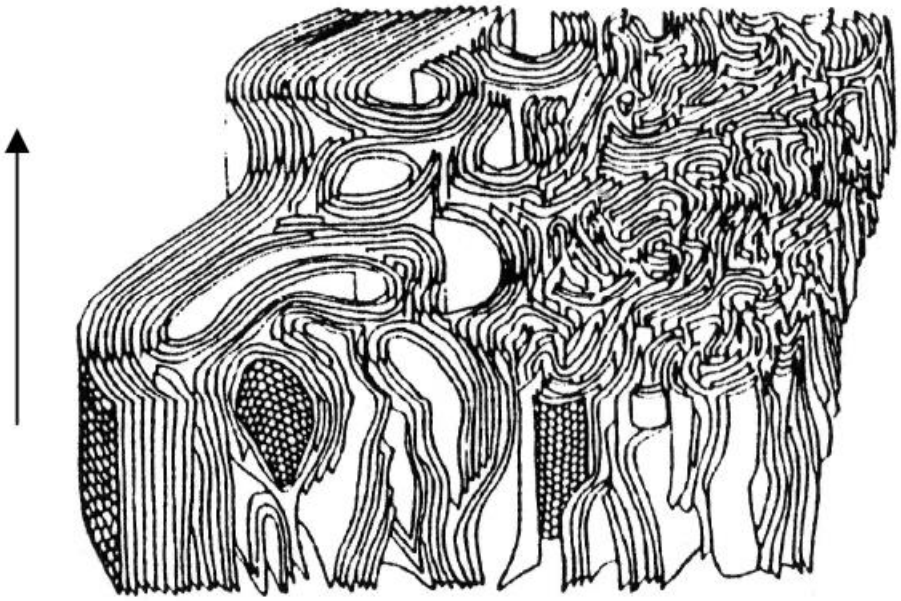

Fig. 2.4: Schematic representation of carbon fiber structure [3].

Aramid fibers

One of the high modulus polymer fibers, containing characteristic –CO–NH– bond with high degree of aromaticity, which exhibit liquid crystalline behaviour in a solution. Aramid fibers are produced by extrusion and spinning processes. Solution of dissolved polymer is passed through a spinneret to develop a high degree of orientation. After the removal of residual solvent, further alignment and ordering of the molecules is done by thermal annealing treatment. Polymer molecules then form rigid planar sheets. Aramid fibers are highly anisotropic and there is a weak inter-chain hydrogen bonding between molecules, which makes the fibers split into fibrils and microfibrils when damaged. [3]

Silicon carbide fibers

These fibers have high stiffness and strength, low density and good thermal stability. The most commonly used are CVD monofilaments with large diameter of fibers (100–150 μm) and PCS multifilaments with fibers of 15 μm in diameter.

CVD monofilaments are formed in reaction chambers, where a gaseous carbon-containing silane is passed through the chamber. The carbon core fiber is heated and the gas dissociates thermally at the fibers surface to deposit SiC. PCS multifilaments are made using the analogous PAN based method using carbonization of polycarbosilane as the selected precursor. [3]

2.1.4 Interphase

The interphase (Fig. 2.5) is a three-dimensional, complex region intermediate to the fiber and the matrix (thickness varying from 0,1 μm to several microns). The properties may be variable across the region and which also may differ from the composition, structure and properties of either of the two constituents. We can distinguish two interfaces at the interphase

region. The first one at the fiber surface is relatively sharp and the second at the matrix is diffused. Interphases greatly influence the mechanical properties of composites.

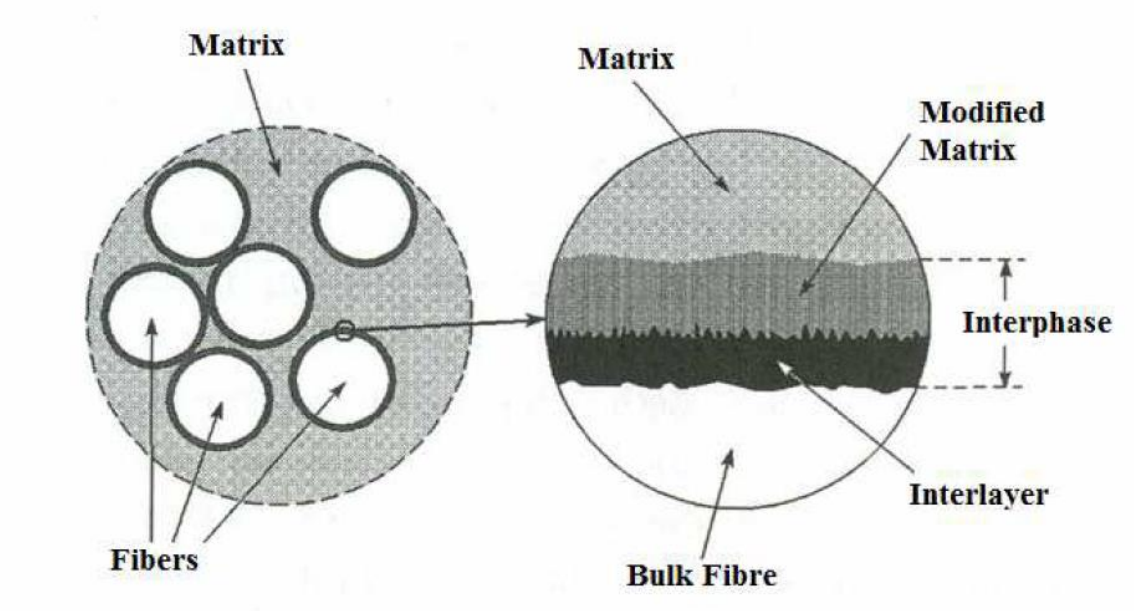

Fig. 2.5: Schematic illustration of a composite interphase [5].

The primary function of the interphase is to transmit stress from the matrix to the fibers and to protect the fibers from environmental damage. The ability to transmit stress is dependent on the interphase strength, as well as mechanical properties of matrix, fiber and the adhesion at interfaces. The surface of fibers needs to be augmented to improve wetting and adhesion to the matrix [5, 7].

2.1.4.1 Adhesion

Adhesion in general can be attributed to mechanisms including, but not restricted to adsorption, wetting, electrostatic attraction, chemical bonding, reaction bonding and exchange reaction bonding. In addition to the major mechanisms, hydrogen bonding, Van der Waals forces and other low energy forces may be involved as well. Generally, a combination of these mechanisms creates the final bond. The nature of bonding is dependent on the atomic arrangement, molecular conformation, chemical constitution of all the phases as well as the morphological properties of the fiber and the diffusivity of elements in each constituent. Different types of bonds are depicted in figure 2.6 [5, 8].

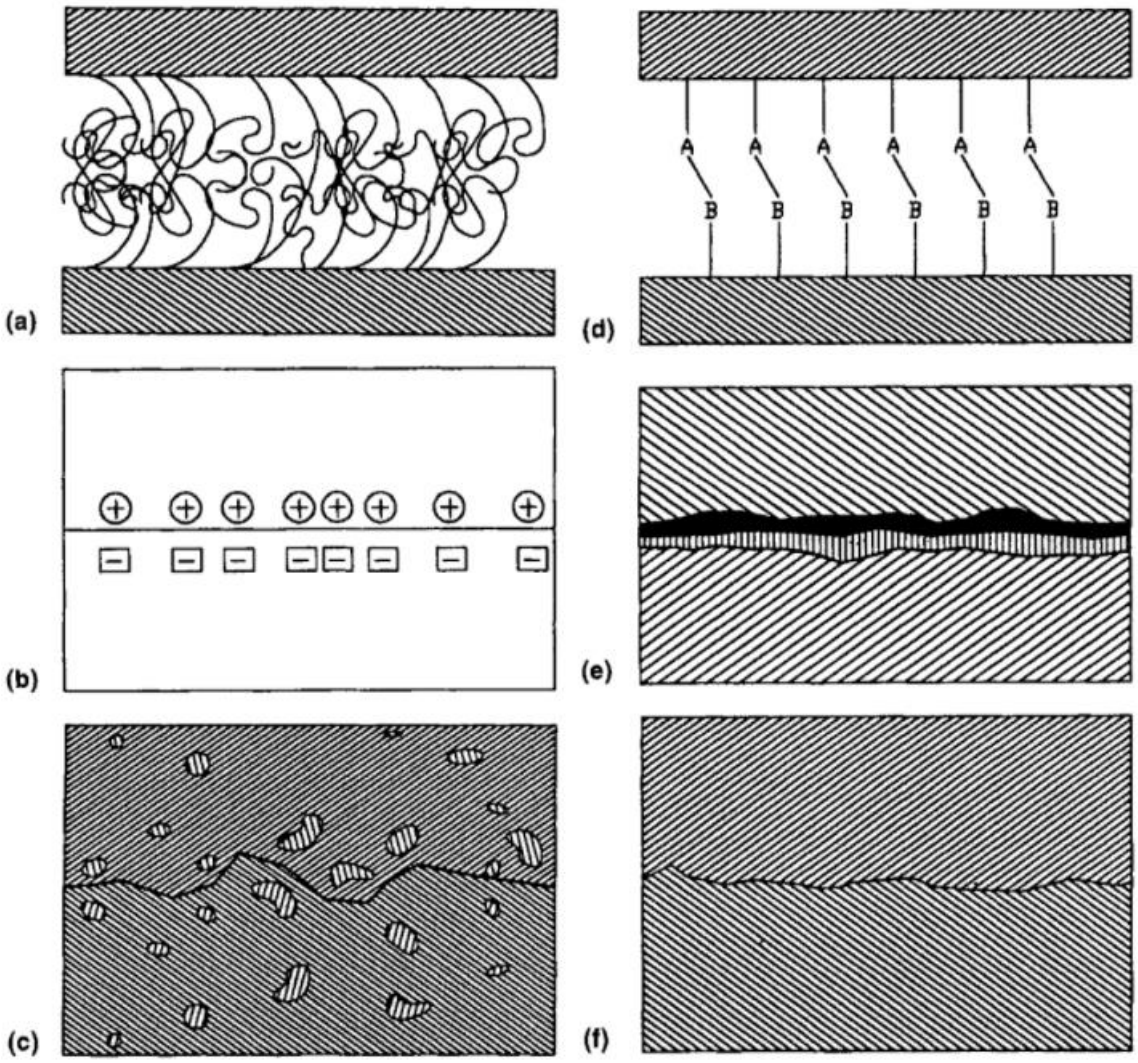

Fig. 2.6: Interface bonds formed by (a) molecular entanglement; (b) electrostatic attraction; (c) interdiffusion of elements; (d) chemical reaction between groups A and B; (e) chemical reaction following forming of a new compound; (f) mechanical interlocking [8].

Good wetting of fibers by matrix during the impregnation is required during the composite construction. Bonding due to wetting involves very short-range interactions of electrons on an atomic scale, where atoms of both constituents are in contact with each other or only few atomic diameters apart. Wetting can be quantitatively expressed in terms of the thermodynamic work of adhesion, W_A, of a luquid to a solid using the Dupre equation:

$$W_A = \gamma_{SL} + \gamma_{SV} - \gamma_{LV}, \tag{1}$$

where γ_{SL} is the surface free energy of the liquid, γ_{SV} is the surface free energy of the solid and γ_{LV} is the interfacial free energy.

The surface energy of a solid must be greater than that of a liquid for proper wetting to take place. This equation can be related to a model of a liquid drop on a solid (Fig. 2.7), where the resolution of forces in the horizontal direction at the point A, where the three phases are in contact is defined with Young's equation

$$\gamma_{SL} \cdot \cos\theta = \gamma_{SV} - \gamma_{LV}\,, \tag{2}$$

where θ is the contact angle. When the contact angle is less than 90°, the liquids are wetting, while liquids with contact angle greater than 90° are called non-wetting. Perfect wetting occurs when the contact angle is 0°.

Glass and carbon fibers can be effectively wetted by thermoset resins at room temperature, while PE fibers need to be surface treated in order to wet them by the same resins. [8]

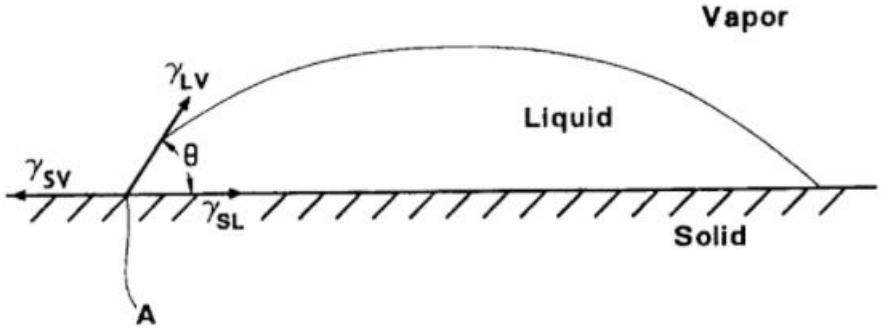

Fig. 2.7: Liquid drop model [8].

2.1.4.2 Glass fiber surface modification

In the presence of water, oxides present in glass fibers (SiO_2, Fe_2O_3, Al_2O_3) react with hydroxyl groups and form hydrogen bonds with other water molecules, adsorbing them onto fiber surface. This significantly decreases the surface free energy of said fibers, reducing the wettability of fibers in polymer matrix. In order to nullify this effect, organosilane sizing is applied. This protective layer blocks the water molecules from adsorbing onto surface as well as increase the adhesion to polymer matrix by forming interfacial covalent bonds between the two constituents.

The type of organosilane ($R–Si–X_3$) is dependent on the application and compatibility with used matrix. The bonding reactions of organosilane are depicted in figure 2.8. Reactive groups X of silane (ethoxy, methoxy, chloride) are hydrolysed in the presence of water, forming silanol, which is then chemisorbed on the fiber surface. The chemisorption is followed by condensation of silanol molecules into a polysiloxane layer with strong chemical bond on the fiber surface. The hydrocarbon chain R is oriented towards the matrix.

Surface treated fibers have increased interlaminar shear, flexural and tensile strengths. Delamination is reduced in favour of microbuckling. All these beneficial effects of improved strength are inevitably accompanied by a loss in the impact fracture toughness of unidirectional laminates, therefore a balance must be sought to ensure adequate strength and toughness properties. The surface treatment is heterogeneous with varying thickness along the coated fibers [6, 8, 9].

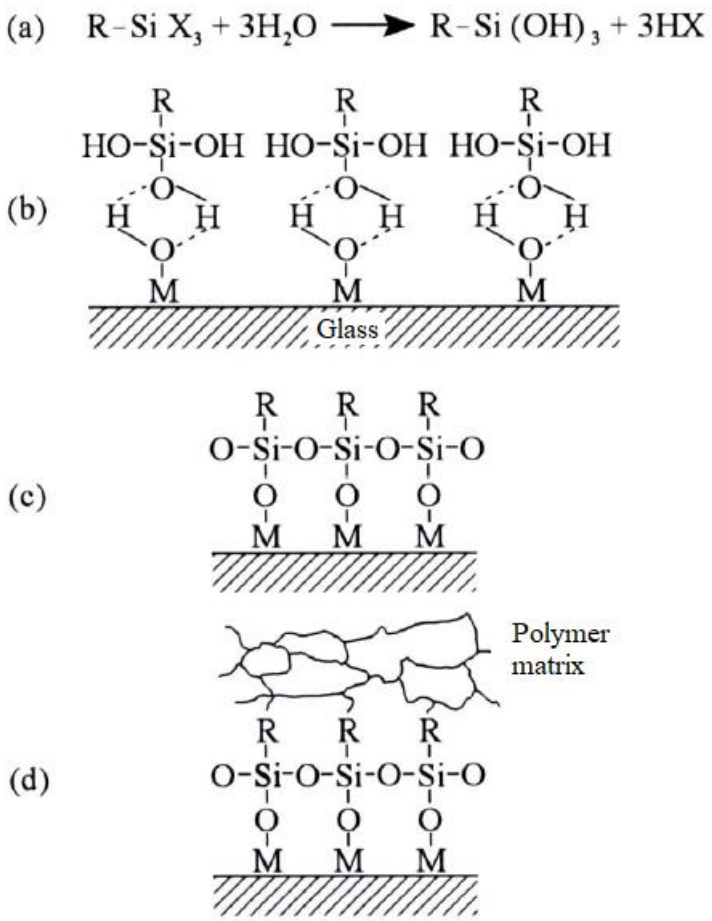

Fig. 2.8: Organosilane bonding reactions (a) hydrolysis; (b) chemisorption; (c) condensation; (d) chemically bond matrix [9]

2.2 Thin film

Thin films are created by the deposition of individual atoms on a substrate. A thin film is defined as a low-dimensional material created by condensing, one-by-one, atomic, molecular or ionic species of matter. It is defined by S/V surface to volume ratio which satisfy the condition that $|S/V| >> 6$ (Fig. 2.9). Thin films differentiate from bulk materials in their physical properties. In general, the thickness of a thin film is $0.1\,\text{nm} - 10\,\mu\text{m}$ [10].

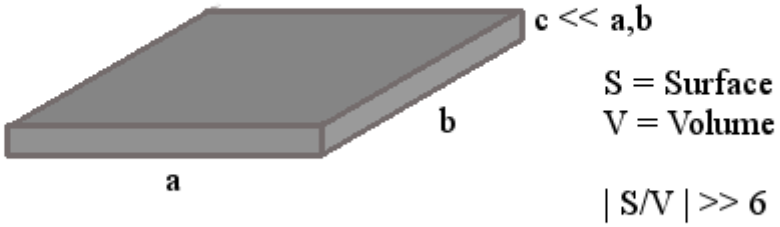

Fig. 2.9: Model of thin layer.

The properties of film, such as film composition, crystal phase and orientation, film thickness and microstructure are manipulated by deposition conditions. Thin films have unique properties that cannot be observed in bulk materials. These are unique material properties resulting from atomic growth process and size effects, including quantum size effects, characterised by the thickness, crystalline orientation and multilayer aspects [10].

Thin films have been used in different types of engineering systems and have been adapted to fulfil a wide variety of functions such as the use of surface coatings to protect structural materials in high temperature environments for example in gas turbine engines. Thin films are integral parts of many micro-electro-mechanical systems designed for sensors or actuators. Extending the durability of components using surface coatings or surface treatments is another use of thin films and can be seen in internal combustion engines, artificial hip and knee implants and computer hard disks for magnetic data storage [11].

2.2.1 Thin film deposition

Thin film deposition methods can be divided into two separate groups. The first is Psychical Vapor Deposition (PVD) and it is based on processes like vaporization or kinetic energy transfer (impact). The second group is Chemical Vapor Deposition (CVD) and is based on chemical reactions. The main factors that distinguish PVD and CVD are mechanisms, by which source atoms enter the gas phase, reduced pressure environment through which the gas atoms are transported, general absence of chemical reactions (in PVD) in gas phase or at the substrate surface. These divisions are not mutually exclusive, because there exist hybrid methods, which incorporate both principles [10, 12].

2.2.1.1 Physical vapour deposition

Two most important methods in PVD are evaporation and sputtering. The goal of these methods is controlled transfer of atoms from a source to a substrate, where film formation and growth proceed atomistically. In the evaporation process, atoms are removed from the source

material thermally in contrast to sputtering, where atoms re dislodged from solid target surfaces by the impact of gaseous ions(Ar) [12].

During the sputtering process (Fig. 2.10), the ions are supplied by glow discharge using CW, AC or RF power supply in an evacuated chamber. The target is a plate of the material that serves as a cathode with several kilovolts applied to it and is deposited onto substrate that can be grounded, electrically floating, biased positively or negatively, heated or cooled. Operational gas pressure is less than 10 Pa [12].

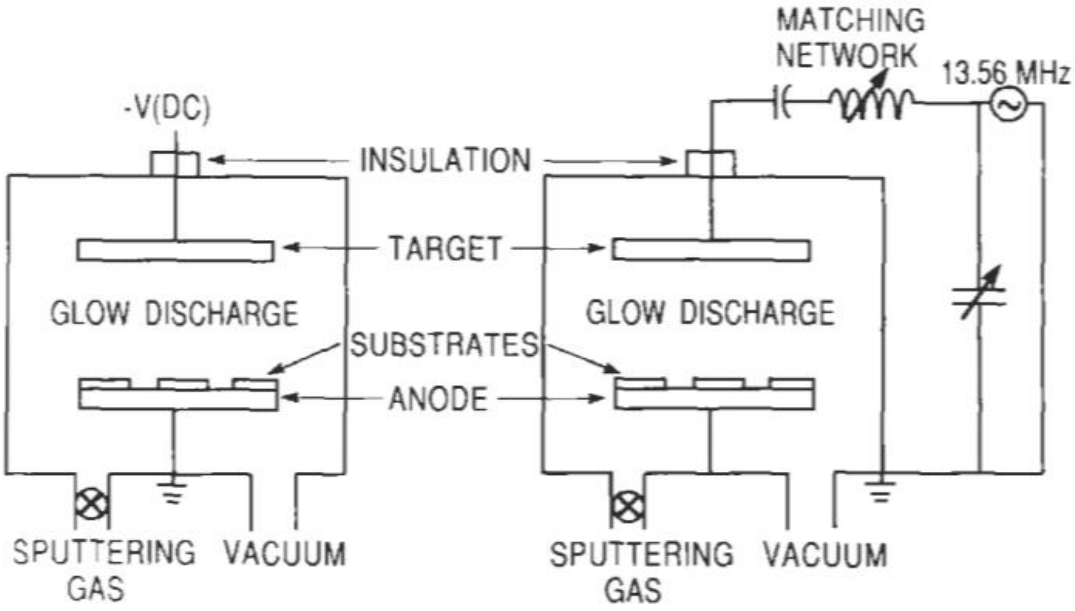

Fig. 2.10: Schematics of a simplified sputtering system [12].

Reactive sputtering is a special type of sputtering using both CVD and PVD methods, using reactive gas in working gas mixture. Reactive gas reacts with sputtered atoms from cathode and forms new chemical substances. Typical example can be oxide formation, which is realized by using oxygen as a reactive gas [10, 12].

2.2.1.2 Chemical vapour deposition

Chemical vapor deposition is the process, where a volatile compound undergoes a chemical reaction in gaseous state and is then deposited atomistically onto a non-volatile solid substrate. Waste gaseous products are formed during this process and must be removed from the reaction chamber. Because of the low requirements on vacuum quality, CVD processes do not require high ammount of energy and thus are economically more friendly than PVD processes. CVD processes are widely used for thin films and coatings, but it is also possible to produce bulk materials and powders of high purity, furthermore, the capability of controllably creating films of widely varying stoichiometry makes CVD unique among deposition techniques. In contrast to PVD processes, CVD have significant advantages such as growing thin films on the whole surface of the substrate including all types of cavities and defects, compared to sputtering, where the substrate needs to be in defined position to the substrate. Many variants of CVD processes have been researched, including low-pressure

(LPCVD), metal-organic (MOCVD), plasma-enhanced (PECVD) and laser-enhanced (LECVD) chemical vapor deposition [12, 13].

Reaction types

There are several types of reactions, which are used in CVD processes. Most reactions during are applied in gas-gas or gas-solid states.

Pyrolisis involves the thermal decomposition of gaseous hydrides, carbonyls and organometallic compounds on hot substrates. Following reaction is an example of high temperature pyrolysis of silane to produce polycrystalline or amorfous silicon films

$$SiH_{4(g)} \rightarrow Si_{(s)} + 2H_{2(g)} \quad (650\,^{\circ}C)$$

Reduction commonly uses hydrogen gas as the reducing agent to for halides, oxyhalides, carbonyl halides, or other oxygen-containing compounds. Common example is the reduction of SiCl, on single-crystal Si wafers to produce epitaxial Si films according to the reaction

$$SiCl_{4(g)} + 2H_{2(g)} \rightarrow Si_{(s)} + 4HCl_{(g)} \quad (1200\,^{\circ}C)$$

Oxidation is used in formation of silicon oxide, applied for its semiconductor and optical properties

$$SiH_{4(g)} + O_{2(g)} \rightarrow SiO_{2(s)} + 2H_{2(g)} \quad (450\,^{\circ}C)$$

Compound formation of nitrides, borides and carbides, need to be in reactive volitile state to be successfully deposited onto a hot surface of substrate, which is to be coated.

$$SiCl_{4(g)} + CH_{4(g)} \rightarrow SiC_{(s)} + 4HCl_{(g)} \quad (1400\,^{\circ}C)$$

Disproportionation reactions are possible when a non-volatile metal can form a volatile compound having different degree of stability depending on the temperature. Example of such system is shown in reaction. [12]

$$2GeI_{2(g)} \xrightarrow{300^{\circ}C} Ge_{(s)} + GeI_{4(g)}$$

$$2GeI_{2(g)} \xleftarrow{600^{\circ}C} Ge_{(s)} + GeI_{4(g)}$$

2.2.2 Plasma enhanced chemical vapour deposition

PECVD is a technique in which electric energy is used to induce plasma in the reaction chamber, where the initiation of homogeneous reactions occurs to produce chemically active ions and radicals. These particles then participate in heterogeneous reactions, which, in turn, lead to layer formation on the substrate. A major advantage of PECVD over regular CVD processes is that deposition can occur at very low temperatures, which allows temperature sensitive substrates to be used [13].

2.2.2.1 Plasma

Plasma is a state of matter in which the electrons, positively and negatively charged particles, neutral atoms and molecules coexist in a highly activated state. Basic characteristics of plasma are high ionisation and very high energy compared to other states of matter such as solid, liquid or gas (Fig. 2.11) [14].

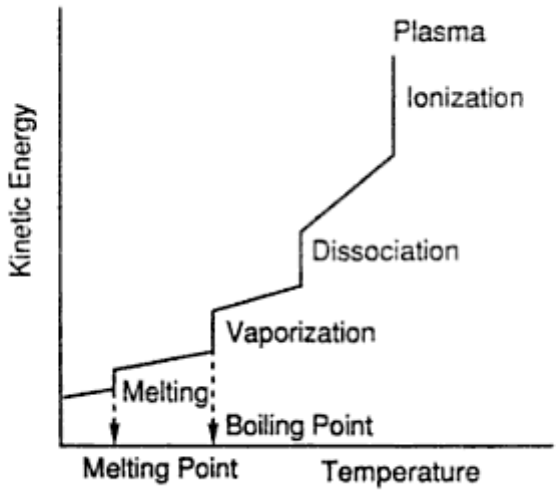

Fig. 2.11: Schematic of transition state [14].

Common division of plasma is according to the temperature into low- (LTP) and high-temperature plasmas (HTP). Further division can be seen in table 2.5, where T_e – electron energy in K ($1\,\mathrm{eV} = 11600\,\mathrm{K}$), T_i – ion energy in K and T_g – translational kinetic energy of gas in K [15].

Table 2.5: Division of plasma [15].

Division of plasma		**Temperature**	**Occurrence**
Low-temperature plasma (LTP)	Thermal LTP	$T_e \approx T_i \approx T_g \lesssim 2\times10^4$ K	arc plasma at normal pressure
	Non-thermal LTP	$T_i \approx T_g \approx 300$ K $T_i \ll T_e \lesssim 10^5$ K	low pressure glow discharge
High-temperature plasma (HTP)		$T_i \approx T_e \gtrsim 10^7$ K	fusion plasmas

The most widely used plasma for PECVD is non-thermal LTP. Due to its high energy of electrons (T_e) and relatively low temperature of the gas (T_g), particles can interact with and activate substrates or reactive gases [16].

Plasma parameters

Quasineutrality is one of the main properties of plasma. This means that under equilibrium with no external forces present, in a volume of the plasma large enough to contain great number of particles and yet sufficiently small compared to the characteristic lengths for variation of macroscopic parameters such as density and temperature, the net resulting electric charge is zero. If either a positively or negatively charged particle is placed into plasma, it disturbs the quasineutrality by influencing other particles around itself. This disturbance decreases in magnitude the further away it is from the placed particle until it has no effect. This is caused by Debye shielding, characterised by Debye length, λ_D, which can be

considered as a measure of the distance over which the fluctuating electric potentials may appear in a plasma [14, 17].

Certain criteria must be met for plasma to occur. The first criterion is large enough dimensions of plasma compared to λ_D. If L is a characteristic dimension of the plasma, then $L \gg \lambda_D$ must be satisfied. Since the Debye shielding is a result of collective particle behaviour, many electrons are needed within a sphere with radius of the Debye length, therefore a second criterion states

$$N_D = n_e \frac{4}{3} \pi \lambda_D^3 \gg 1, \tag{3}$$

where n_e is the concentration of electrons, N_D is number of charged particles and λ_D is Debye length [14, 17].

The third criterion is plasma frequency, which is a natural frequency of particle oscillations. This is caused by the disturbance in plasma, creating internal electric field and subsequent movement of electrons towards equilibrium. These electrons move beyond the point of equilibrium and an electric field is produced in the opposite direction. Plasma frequency is given by

$$\omega = \sqrt{\frac{n_e e^2}{m_e \varepsilon_0}}\,. \tag{4}$$

Ionised gas can be considered plasma only when $\omega\tau > 1$, where τ states the average travel time of an electron between collisions with neutral particles and ω represents the angular frequency of typical plasma oscillation [17].

2.2.2.2 Mechanism of plasma polymerization

Plasma polymerization is a thin film-forming process in which the film is deposited directly on surface of the substrate without any fabrication. In this process, low-molecular weight monomers grow into high-molecular weight polymers. Plasma polymerization differs greatly from conventional polymerization in the product of the polymerization, its structure, physical and chemical properties. It is possible that the oxygen from residual air may be incorporated into the plasma polymer. Plasma is the source of energy and initiator, which activates the electrons, ions and radicals of the monomer. The most suitable plasma for this process is the non-thermal LTP [14, 18].

The mechanism of plasma polymerization implements elemental reactions occurring in plasma, which are the fragmentation of monomer molecules, the formation of active sites (radicals) and recombination of the activated fragments. In plasma polymerization, it is not necessary for the constituents to contain polymerizable bonds such as double bond, triple bond or cyclic structure. The propagation reaction in plasma polymerization is a stepwise reaction of recombination between biradicals that are formed from fragmentation of the starting molecules by plasma. This effect causes differentiation in the sequence of molecules before and after the polymerization [14, 16]. The scheme of plasma polymerization is illustrated in figure 2.12.

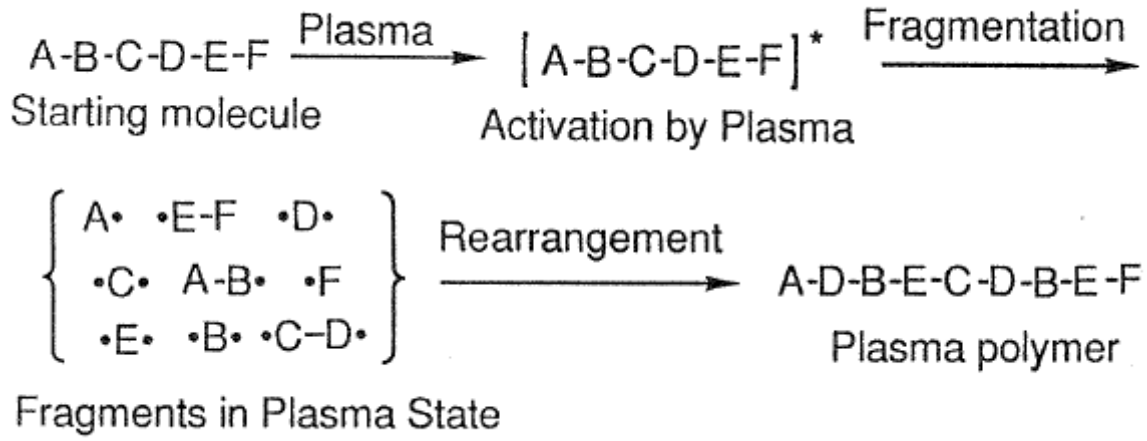

Fig. 2.12: Schematic of presentation of plasma polymerization [14].

The fragmentation of starting molecules in plasma is represented by two types of reactions: the elimination of the hydrogen atom and the C – C bond scission (Fig. 2.13).

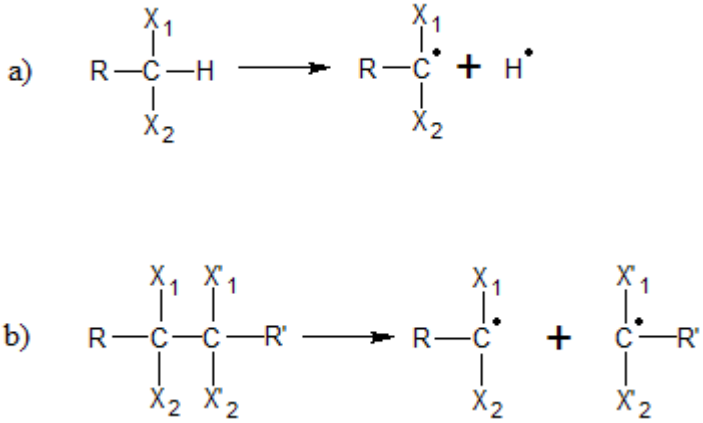

Fig. 2.13: Schematic of hydrogen elimination (a) and C – C bond scission (b) [14].

Hydrogen elimination is considered to contribute greatly to the polymer-forming process in plasma polymerization.

It is more likely for the hydrogen atoms to be eliminated from the monomer molecules by the plasma, forming monoradicals $M_i^\bullet$ and biradicals $^\bullet M_k^\bullet$, and the addition of the radicals to monomer and the recombination between the two radicals proceed to make large molecules with or without radical. Figure 2.14 shows the polymer-forming process in plasma polymerization. Monoradical $M_i^\bullet$ adds to the monomer to form a new radical $M_j^\bullet - M^\bullet$ (reaction a). Monoradical $M_i^\bullet$ can also recombine with monoradical $M_j^\bullet$ to form a neutral molecule $M_i - M_j$ (reaction b) or recombines with biradical $^\bullet M_k^\bullet$ to form a new monoradical $M_i - M_k^\bullet$ (reaction c). Biradical $^\bullet M_k^\bullet$ is added to monomer to form a new biradical $^\bullet M_k - M^\bullet$ (reaction d). Biradical $^\bullet M_k^\bullet$ recombines with biradical $^\bullet M_j^\bullet$ to form a new biradical $^\bullet M_k - M_j^\bullet$ (reaction e). The new neutral molecule $M_i - M_j$ is again activated by plasma to form mono- or biradicals and cycle I repeats. The new monoradicals $M_i - M_k^\bullet$ and biradicals $^\bullet M_k - M_j^\bullet$ are further recombined to form larger radicals in cycle II [14].

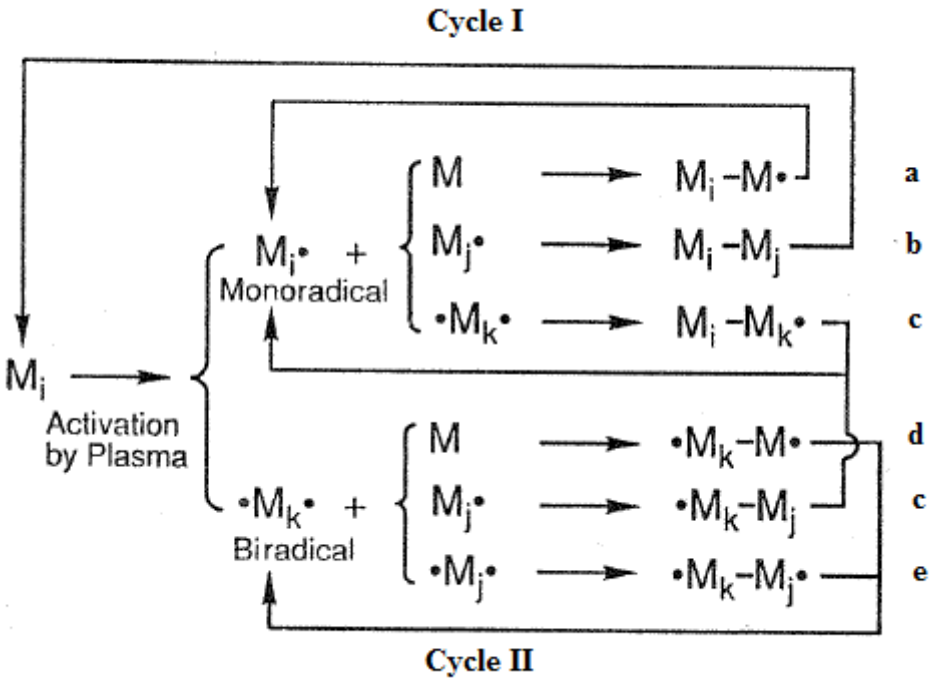

Fig. 2.14: Overall plasma polymerization mechanism [14].

2.2.2.3 Operational parameters of plasma polymerization

Deposition and ablation

When the monomer gains enough energy from plasma, it is fragmented into smaller, highly activated molecules. These molecules merge together to form larger molecules which are deposited onto the surface of a substrate. The deposited polymers are continuously irradiated by the plasma. In such conditions, a deterioration of the deposited polymers occurs, and their chemical structure is changed. This change is caused by the simultaneous deposition and ablation of the polymer on the substrate (Fig. 2.15). The process of ablation and polymerization has competitive character [14].

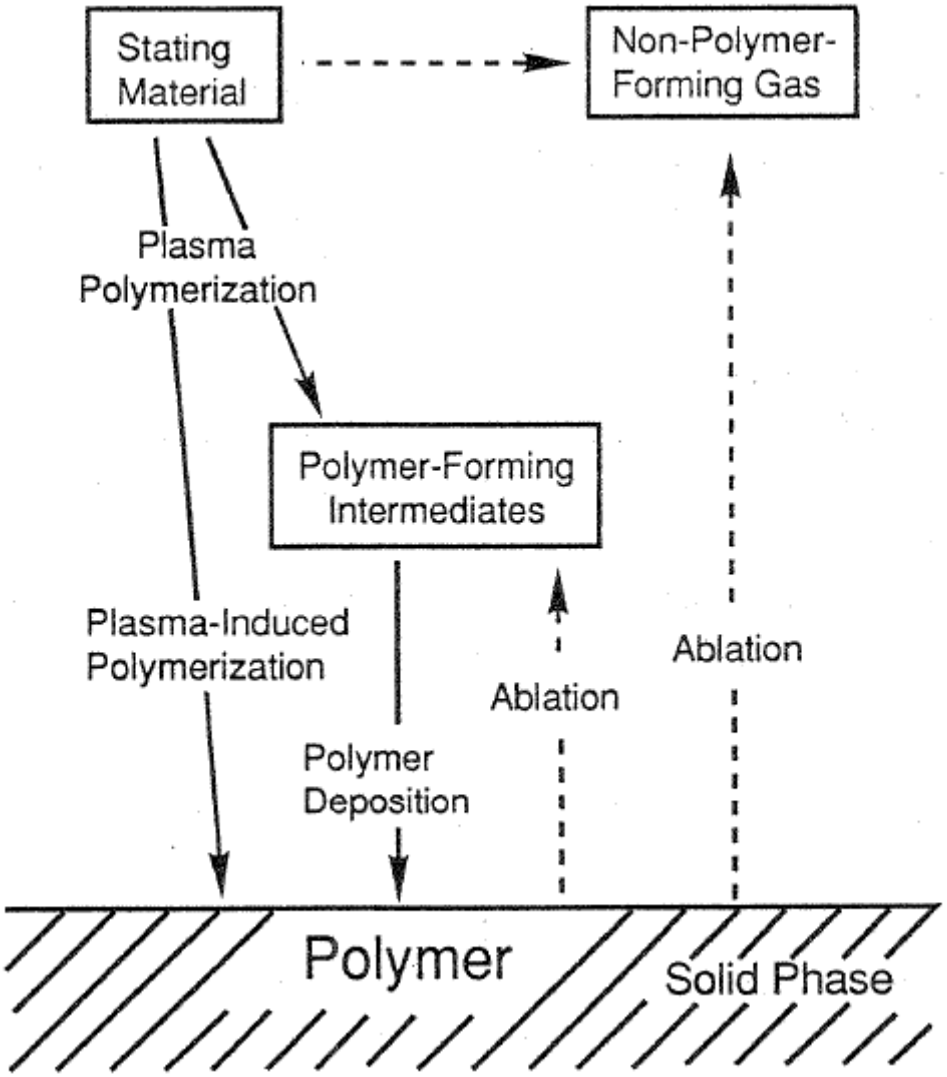

Fig. 2.15: Overall reactions of plasma polymerization [14].

W/FM parameter

The activation of monomers and reactivation of the recombined molecules is due to fragmentation by plasma. The fragmentation process depends on how much of electric energy was used to maintain plasma, the amount of monomer that was added into plasma and where the monomer molecules interacted with activated species of the plasma. Therefore, a controlling parameter of W/FM (W – power of generator [W], F – monomer flow rate $[\,\mathrm{mol}\cdot\mathrm{s}^{-1}]$, M – molecular weight of the monomer $[\,\mathrm{kg}\cdot\mathrm{mol}^{-1}]$) was introduced to control the process of plasma polymerization. The magnitude of W/FM parameter is proportional to the concentration of activated particles in plasma. The polymer deposition rate increases with increasing W/FM parameter under the operational condition, where the activated species have considerably lower concentration than monomer molecules in plasma. These conditions refer to monomer sufficient region (Fig. 2.16). Afterwards the polymer formation rate levels off in the competitive region and with the increasing W/FM parameter the polymer formation rate decreases due to insufficient amount of monomer molecules. These conditions refer to monomer deficient region. In the monomer sufficient region, monomer molecules are subjected to less fragmentation to be plasma-polymerised. In the monomer-deficient region,

the monomer molecules are heavily fragmented and plasma polymers with great rearrangement are formed. The ideal conditions for plasma polymerization are in the competitive region, where the deposition rate is at its peak [14, 16].

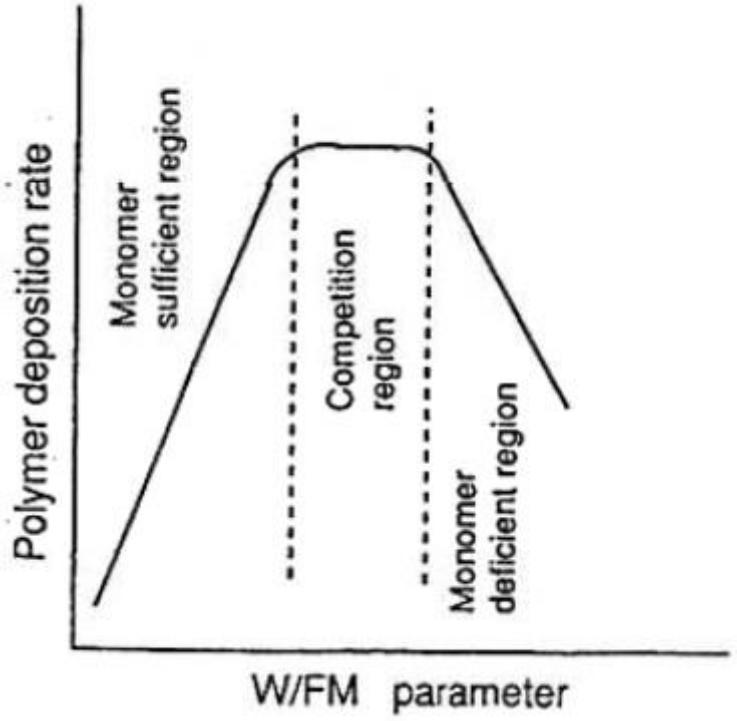

Fig. 2.16: Domain of plasma polymer deposition [14].

2.2.2.4 Organosilicon plasma polymerized films

Plasma polymerized organosilicons constitute a class of materials with a rich and varied scientific background. Plasma polymer films deposited by low pressure plasma from organosilicon monomers constitute a special class of dielectric coatings with controllable organic/inorganic character and cross-linking that enable optimization of their dielectric, optical, mechanical, and surface properties. Such films are used as transparent protective coatings, optical filters, or low-*k* materials [19, 20].

Most commonly used monomers are Hexamethyldisiloxane (HMDSO), Tetraethoxysilane (TEOS) and Hexamethyldisilazane (HMDSN), which contains two Si-N bonds. These monomers are mostly used in mixtures with rare gas such as Argon and with an active gas like O_2 or N_2O. The atomic oxygen is created during the plasma phase and this oxygen reacts in the gas and at the plasma surface interface with organic parts of the organosilicon precursor. The mostly commonly used organosilicon precursors are in table 2.6 [21].

Table 2.6: Main organosilicon precursors and growth conditions for plasma films [21].

Name and shortcut	Plasma source	Pressure range	Power range	Reference
Hexamethyldisiloxane HMDSO	RF, μW, LF	10^{-1} – 10^{2} Pa	3–100 W	[22, 23, 24, 25, 26]
Tetraethoxysilane TEOS	RF, μW,	10^{-1} – 10^{2} Pa	3–100 W	[27, 28, 29, 30]
Tetramethyldisiloxane TMDSO	13,56 MHz, Inductive coupling	1.3 Pa	25 W	[31]
Divinyltetramethyldisiloxane DVTMDSO	13,56 MHz, Capacitive coupling remote plasma	1–10 Pa	14–200 W	[32]
Methyltrimethoxysilane TMOS	13,56 MHz, Parallel plate	14.7 Pa	300 W	[33]
Octamethylcyclotetrasiloxane OMCATS	13,56 MHz, Capacitive coupling remote plasma	1–10 Pa	14–200 W	[32]
Bis(Trimethylsilyl)methane BTMSM	13,56 MHz, inductive coupling	1.3 Pa	50–150 W	[34]
Hexamethyldisilane HMDS	13,56 MHz, inductive coupling	1.3 Pa	50–150 W	[34]
Tetramethylsilane TMS	13,56 MHz, Inductive coupling	1.3 Pa	25 W	[31]
Tetravinylsilane TVS	13,56 MHz helical coupling	0.1–4.4 Pa	0.05–10 W	[35]

2.3 Testing methods, analysis

Mechanical tests of fiber-reinforced composites measure the adhesion between the fibers and matrix. Mechanical properties of materials can be determined by applying tensile, compressive and shear loadings. Flexure test includes all of the above-mentioned loads. Another division of loadings is based on type and time into static, impact and fatigue loadings. Most commonly used are static tests, as they represent the response of material to monotonal load over short period of time (seconds to minutes). Mechanical tests are divided into direct, indirect and shear test methods [36, 37].

2.3.1 Direct methods

Direct measurement methods are difficult to perform, because the fiber can often break before the interface. It is assumed that the stress is constant along the length of the fiber and that the fibers are unidirectional and wetted without any defects to avoid local stress concentrations.

These involve a single fiber embedded into a resin disk or a microdroplet. The force needed to pull the fiber from the resin is related to the interfacial bond strength using equation:

$$\tau_{\text{int}} = \frac{\text{F}}{\pi \text{D}_\text{f} \text{l}}, \tag{5}$$

where F is the pull-out force and $\pi \text{D}_\text{f} \text{l}$ is the interfacial area [37].

2.3.2 Indirect methods

Indirect tests involve elongating a specimen with only one fiber embedded in the matrix. The matrix elongates more than the fiber, the fiber is then forced to either break or to delaminate from the matrix with the interface. The matrix should be transparent for the fiber fragments to be visible. As more load is applied to the specimen, the fiber breaks into more and more halves to the point the fiber can no longer breaks and reaches critical length l_c. σ_{uf} is the inferfacial shear stress of fragmens.

$$\tau_{\text{int}} = \frac{\sigma_{\text{uf}} D_f}{2 l_c}. \tag{6}$$

Fiber microindentation is another indirect way to measure τ_{int}. Specimens are cut perpendicular to the fiber direction and a single fiber is compressed with a probe. The force needed to debond the fiber from the matrix is proportional to τ_{int}.

$$\tau_{\text{int}} = \text{A}\left(\frac{4\text{F}}{\pi \text{D}_\text{f}^2}\right)\left(\frac{\text{G}_m}{\text{E}_\text{f}}\right)^{\frac{1}{2}}, \tag{7}$$

where the first factor in parentheses is the nominal fiber compressive stress, G_m is the shear modulus of the matrix, E_f is the tensile modulus of the fiber. Constant A is determined by finite element modelling as a function of the fiber nearest-neighbour spacing [37].

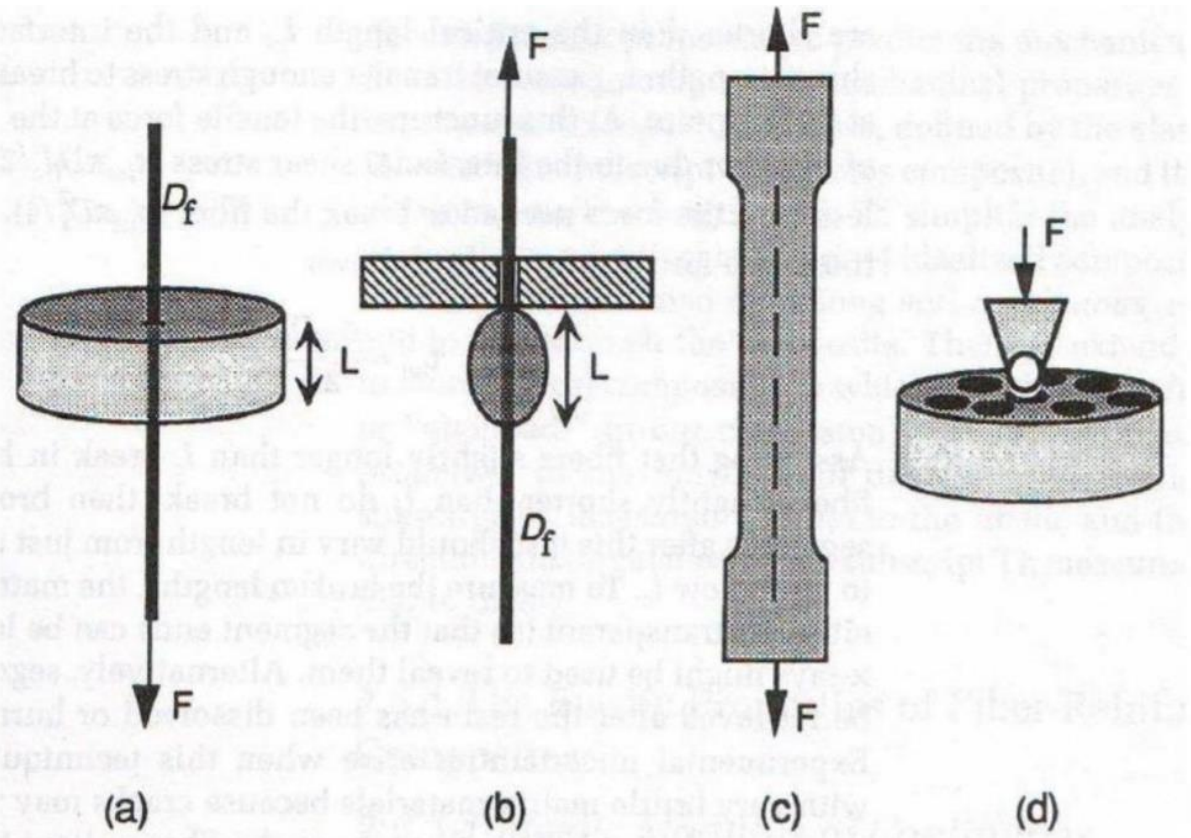

Fig. 2.17: Interfacial shear strength testing methods: (a) single fiber pull-out test; (b) single fiber microdroplet test; (c) single fiber fracture test; (d) fiber microindentation test [37].

2.3.3 Shear test methods

These methods measure the shear properties of composite materials. Focused mainly on interlaminar shear (short beam shear test method) due to the fact that this type of measurements was done to measure adhesion between matrix and glass fibers of created composites and their plasmochemical modifications.

Shear test methods involve 4-point shear and 3-point shear tests. In 3-point shear, the load is concentrated in the middle of the specimen, while in 4-point shear the maximum load is dispersed throughout the specimen due to implementation of additional loading point.

In short beam shear test, the span length is substantially shorter, thus a very small amount of composite material is needed for this test. The bending stress is directly proportional to the applied load and span length. By shortening the support span length, the specimen is exposed to interlaminar shear. Figure 2.18 depicts types of deformation during the test, where (a) is desired deformation. Other deformation types cause inaccuracy or outright failure to measure interlaminar shear. The specific span length to specimen thickness is defined by ASTM (American Society for Testing and Materials) [36].

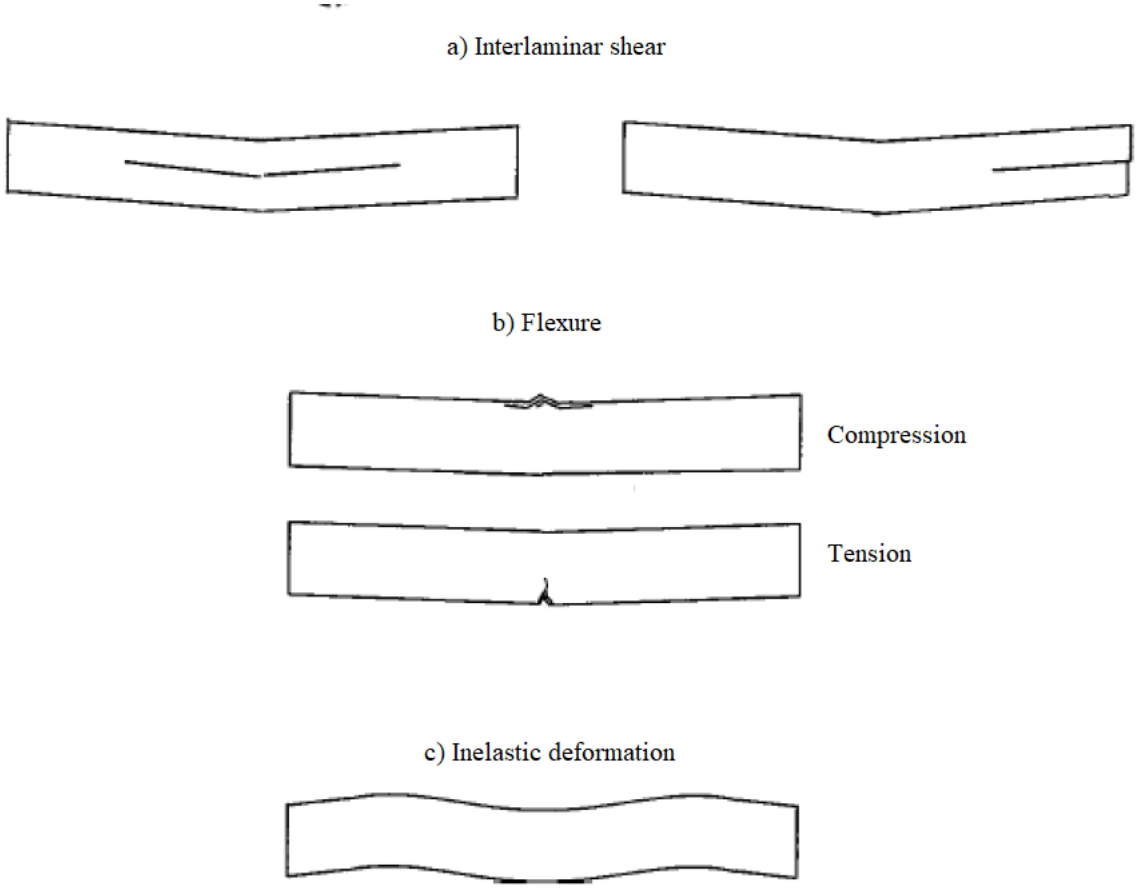

Fig. 2.18: Types of deformation during short beam shear test [38].

3 EXPERIMENTAL PART

3.1 Used materials

3.1.1 Polymer matrix

Unsaturated isophthalic polyester resin POLY DS 183 B1 was used for the preparation of composites. Properties are listed in table 3.1, supplier of this resin is Skolil Kompozit spol. s.r.o.. The ratio between components was kept according to table 3.2.

Table 3.1: Selected properties of POLY DS 183 B1

Parameter	**Value**
Viscosity	900–1100 mPa·s
Styrene content	33–37 %
Tensile strength	80 MPa
Flexural strength	130 MPa
Volume contraction	8,3 %

3.1.1.1 Polymer matrix additives

Styrene

Bonding agent, CAS: 100-42-5

Mr = 104.152 g · mol^{-1}

ρ (20 °C) = 0.906 g · cm^{-3}

T_m = -30.628 °C

T_b = 145.14 °C

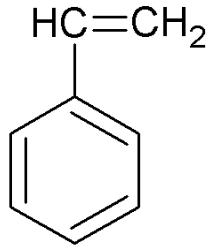

Peroxan BP-Paste 50 PF

dibenzoyl peroxide 50% with isononyl benzoate, CAS: 94-36-0

Manufacturer: PERGAN GmbH, Bocholt, Germany

High temperature initiator, white paste

Mr = 242.2 g · mol^{-1}

ρ (20 °C) = 1.17 g · cm^{-3}

SADT 50 °C

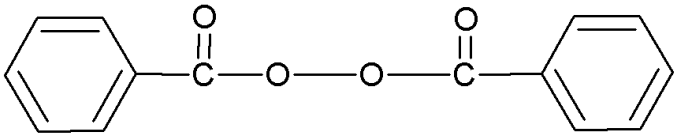

Perkadox 16

Di(4-tert-butylcyclohexyl) peroxydicarbonate, CAS: 15520-11-3

Manufacturer: Akzo Nobel Polymer Chemicals BV Amersfoort, Netherlands

Low temperature initiator, white powder

Mr = 398.5 g · mol^{-1}

ρ (20 °C) = 0.113 g · cm^{-3}

bulk ρ (20 °C) = 450–480 kg · m^{-3}

SADT 40 °C

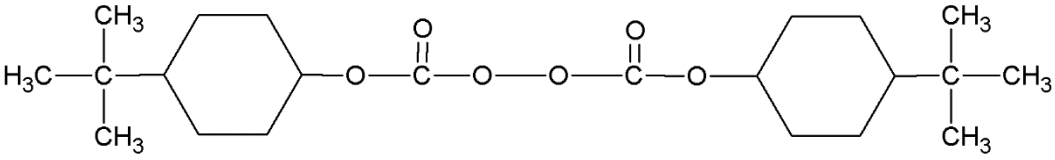

Uvasorb MET

2-hydroxy-4-methoxy-benzophenone, CAS: 131-57-7

Manufacturer: 3V Sigma S. p. A., Bergamo, Italy

Ultraviolet light absorber, yellow powder

Mr = 228.2 g · mol^{-1}

ρ (20 °C) = 0.906 g · cm^{-3}

T_m = 63–64.5 °C

MOLD WIZ INT-PUL-24

Manufacturer: Axel Plastics Research Laboratories Inc., USA

Contains organic esters, acids, amines and neutralizing agents, serves as a lubricant for improved fiber wettability

Table 3.2: Resin composition for composite samples.

Component	**Wt.%**
POLY DS 183 B1	96.1
Styrene	2.0
Peroxan BP-Paste 50 PF	1.0
MOLD WIZ INT-PUL-24	0.50
Perkadox 16	0.20
Uvasorb MET	0.20

3.1.2 Glass fiber reinforcement and planar substrates

Type E glass fiber rowing from Saint-Gobain Adfors CZ, s.r.o., Litomyšl, ČR was used as a reinforcement in the prepared composite. The diameter of the fiber is 19 μm, tex 1200, one bundle contains 1600 filaments. Plasmochemical modification was done on unsized glass fibers.

Two types of planar substrates were used. Infrared-transparent double polished silicon wafers (ON Semiconductor Czech Republic s.r.o.) with dimensions 10 × 10 × 0.6 mm. These substrates are required in IR spectroscopy and scratch test. The second type were 1 mm thick glass substrates (Paul Marienfeld GmbH & Co. KG, Germany) cut into 10 × 10 mm pieces, used in profilometry along with silicon wafers.

3.2 Plasmochemical modification for fiber reinforcement

The method of PECVD was used to create a thin film of tetravinylsilane (TVS) on unsized glass fibers type E. This process was done on deposition apparatus A4.

3.2.1 Monomer and used gases

Tetravinylsilane, $Si\text{-}(CH=CH_2)_4$, CAS: 1112-55-6

Manufacturer: Sigma Aldrich

Mr = 136.27 g · mol^{-1}

ρ (20 °C) = 0.8 g · cm^{-3}

T_b = 130 °C

Refractive index: 1.461

Purity: 97%

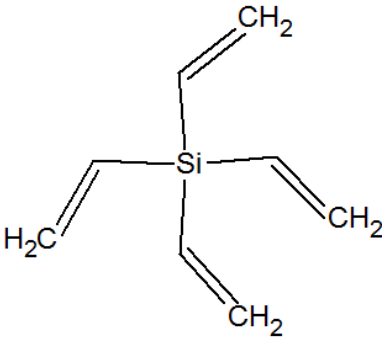

Used gases:

Argon 5.0 (Linde gas) with 99.999% purity is used as a cleaning medium of the reaction chamber, which also serves as an inert atmosphere for free radical quenching in the reaction chamber after the deposition.

Oxygen 4.5 (Linde gas) with 99.995% purity is used for pre-treatment of substrates to remove surface contamination and activate surface states.

3.2.2 Vacuum system

The pumping system of aparature A4 uses HiCube 80 Eco system (Pfeiffer Vacuum) which consists of:

- Turbomolecular pump HiPace 80 with pumping speed for N_2 of $67\,l\cdot s^{-1}$ and operating frequency of 1500 Hz (pressure range $2200 - 10^{-5}$ Pa).
- Membrane pump MVP 015 with pumping speed of $0{,}7\ m^3\cdot h^{-1}$ (range atm. – 350 Pa).
- Turbomolecular pump cooling system.

Pressure control system consists of:

- Butterfly valve with sealing function VAT 615 DN.
- Solenoid controlled pneumatic valve VAT N 7557.
- Solenoid controlled pneumatic valve AVC 016 PA.
- Capacitance gauge CMR 362 (pressure range $1-10^4$ Pa).
- Capacitance gauges CMR 364 (pressure range $10^{-2} - 110$ Pa).

- Capacitance gauge Leybold CTR 100 (range $0{,}13-133\,\mathrm{Pa}$).
- Fullrange gauge PKR 251 (pressure range $5\cdot10^{-7}-10^{5}\ \mathrm{Pa}$).
- Pirani gauge TPR 280 (pressure range $5\cdot10^{-2}-10^{5}\ \mathrm{Pa}$).
- Controller Leybold Capacitron DM 22.
- Controller Pfeiffer MaxiGauge TPG 256.

Monomer and gas control system consists of:

- Solenoid controlled AP Tech Diaphragm valve AP3540.
- Solenoid controlled AP Tech Diaphragm valve AP4540.
- Mass flow meter Bronkhorst F-201CV
- Mass flow meter Bronkhorst F-201DV
- Gas flow controllers

3.2.3 Deposition system

Deposition system (Fig. 3.1, Fig. 3.3) was designed mainly for fiber surface modification with the possibility to prepare thin films on planar substrates. The reaction chamber (Fig. 3.2) is made of glass tube (SIMAX, Merci, s.r.o.) with an inner diameter of 4 cm and a length of 1 m. The tube is equipped with 7 live and 8 grounding electrodes alternating one after the other to ensure stable plasma discharge throughout the whole length of reaction chamber.

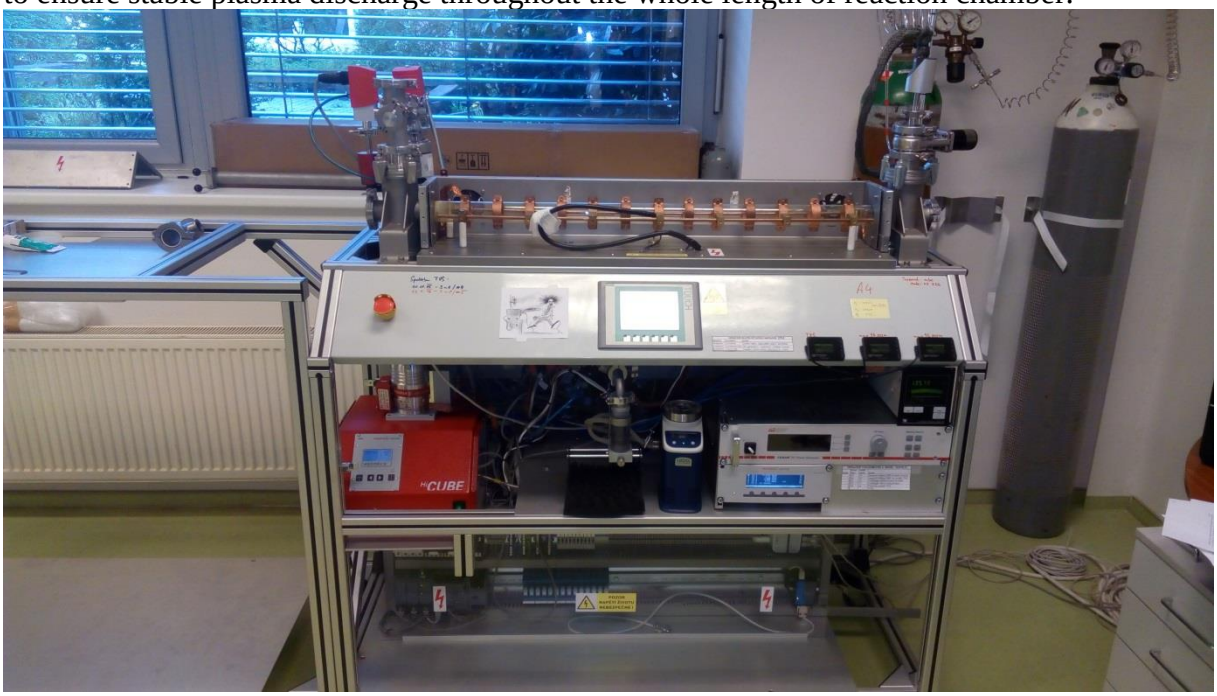

Fig. 3.1: Deposition apparatus “A4”

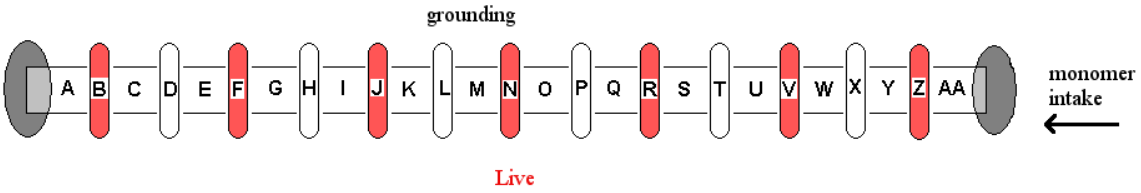

Fig. 3.2: Reaction chamber scheme with labelled positions.

The glow discharge is powered by Cesar 1310 RF Generator (Advanced Energy) with frequency of 13.56 MHz with maximum power output of 1000 W into a 50 Ω load. The RF generator is controlled manually. It is able to work both in pulsed and continuous wave (CW) modes. The principle of pulse mode is in alternation between intervals when the discharge is on (t_{on}) and when the discharge is off (t_{off}). The effective power is defined as:

$$P_{eff} = P_{total} \frac{t_{on}}{t_{on} + t_{off}}. \tag{8}$$

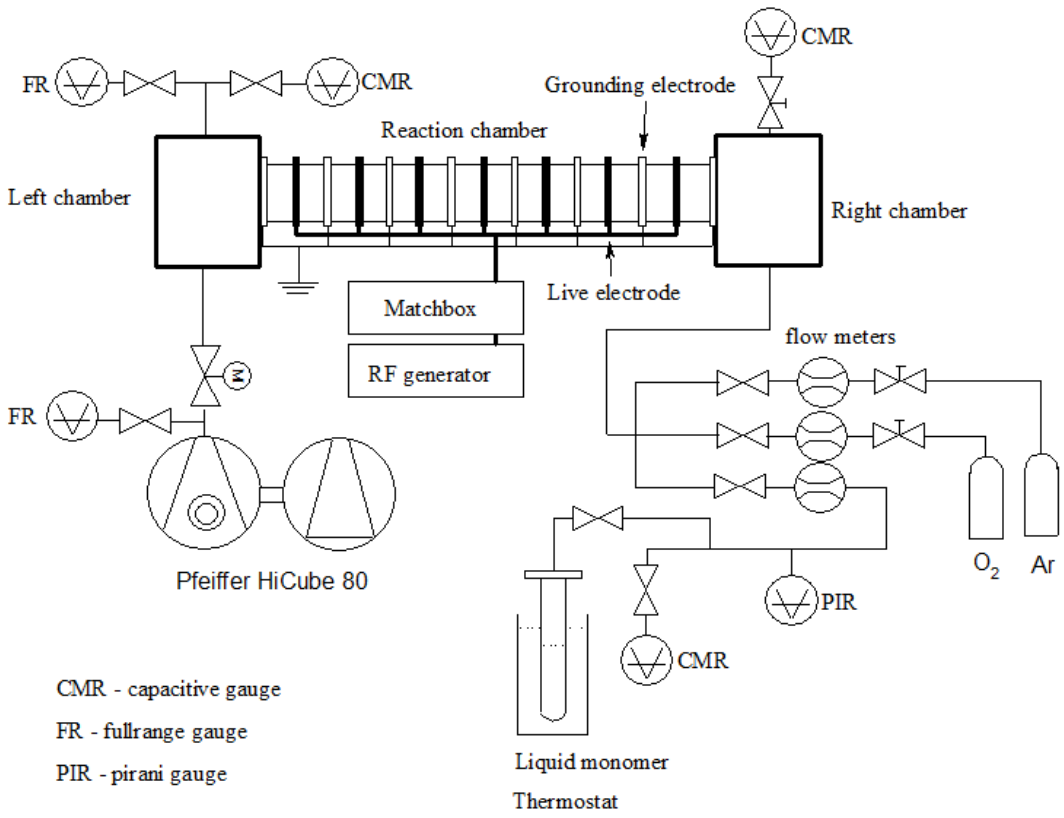

Fig. 3.3: Schematic illustration of deposition apparatus “A4”.

3.2.4 Plasma polymer film preparation procedure

Particular steps during the deposition procedure are described in the following table 3.3.

Table 3.3: Procedures for plasma polymer film preparation.

.1	Sample was placed into the reaction chamber. The reaction chamber is then shut off the outer atmosphere and vacuum system is turned on to establish vacuum of at least $5 \cdot 10^{-4}$ Pa.
2.	Argon throttling – 10 sccm Ar, setting main VAT valve to achieve 5.7 Pa in the reaction chamber
2.	Oxygen pre-treatment: 1. 10 sccm O_2, pressure inside chamber ~ 5.2 Pa 2. configure RF generator to continuous discharge (30 W, 10 minutes for planar substrates, 100 W, 30 minutes for glass fiber modification) 3. after set time turn off discharge and stop O_2 flow
3.	Reservoir with monomer: Release the accumulated monomer vapour to the pressure of 1000 Pa.
4.	Deposition 1. set desired TVS and O_2 flow rates 2. set RF generator to desired power and time 3. after the deposition turn off RF generator and stop respective gas flow and close valves.
5.	Post-deposition treatment: Set Ar flow meter to 10 sccm for 1 hour (radical quenching).
6.	The samples are kept in vacuum until next day and then the vacuum system is shut down and samples are taken to further processing.

3.3 Composite sample preparation

Samples were prepared as fiber bundles clad in polyester resin, that were put in moulds of pre-defined proportions.

3.3.1 Mould preparation

Moulds were prepared from two-component silicone rubber Lukopren N 1522 (Lučební závody a. s. Kolín), final moulds have two chambers with dimensions $3 \times 10 \times 250$ mm. Catalyst C21 (3 wt.%), consisting of dibutyltin dilaurate (CAS 77-58-7) and tetraethyl orthosilicate (CAS 78-10-4), was used for curing at room temperature for 24 hours. Thermal stability of cured mould is –50 to 180 °C.

3.3.2 Composite beam preparation

The prepared matrix with all necessary additives needs to be thoroughly homogenized and kept at rest for 30 minutes to get rid of air bubbles that are created during the homogenization. The following step is to fill a syringe with matrix and create a layer at the bottom of the mould chamber and systematically adding bundles of fiber. The fibers must be well saturated, straightened (using steel spatulas) so that fibers do not cross each other, excess matrix and

voids are eliminated from the mould. When the mould is filled with required number of bundles, rest of the mould is filled with slight excess of matrix to counter the volume contraction in curing process.

Entire mould is then cured following set program:

- Heat up to 45 °C, duration 5 minutes.
- Tempering at 45 °C, duration 30 minutes.
- Heat up to 100 °C, duration 30 minutes.
- Tempering at 100 °C, duration 30 minutes.
- Heat up to 140 °C, duration 30 minutes.
- Tempering at 140 °C, duration 60 minutes.
- Cooling to room temperature

The composite beam is then cut down to 20 mm and every sample was grinded to dimensions of 18.00 ± 0.30 mm , 10.00 ± 0.50 mm and 3.00 ± 0.15 mm using metallographic grinder.

3.4 Testing methods

3.4.1 Short beam shear test

Short beam shear was measured on universal testing machine Zwick Z010/TH2A (ZwickGmbH & Co, Ulm, Germany) at room temperature. The exact size of samples was measured with Absolute Digimatic Caliper (Mitutoyo Ltd., U.K.).

Fig. 3.4: Testing machine Zwick Z010/TH2A.

All samples were tested according to test method ASTM D 2344/D 2344M. Samples in this method are subjected to three-point bending with very short span length. This arrangement eliminates the flexural deformation, making the applied force directly proportional to shear stress. This testing method suggests that the length to thickness ratio is 6, width to thickness ratio is 2, as well as span length to thickness ratio to be 4. The diameter of supporting spans and loading nose are R_1 = 1.5 mm and R_2 = 3 mm respectively. The loading nose speed is $1\ \mathrm{mm} \cdot \mathrm{min}^{-1}$. The test ends when the sample breaks or the force on loading head drops below 30% of maximum. The interlaminar shear strength τ_{int} is calculated using equation:

$$\tau_{\mathrm{int}} = \frac{3 \cdot F_{\mathrm{max}}}{4 \cdot t \cdot b} \left[\mathrm{MPa}\right], \tag{9}$$

where F_{max} is the maximum loading force [N], t is sample thickness [mm], b is sample width [mm] [36, 38].

Measurement settings:

- Sample dimensions: L = 18 mm, t = 3 mm, b = 10 mm
- Load head: 10 kN
- R_1 = 1.5 mm
- R_2 = 3 mm
- Pre-load: 20 N
- Loading nose speed: $1\ \mathrm{mm} \cdot \mathrm{min}^{-1}$
- Measurement termination: F drop below 30 % of F_{max}

3.4.2 Profilometry

The thickness of deposited layer on planar Si substrates was measured on Dektak XT stylus profiler (Bruker). All samples were measured in hills and valleys mode using stylus with diameter of 12.5 µm and applied force of 2 mg. Part of the layer was mechanically eliminated using a dull object of appropriate size (screwdriver) and used as a base line. It is necessary to do this step with caution, because exerting higher force can damage the substrate itself, resulting in inaccurate measurement. The acquired sample profile was then compared to the base line, creating height difference equal to the thickness of the deposited layer.

3.4.3 IR spectrometry

For measuring IR spectra of planar substrates, FT-IR (Fourier transform infrared) spectrometer Vertex80v (Bruker Optics) was used and operated at vacuum applying a pressure of 160 Pa and with standard optical components: KBr beamsplitter, DLaTGS detector and MIR source, which can achieve spectral range of middle IR: 8000 to 350 cm^{-1}. It is based on UltraScan™ interferometer, providing high spectral resolution. The spectrometer eliminates atmospheric moisture absorptions, it can increase the sensitivity and stability of the spectrometer [39].

Vertex80v has separate chamber for samples and for optical components, allowing the samples to be inserted without breaking the vacuum and contaminating the optical components. All functions of the spectrometer are controlled via PC using OPUS software.

Corresponding experiment must be selected before the start of the measurement. After an experiment is loaded, it is necessary to measure background noise by choosing the background single channel in the measurement menu. After the background channel is scanned, it is possible to measure a sample with the sample single channel option in the measurement menu. When the sample spectrum is acquired it can be now processed using software tools such as water compensation, cut and subtraction to get optimal results. The absorption spectrum of silicon substrate was subtracted using the measurement of undeposited silicon wafer to obtain the absorption spectrum of the thin film. The samples were measured in range from 400 to 4000 cm^{-1} with a resolution of 4 cm^{-1}.

3.4.4 Scratch test

The test was done on NTEGRA Prima/Aura with loading head TriboScope TS-75 (Hysitron Inc.). Diamond tip with a shape of a three-sided pyramid (142.35° angle between sides), and curvature radius of 50 nm was used during this measurement. The samples used for scratch test were silicon wafers with 0.1 μm thick deposited TVS film. During this test the indentor moves along the surface of the sample, applying increasing load (maximum load 10 mN) onto the surface until the bond between the silicon wafer and deposited film breaks, causing delamination.

3.4.5 Scanning electron microscopy (SEM)

This measurement was done at faculty of mechanical engineering, Brno university of technology using scanning electron microscope Phillips XL30. Already tested and delaminated composite samples were used for the microscopy. The surface of samples was deliberately damaged in order to obtain details on the fiber-matrix interface and observe the adhesion of various treatments of samples. All samples were treated with a thin gold layer to increase the conductivity needed for the measurement. Secondary electrons with accelerating voltage of 20 kV were used to conduct the measurement.

4 RESULTS AND DISCUSSION

4.1 A4 characterization

4.1.1 Pressure profile

The behaviour of used gases was observed in the reaction chamber using mass flow rate of 10 sccm for Ar and O_2 and 4 sccm for TVS during CW discharge of increasing RF power (0–200 W). The result of this test is depicted in figure 4.1. Argon had constant pressure value throughout the test. We can see an increase of oxygen pressure at lower RF power values followed by a slight decrease to a constant value. This is caused by dissociation of oxygen molecule and its subsequent recombination. There is a substantial decrease in pressure for TVS caused by deposition of reactive fragments onto the chamber surface, having significant effect at lower power values. At higher RF power the pressure is at a constant level due to the fact that the deposition is rivalled by ablation.

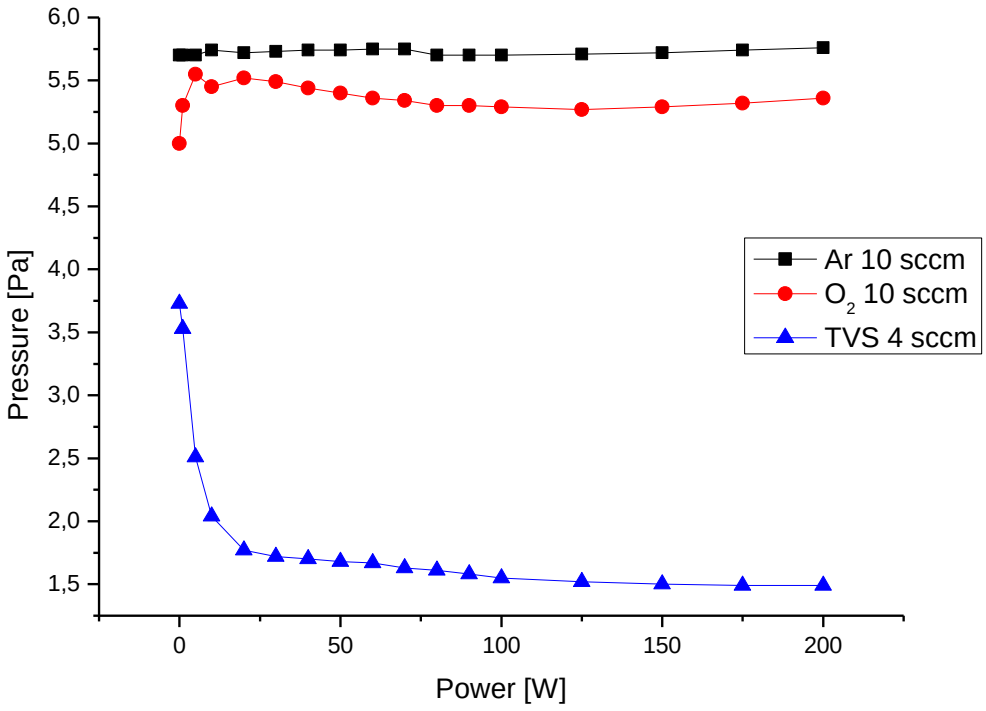

Fig. 4.1: Pressure of used gases with increasing RF power, taken from [41].

4.1.2 Deposition speed

Polished silicon and glass wafers were deposited, and the deposition speed was then calculated based on the film thickness and duration using profilometry (Fig. 4.2). Planar substrates were also used in FTIR to obtain IR spectra and in scratch test to measure critical load of selected samples. Substrates were placed in positions (Fig. 3.2) A, G, N, O, U and AA along the glass tube axis using glass substrate holders. Position "O" was always filled with a silicon wafer.

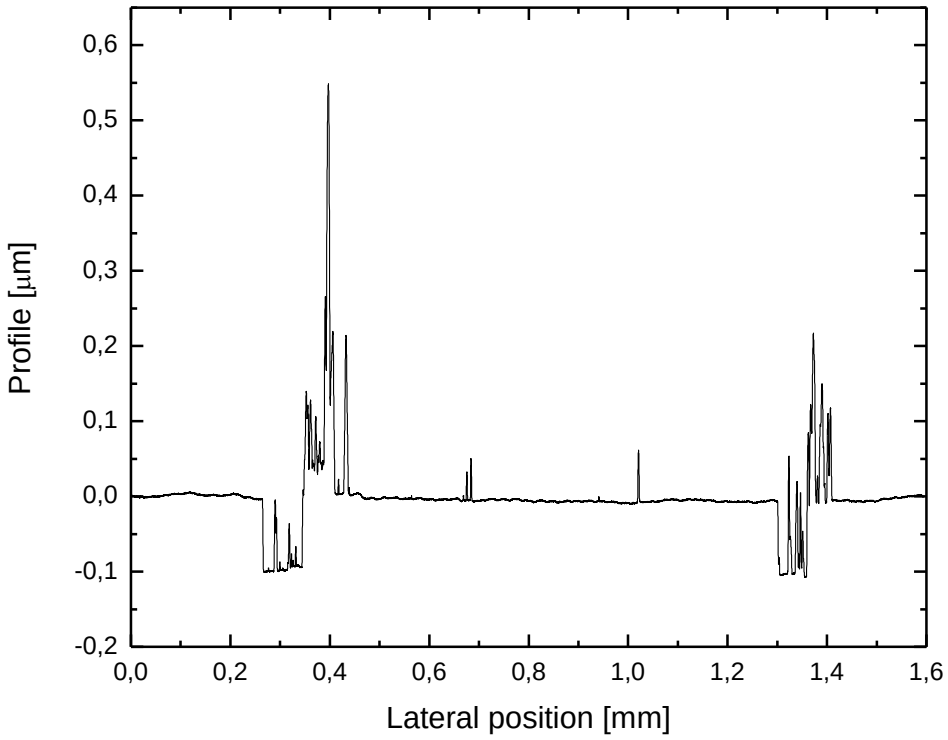

Fig. 4.2: Profile of a sample with 0.1 µm thick film.

4.1.2.1 Deposition speed with increasing RF power in CW mode

Deposition speed throughout the reaction chamber in CW mode, using TVS flow rate of 4 sccm and RF power range 2–100 W can be seen in figure 4.3. Samples deposited under 100 W have higher deposition speed at the monomer intake, but the deposition rate drops down further in the chamber, having the lowest deposition speed at the end of the reaction chamber. With decreasing RF power, all samples follow this trend with an exception of 2 W samples, which have their deposition speed relatively balanced throughout the chamber. Samples using 2–10 W have balanced deposition speed throughout the reaction chamber. Table 4.1 shows that the average deposition speed increases significantly between 2 and 5 W, with only a slight increase at 10 W. Further increase in power does not increase the overall deposition speed.

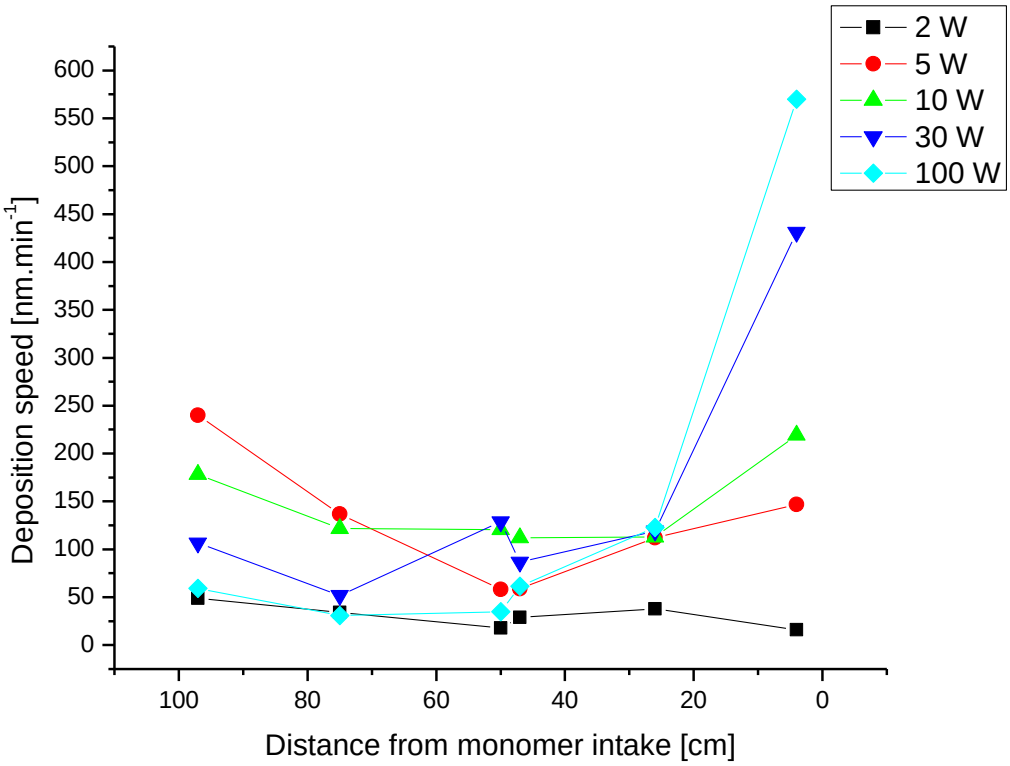

Fig. 4.3: Deposition speed with different RF power using CW mode, TVS flow rate of 4 sccm, taken and modified from [42].

Table 4.1: Average deposition speed in CW mode.

Power [W]	Deposition speed [nm·min^{-1}]
2	31
5	125
10	144
30	154
100	146

4.1.2.2 Deposition speed with increasing RF power in pulse mode

Deposition speed using pulse mode with TVS flow rate of 4 sccm with effective power range of 2–150 W is shown in figure 4.4. Samples in pulse mode follow a similar trend as in CW mode with higher deposition speed at the ends of the reaction chamber. This occurred because the intensity of plasma discharge at both ends of the reaction chamber was significantly higher than at the centre. The overall speed in pulse mode is lower and the deposition speed throughout the reaction chamber is more balanced with the exception of samples with effective power of 150 W, where the deposition speed is significantly higher at the monomer inlet compared to the rest of the reaction chamber. Samples treated with 10 W_{ef}

have their deposition speed quadrupled at both reaction chamber ends. Further testing was done using 2 W_{ef} deposition conditions. Table 4.2 shows the pulse mode setting and average deposition speed of samples deposited in pulse mode, having two peaks at 10 W_{ef} and 150 W_{ef}. The deposition speed at 2 W_{ef} is mostly the same as 2 W samples in CW mode.

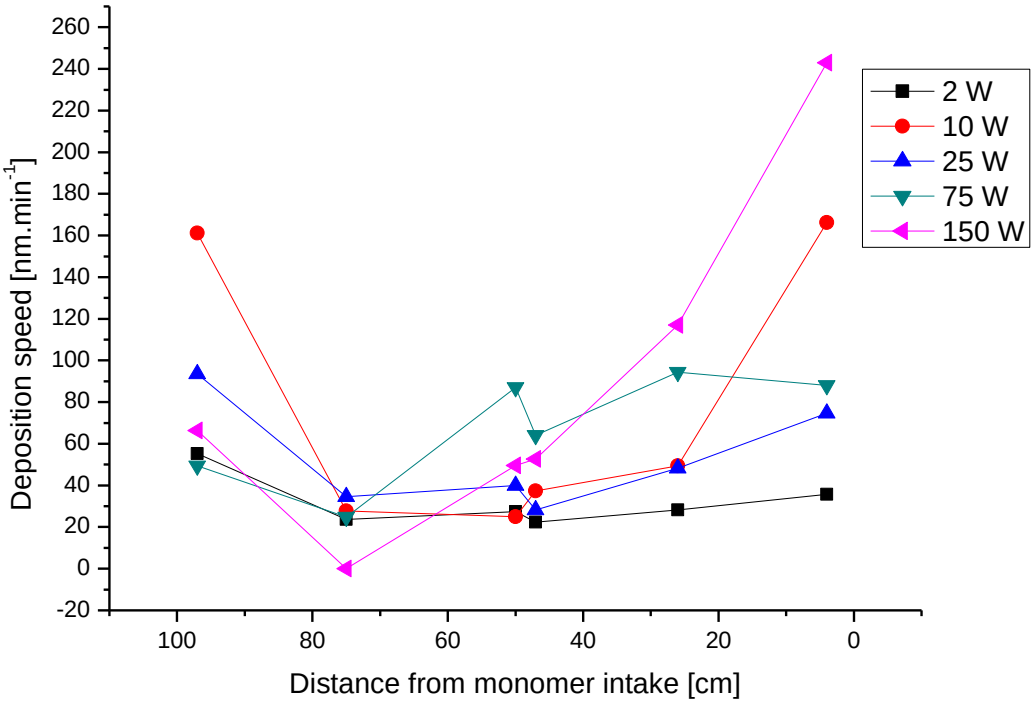

Fig. 4.4: Deposition speed with different RF power using pulse mode according to Table 4.2, TVS flow rate of 4 sccm.

Table 4.2: Pulse mode setting and average deposition speed.

Effective power [W_{ef}]	Total power [W]	$t_{on} : t_{off}$ [ms]	Deposition speed [nm·min^{-1}]
2	10	1:4	32
10	50	1:4	77
25	200	1:7	53
75	300	1:3	66
150	300	1:1	90

4.1.2.3 Deposition speed with different gas mixtures

Using the previous deposition conditions (RF pulsed, 2 W_{ef}, duty cycle 1:4), different mixtures of gases (2 sccm O_2 + 2 sccm TVS, 10 sccm O_2 + 4 sccm TVS, 4 sccm TVS) were used during the process. Figure 4.5 shows that adding oxygen into the monomer during deposition generally increases the deposition speed (averages in table 4.3), creating more covalent bonds and activating the sample surface for monomer to attach to.

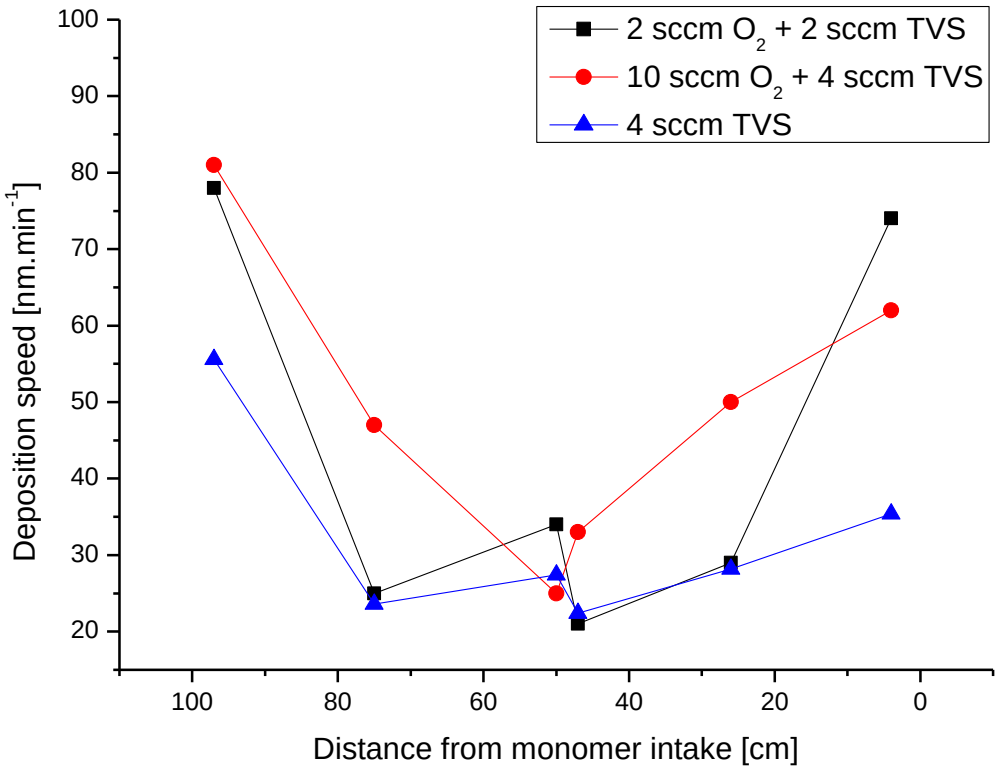

Fig. 4.5: Deposition speed of different gas mixtures using pulse mode 2 W_{ef}, duty cycle 1:4.

Table 4.3: Average deposition speed using different gas mixtures.

TVS flow rate [sccm]	O_2 flow rate [sccm]	Deposition speed [nm·min^{-1}]
2	2	43
4	4	50
4	0	32

Further testing was done using the previous parameters (RF pulsed, 2 W_{ef}, duty cycle 1:4), constant TVS flow rate (4 sccm) and changing concentration of O_2 in the mixture at position "O" from 0 to 71 %. The result in figure 4.6 shows that the O_2 concentration has negligible effect on deposition speed with minimum (O_2 = 0 %) at 29 nm·min^{-1} and maximum (O_2 = 61 %) at 34 nm·min^{-1}.

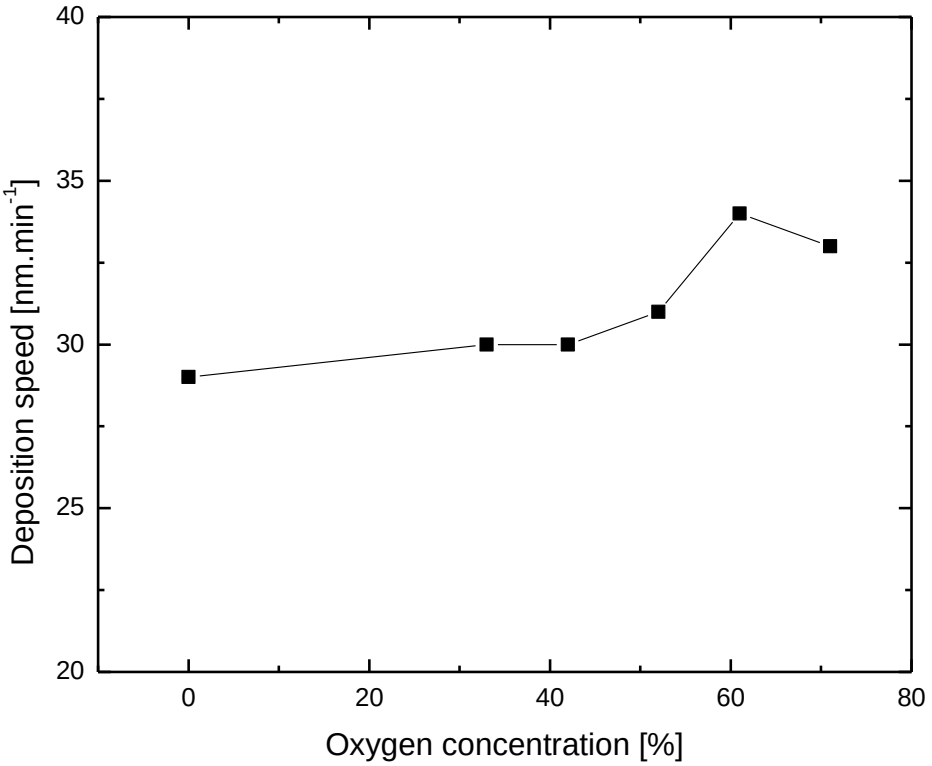

Fig. 4.6: Deposition speed with different O_2 concentration at position “O”.

4.1.3 FTIR

IR spectra of selected planar substrates (Si wafer) with 0.1 µm thick film were obtained using the FT-IR spectroscope. The absorption bands were assigned according to table 4.4 containing the typical wavenumber of the absorption band. This measurement was done right after the samples were taken out from vacuum to minimize oxidation effects in the atmosphere. Three series were prepared with changing chamber position, RF power and O_2 content in the gas mixture.

Table 4.4: Functional groups and their respective absorption bands [40].

Wavenumber [cm^{-1}]	**Assignment**
3461	O-H stretching
2921-2894	CH_x stretching $(x = 1,2,3)$
2194-2116	Si-H stretching
1708	C=O stretching
1608	C=C stretching in vinyl
1457	CH_2 scissoring
1408	CH_2 deformation in vinyl
1266-1257	CH_2 wagging in Si-CH_2-R
1067-1056	Si-O-C stretching
1010	=CH wagging in vinyl
950	=CH_2 wagging in vinyl
885-830	Si-O bending
780-745	Si-C stretching

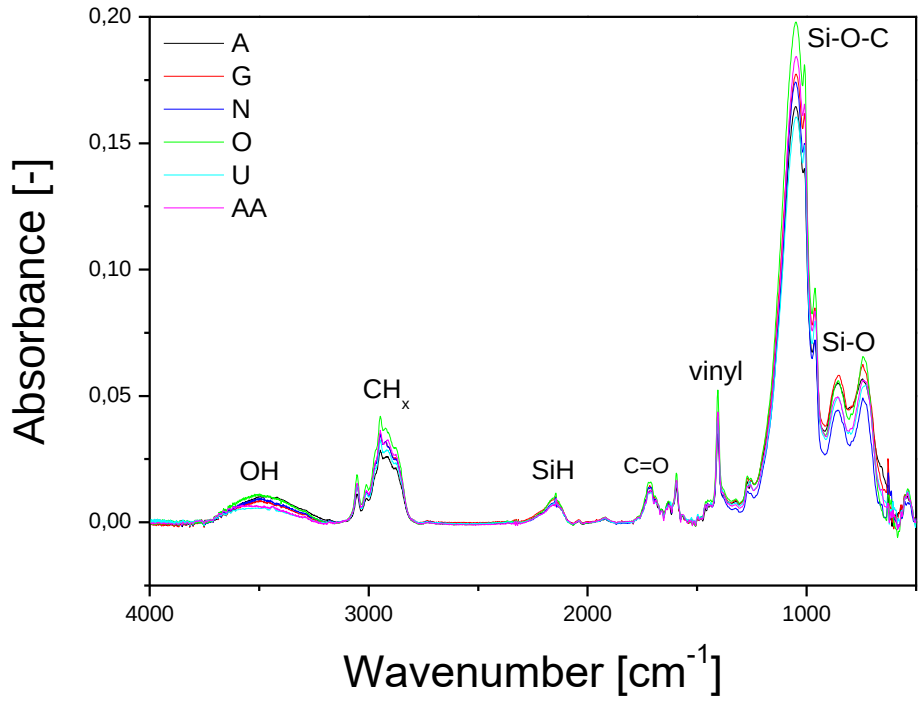

Fig. 4.7: FTIR – positional series.

Positional series (2 W_{ef}, pulsed, 4 sccm TVS + 10 sccm O_2) in figure 4.7 shows that the sample composition is the same regardless the position in the reaction chamber. Functional group C=O is present due to the oxidation of sample surface. The abundance of Si–O–C and Si–O–Si groups confirms the covalent bonds between deposited film and substrate.

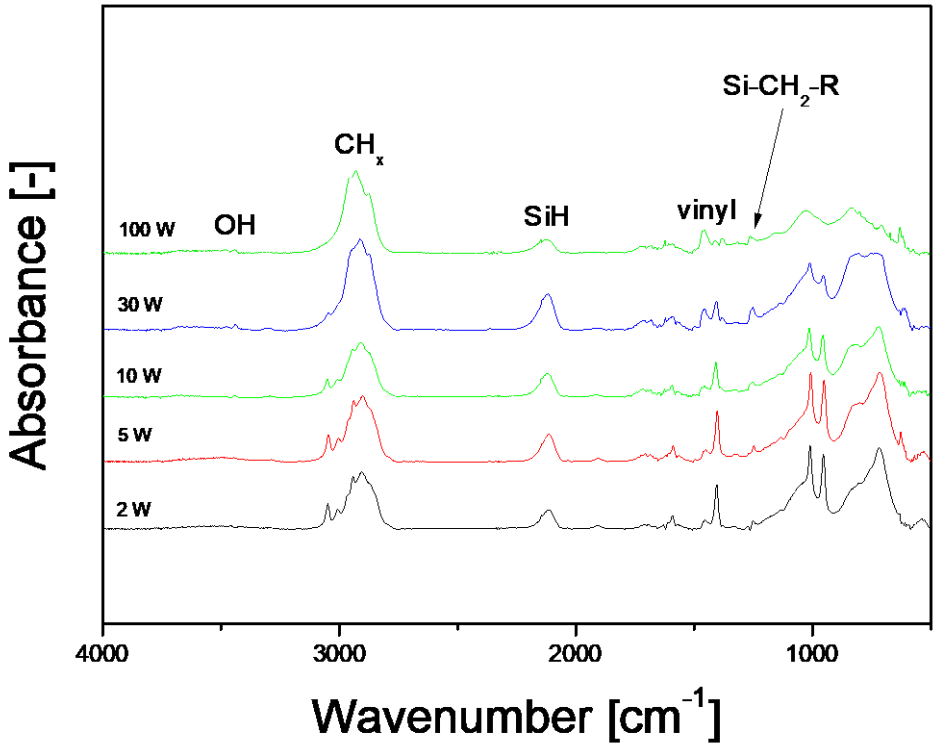

Fig. 4.8: FTIR – power series.

Power series (2–100 W, CW, 4 sccm TVS) in figure 4.8 shows the change in the composition of the samples. With increasing power, the number of vinyl groups decreases, while there is a clear rise of CH_x groups. These samples were deposited without any oxygen but a number of OH groups are still present in all samples due to exposure to the atmospheric oxygen.

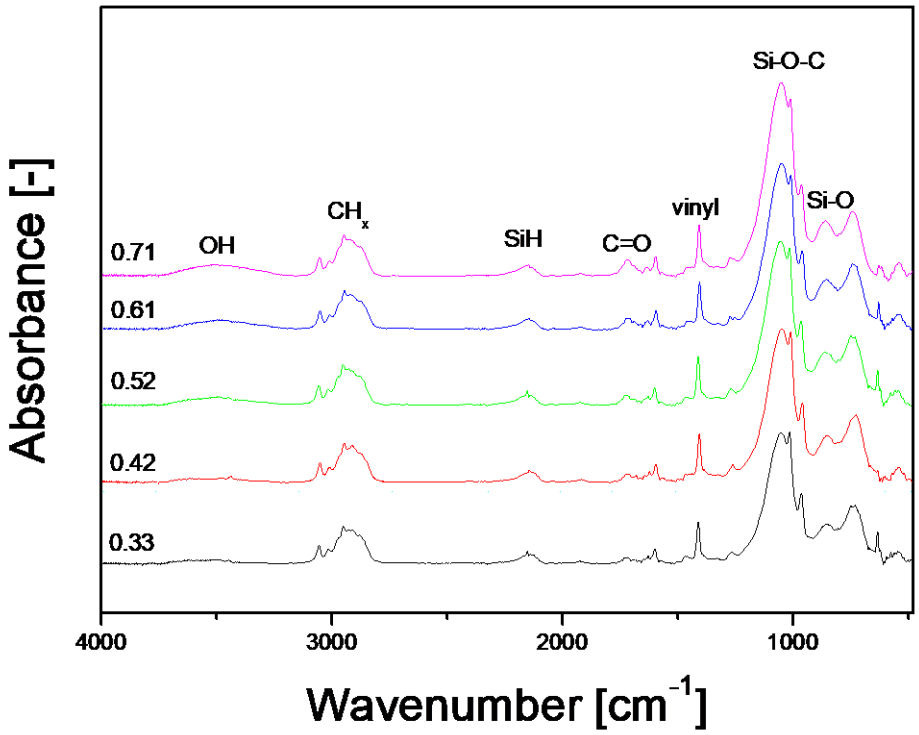

Fig. 4.9: FTIR –series with increasing oxygen content in the gas mixture: 0.33 (black, 2 sccm O_2), 0.42 (red, 2.9 sccm O_2). 0.52 (green, 4.3 sccm O_2), 0.61 (blue, 6.2 sccm O_2) and 0.71 (purple, 10 sccm O_2)

The O_2 concentration series (2 W_{ef}, pulsed, 4 sccm TVS + 2–10 sccm O_2) in figure 4.9 shows a gradual increase of OH, C=O, Si–O–Si and Si–O–C groups with increasing O_2 concentration in the gas mixture. With rising oxygen content, only a marginal decrease in vinyl and CH_x groups has been observed.

4.1.4 Scratch test

Series of samples deposited with 0.1 µm thick TVS layer on silicon substrate were prepared. Scratch test measures the load at which the deposited layer delaminates. Three series were prepared with changing chamber position, RF power and O_2 concentration. The critical load along with the layer thickness measured using profilometry were put into the graphs below.

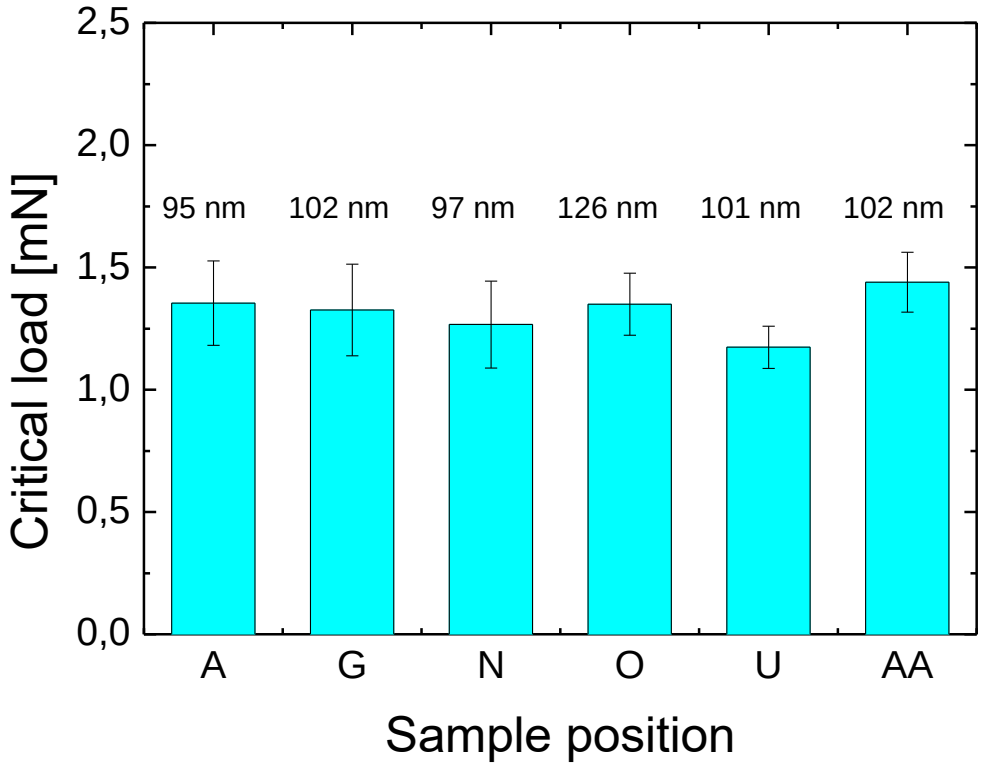

Fig. 4.10: Critical load and sample thickness – positional series.

The positional series (2 W_{ef}, pulsed, 4 sccm TVS + 10 sccm O_2) was done first to confirm the homogeneous conditions throughout the reaction chamber. This is confirmed by figure 4.10, where the critical load is 1.3 ± 0.2 mN in all positions. Further testing with changing power and O_2 concentration was done in position "O" using a common point at 2 W and 0 sccm O_2.

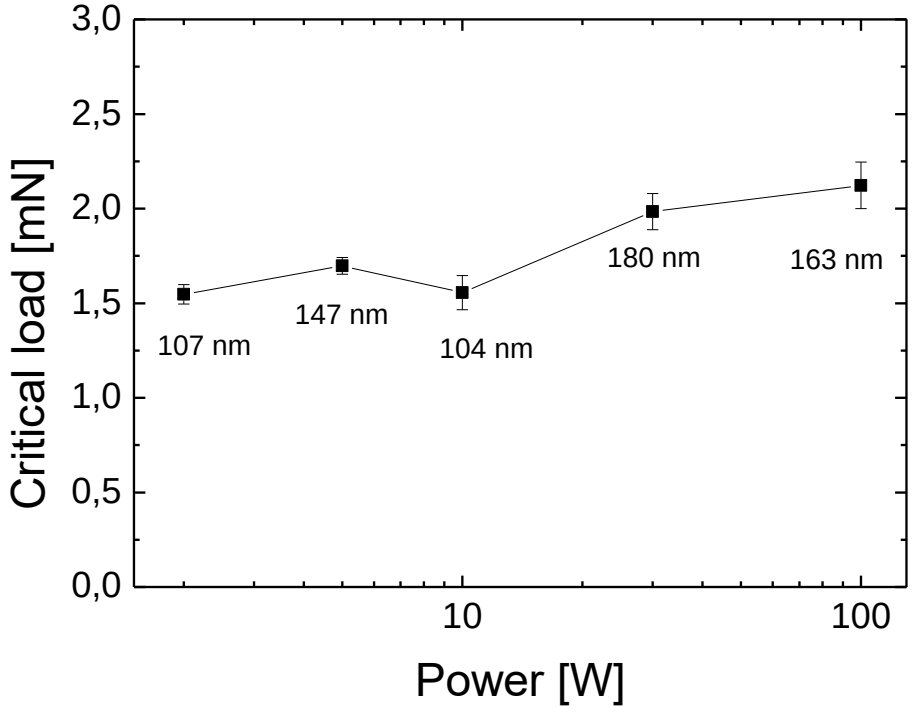

Fig. 4.11: Critical load and sample thickness – power series.

The power series (2–100 W, CW, 4 sccm TVS) in figure 4.11 shows an increasing trend of critical load with higher power, however the sample thickness of some of the samples in this series is higher than 0.1 µm. This was done unintentionally in the preparation step, causing any potential change in the critical load to be overshadowed by increased sample thickness. While further testing is required to obtain reliable data on this matter, we can assume that the change in the critical load will be minimal with values around 1.5 mN.

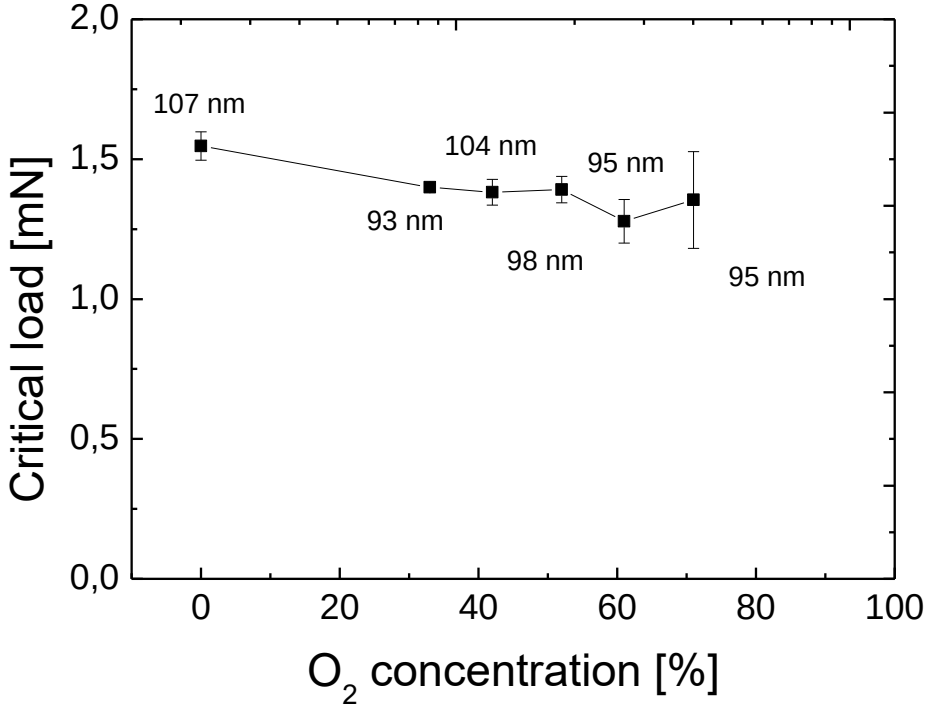

Fig. 4.12: Critical load and sample thickness – oxygen fraction in TVS/O_2 mixture.

The oxygen fraction in TVS/O_2 mixture (2 W_{ef}, pulsed, 4 sccm TVS + 0–10 sccm O_2) in figure 4.12 shows a declining trend. With increasing concentration, the critical load is slightly decreasing to a minimum of 1.3 mN.

4.2 Short beam shear test

Prepared composite beams were tested according to test conditions in chapter 3.4.1. The result of the test yields the dependence of applied force on the strain of the specimen with sample failure at the force maximum (F_{max}). With specimen thickness (*t*) and width (*b*), interlaminar shear strength (τ_{int}) was acquired. Composites made of unsized, sized glass fibers as well as pre-treated and plasmochemically modified samples were tested. The deposition conditions of plasmochemically treated composites have two series, one with increasing RF power (2–100 W, 4 sccm TVS) and second with increasing O_2 concentration (constant RF power 2 W_{ef}, 4 sccm TVS + 0–10 sccm O_2). The time of the deposition was set individually to maintain a minimum of 0.2 µm thick layer in positions with the lowest deposition speed. Following figures and tables show the test progression and resulting interlaminar shear strength.

4.2.1 Unsized GF

The resulting force-strain curve of composite samples using unsized glass fibers is depicted in figure 4.13 with the resulting mechanical properties shown in table 4.5.

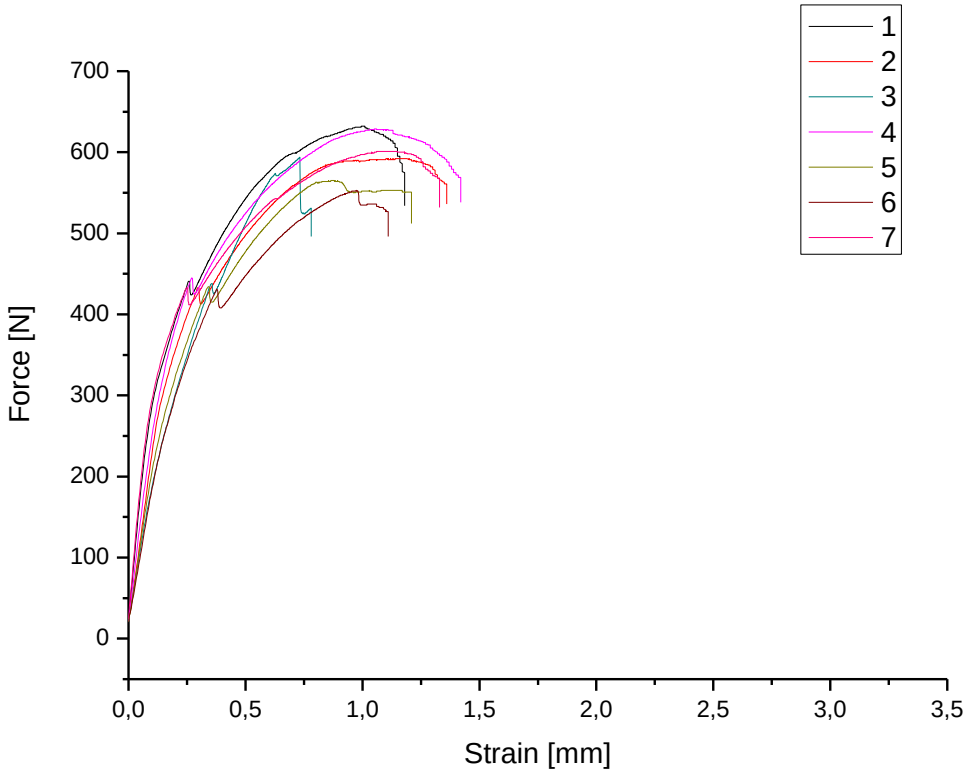

Fig. 4.13: Force-strain curve of composites using unsized glass fibers.

Table 4.5: Mechanical properties of composites using unsized glass fibers.

Specimen number	t [mm]	b [mm]	F_{max} [N]	τ_{int} [MPa]
1	2.87	10.02	632.1	16.5
2	3.09	9.71	592.0	14.8
3	3.09	9.55	594.2	15.1
4	3.05	9.60	628.6	16.1
5	3.03	9.95	564.9	14.1
6	3.05	9.84	552.6	13.8
7	3.01	9.66	601.3	15.5
	Average :		595.1	15.1
	σ :		29.6	1.0
	σ_r [%]:		5.0	6.6

Average interlaminar shear strength for unsized fiber composites is 15.1 ± 1.0 MPa. Some of the fibers broke before the peak at which the composite delaminated. This was due to various strain on respective fiber bundles which was caused during the composite preparation, where some bundles were more tightly packed than others, resulting in overall lower shear strength.

4.2.2 Sized GF

The resulting force-strain curve of composite samples using commercially sized glass fibers is depicted in figure 4.14 with the resulting mechanical properties shown in table 4.6.

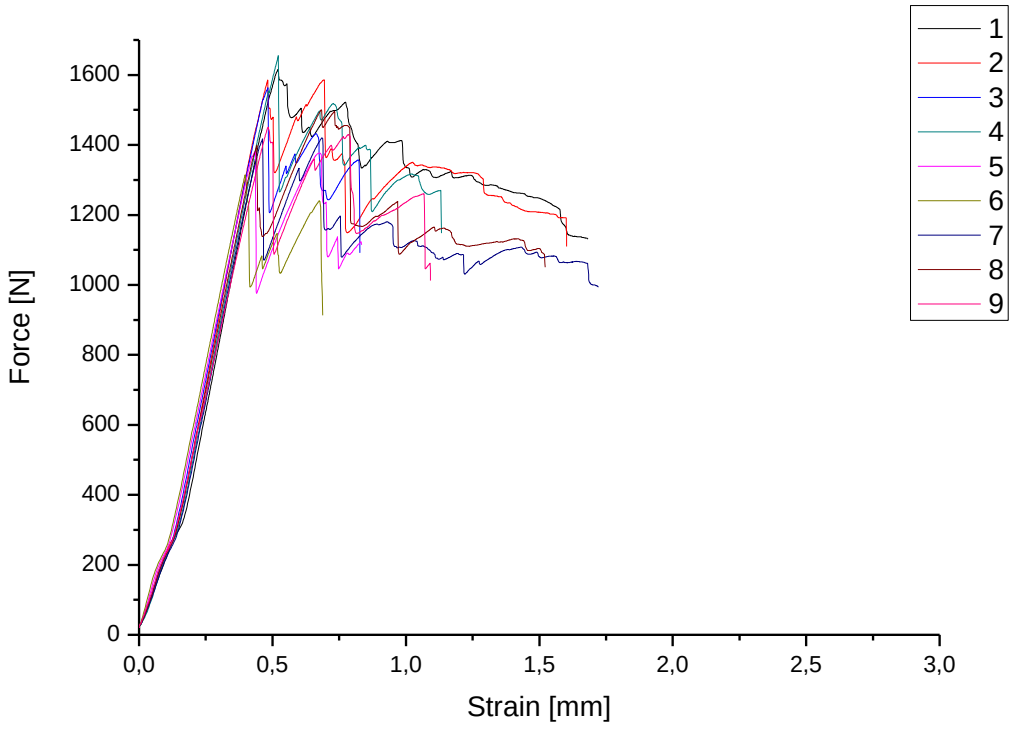

Fig. 4.14: Force-strain curve of composites using commercially sized glass fibers.

Table 4.6: Mechanical properties of composites using commercially sized glass fibers

Specimen number	t [mm]	b [mm]	F_{max} [N]	τ_{int} [MPa]
1	2.93	9.89	1615.6	41.8
2	2.96	9.94	1586.1	40.4
3	2.98	9.93	1563.4	39.6
4	2.93	9.85	1655.3	43.0
5	2.90	9.68	1381.3	36.9
6	2.89	9.68	1314.6	35.2
7	2.92	9.74	1420.2	37.5
8	2.91	9.78	1500.8	39.5
9	2.91	9.75	1450.7	38.3
	Average :		1498.6	39.2
	σ :		115.2	2.4
	σ_r [%]:		7.7	6.2

Average interlaminar shear strength for commercially sized fiber composites is 39.2 ± 2.4 MPa. The sizing improves the adhesion between fibers and matrix, resulting in significantly higher shear strength compared to composites made from unsized fibers.

4.2.3 Pre-treated GF

The resulting force-strain curve of composite samples modified with O_2 pre-treatment (10 sccm O_2, RF power 100 W, CW mode, 30 min) is depicted in figure 4.15 with the resulting mechanical properties shown in table 4.7.

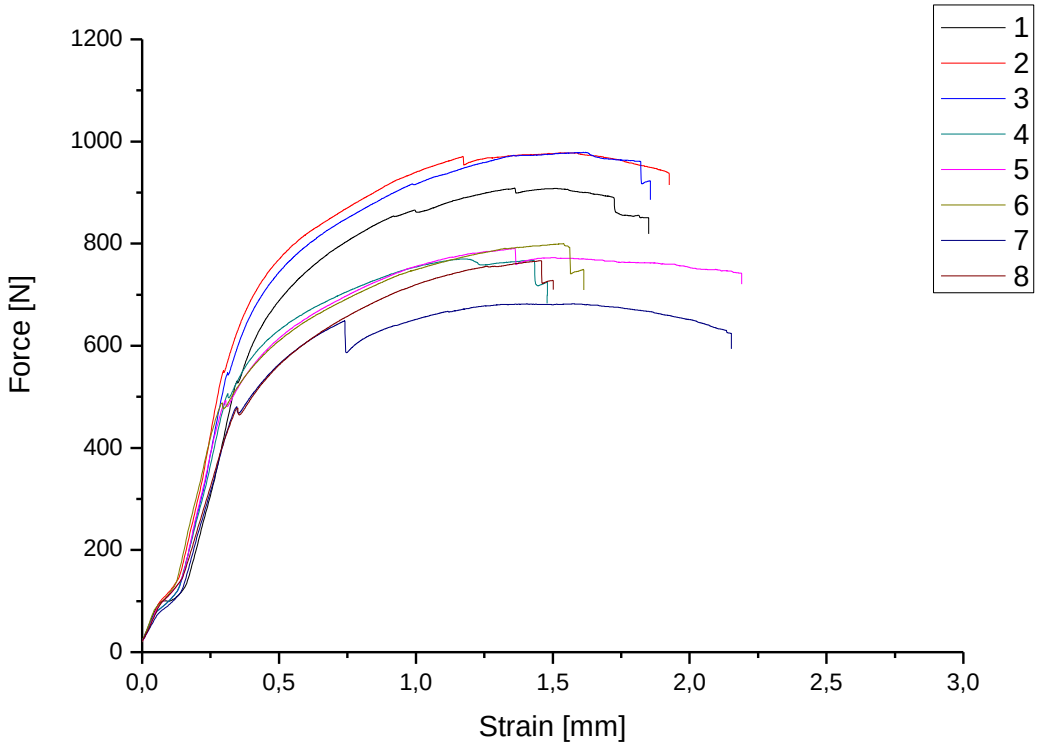

Fig. 4.15: Force-strain curve of O_2 pre-treated composites.

Table 4.7: Mechanical properties of O_2 pre-treated composites.

Specimen number	t [mm]	b [mm]	F_{max} [N]	τ_{int} [MPa]
1	2.86	9.72	908.7	24.5
2	2.91	9.74	977.8	25.9
3	2.98	9.63	978.6	25.6
4	2.91	9.45	770.1	21.0
5	2.95	9.35	790.9	21.5
6	2.88	9.46	800.0	22.0
7	2.91	9.57	682.0	18.4
8	2.91	9.53	766.6	20.7
	Average :		834.3	22.4
	σ :		108.2	2.6
	σ_r [%]:		13.0	11.7

Average interlaminar shear strength for O_2 pre-treated composites is 22.4 ± 2.6 MPa. The behaviour during the test was still similar to unsized samples, namely bending during test.

4.2.4 Plasmochemically modified GF

Figures 4.16–20 show the force-strain curves of samples in the power series with their mechanical properties shown in tables 4.8–12. O_2 concentration series and their force-strain curves are shown in figures 4.21–25 with their mechanical properties in tables 4.13–17.

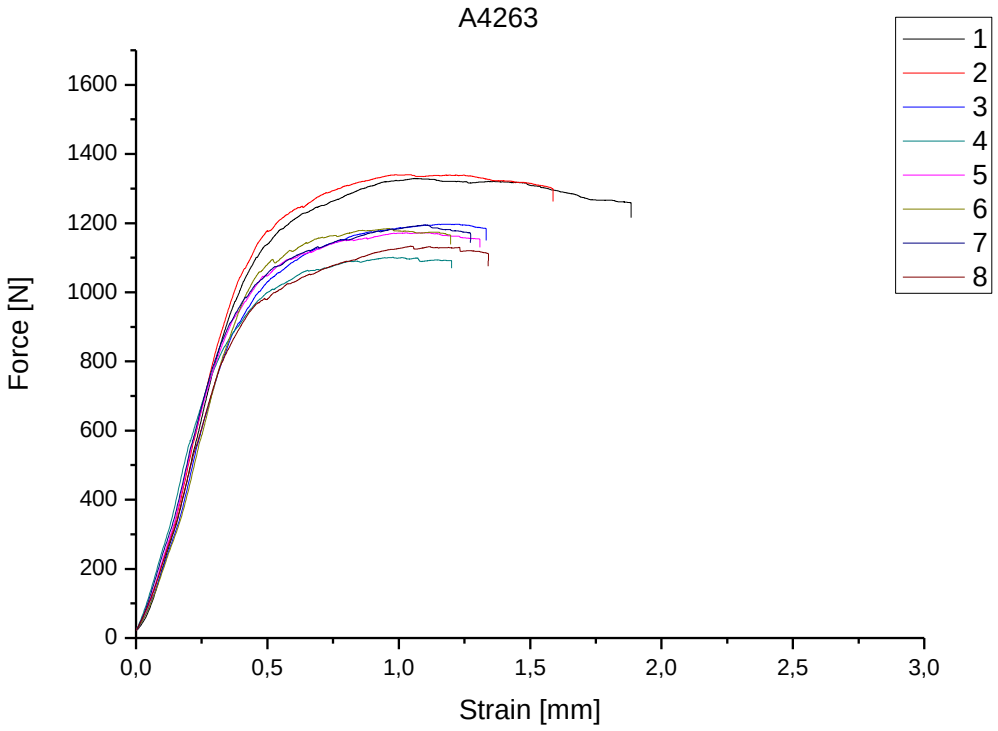

Fig. 4.16: Force-strain curve of plasmochemically treated composites – 2 W, CW, 4 sccm TVS

Table 4.8: Mechanical properties of plasmochemically treated composites – 2 W, CW, 4 sccm TVS

Specimen number	t [mm]	b [mm]	F_{max} [N]	τ_{int} [MPa]
1	2.96	9.84	1329.2	34.2
2	2.99	9.81	1340.4	34.3
3	2.95	9.76	1197.0	31.2
4	2.91	9.57	1101.5	29.7
5	2.96	9.58	1172.4	31.0
6	2.91	9.55	1184.3	32.0
7	2.95	9.67	1195.2	31.4
8	2.92	9.68	1133.4	30.1
	Average :		1206.7	31.7
	σ :		85.5	1.7
	σ_r [%]:		7.1	5.4

Average interlaminar shear strength for 2 W plasma treated composites is 31.7 ± 1.7 MPa.

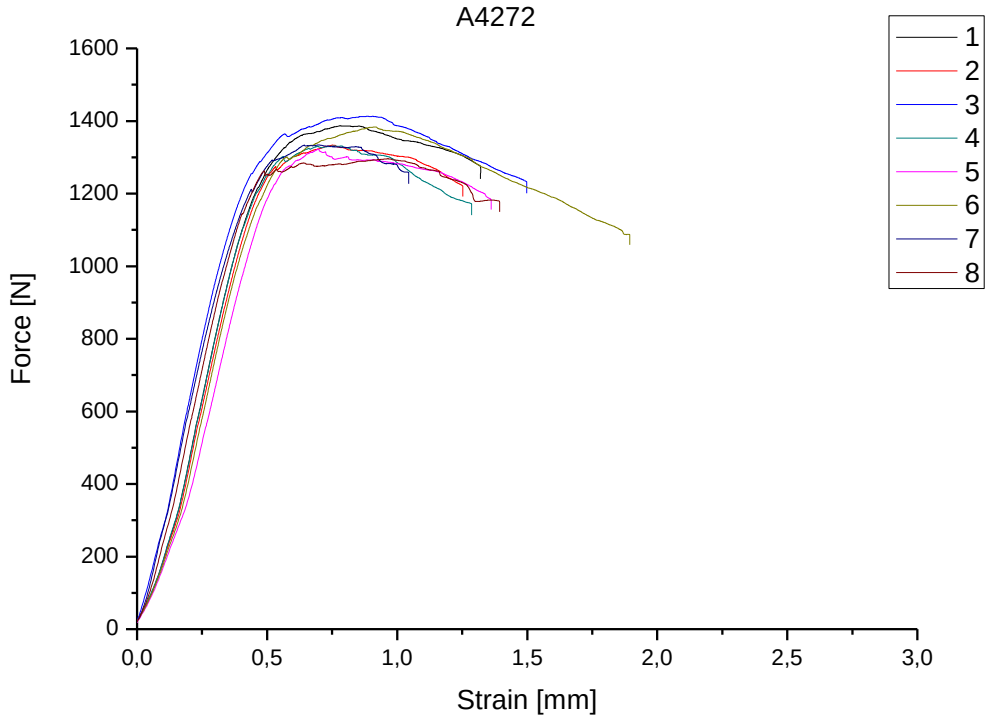

Fig. 4.17: Force-strain curve of plasmochemically treated composites – 5 W, CW, 4 sccm TVS

Table 4.9: Mechanical properties of plasmochemically treated composites – 5 W, CW, 4 sccm TVS

Specimen number	t [mm]	b [mm]	F_{max} [N]	τ_{int} [MPa]
1	2.90	10.13	1387.0	35.4
2	2.86	9.95	1333.6	35.1
3	2.90	9.94	1413.2	36.8
4	2.86	10.15	1331.7	34.4
5	2.89	10.21	1322.7	33.6
6	2.83	10.28	1383.5	35.7
7	2.82	10.31	1334.3	34.4
8	2.82	10.31	1296.3	33.4
	Average :		1350.3	34.9
	σ :		39.6	1.1
	σ_r [%]:		2.9	3.2

Average interlaminar shear strength for 5 W plasma treated composites is 34.9 ± 1.1 MPa. With slighty better results than 2 W, these samples yield consistent results with relative standard deviation of 3.2 %.

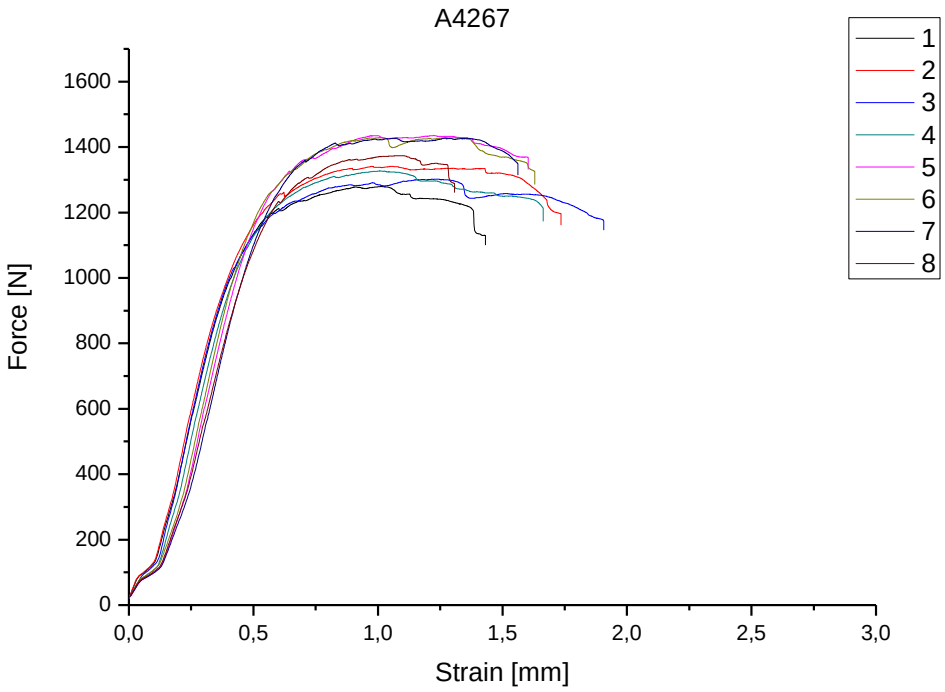

Fig. 4.18: Force-strain curve of plasmochemically treated composites – 10 W, CW, 4 sccm TVS

Table 4.10: Mechanical properties of plasmochemically treated composites – 10 W, CW, 4 sccm TVS

Specimen number	t [mm]	b [mm]	F_{max} [N]	τ_{int} [MPa]
1	2.86	10.18	1279.7	33.0
2	3.03	10.12	1341.3	32.8
3	2.90	10.12	1302.0	33.3
4	2.90	10.10	1327.1	34.0
5	2.95	10.00	1435.1	36.5
6	2.86	9.95	1428.9	37.7
7	2.96	10.03	1427.0	36.0
8	2.88	9.97	1373.7	35.9
	Average :		1364.4	34.9
	σ :		61.1	1.9
	σ_r [%]:		4.5	5.3

Average interlaminar shear strength for 10 W plasma treated composites is 34.9 ± 1.9 MPa. Together with 5 W, this RF power range represents optimal setting with best fiber to matrix adhesion.

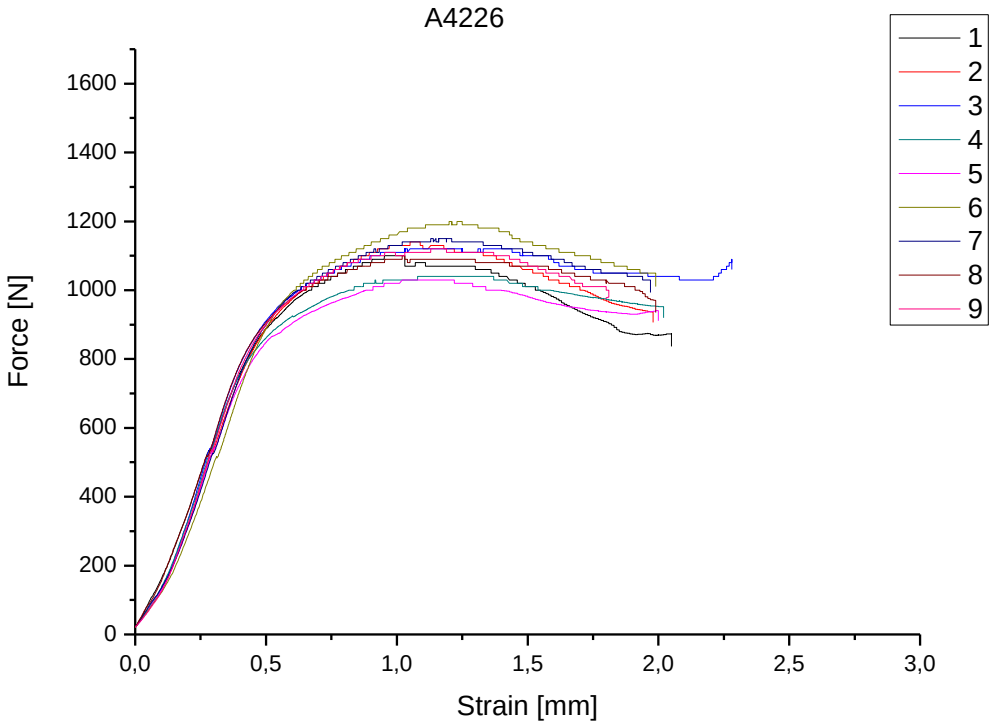

Fig. 4.19: Force-strain curve of plasmochemically treated composites – 25 W, pulsed, 4 sccm TVS

Table 4.11: Mechanical properties of plasmochemically treated composites – 25 W, pulsed, 4 sccm TVS

Specimen number	t [mm]	b [mm]	F_{max} [N]	τ_{int} [MPa]
1	2.97	9.86	1101.0	28.2
2	3.01	9.83	1140.4	28.9
3	3.05	9.72	1118.3	28.3
4	2.97	9.66	1044.3	27.3
5	2.98	9.80	1030.5	26.5
6	3.03	10.01	1196.6	29.6
7	2.98	10.04	1146.0	28.7
8	2.98	9.96	1095.5	27.7
9	3.01	9.99	1116.1	27.8
	Average :		1109.9	28.1
	σ :		50.9	0.9
	σ_r [%]:		4.6	3.3

Average interlaminar shear strength for 25 W plasma treated composites is 28.1 ± 0.9 MPa. Compared to samples treated with lower RF power, these composites have lower shear strength. This power setting has already less beneficial impact on the adhesion than the previous ones.

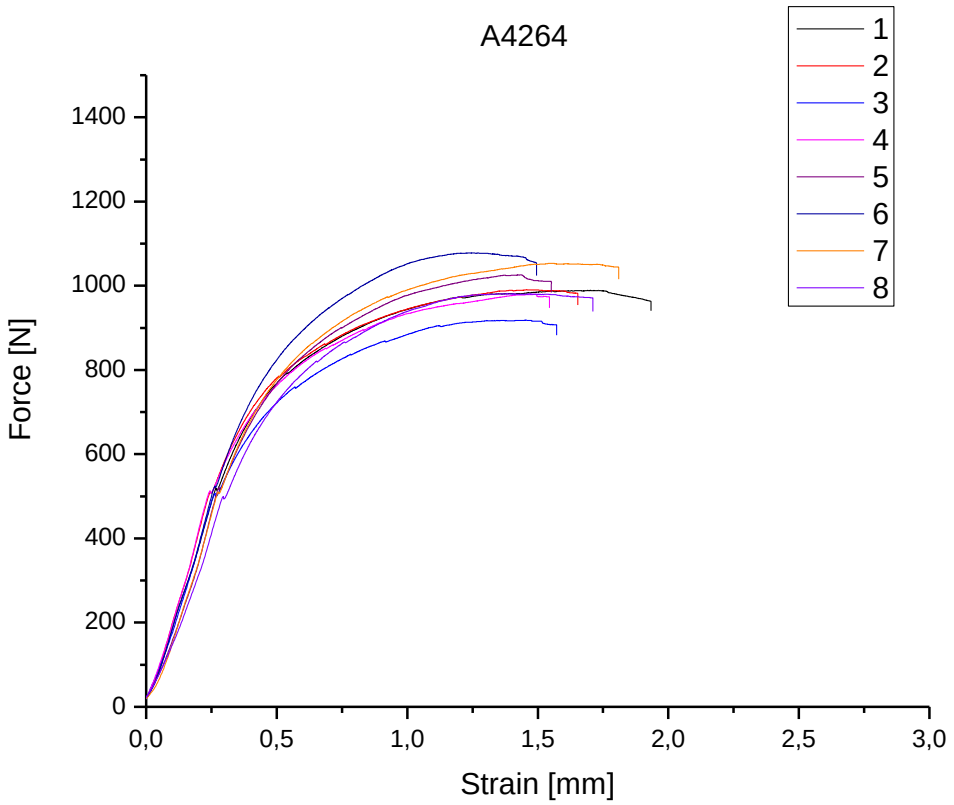

Fig. 4.20: Force-strain curve of plasmochemically treated composites – 100 W, CW, 4 sccm TVS

Table 4.12: Mechanical properties of plasmochemically treated composites – 100 W, CW, 4 sccm TVS

Specimen number	t [mm]	b [mm]	F_{max} [N]	τ_{int} [MPa]
1	2.92	9.75	988.9	26.1
2	2.95	9.72	990.5	25.9
3	2.91	9.57	918.5	24.7
4	2.97	9.60	979.7	25.8
5	2.94	9.79	1025.9	26.7
6	2.94	9.87	1078.1	27.9
7	2.94	9.79	1053.2	27.4
8	2.96	9.88	981.3	25.2
	Average :		1002.0	26.2
	σ :		49.6	1.1
	σ_r [%]:		4.9	4.1

Average interlaminar shear strength for 100 W plasma treated composites is 26.2 ± 1.1 MPa. Composite behaved partially like unsized fibers in a sense that the samples were bent before delaminating, having wider peak. Lower shear strength is caused by sub-

optimal adhesion between fibers and matrix due to high RF power in which the occurrence of vinyl groups is substantially lower (Fig. 4.8) because of their fragmentation.

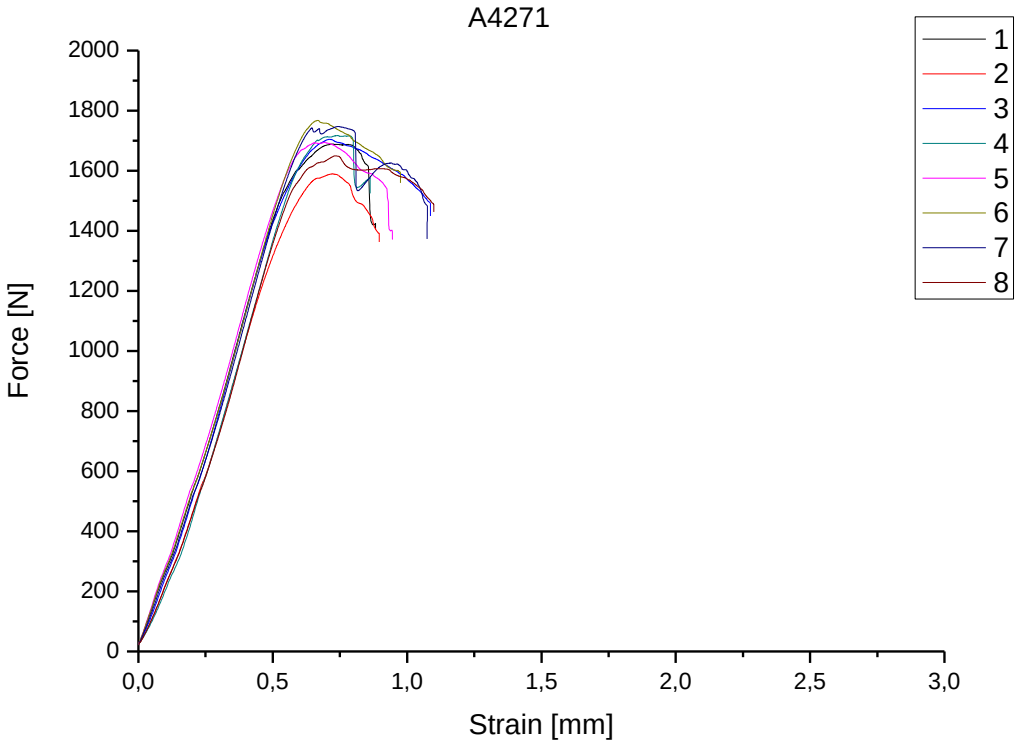

Fig. 4.21: Force-strain curve of plasmochemically treated composites – 33 % O_2 concentration

Table 4.13: Mechanical properties of plasmochemically treated composites – 33 % O_2 concentration

Specimen number	t [mm]	b [mm]	F_{max} [N]	τ_{int} [MPa]
1	2.82	10.20	1689.0	44.0
2	2.73	10.19	1589.5	42.9
3	2.81	10.29	1704.2	44.2
4	2.90	10.10	1717.5	44.0
5	2.84	10.30	1694.4	43.4
6	2.82	10.25	1767.8	45.9
7	2.82	10.37	1747.3	44.8
8	2.74	10.34	1649.6	43.7
	Average :		1694.9	44.1
	σ :		55.9	0.9
	σ_r [%]:		3.3	2.1

Average interlaminar shear strength for plasma treated composites with 33 % O_2 is 44.1 ± 0.9 MPa. Compared to samples that don't use oxygen in their mixture, these samples have substantially improved fiber-matrix adhesion.

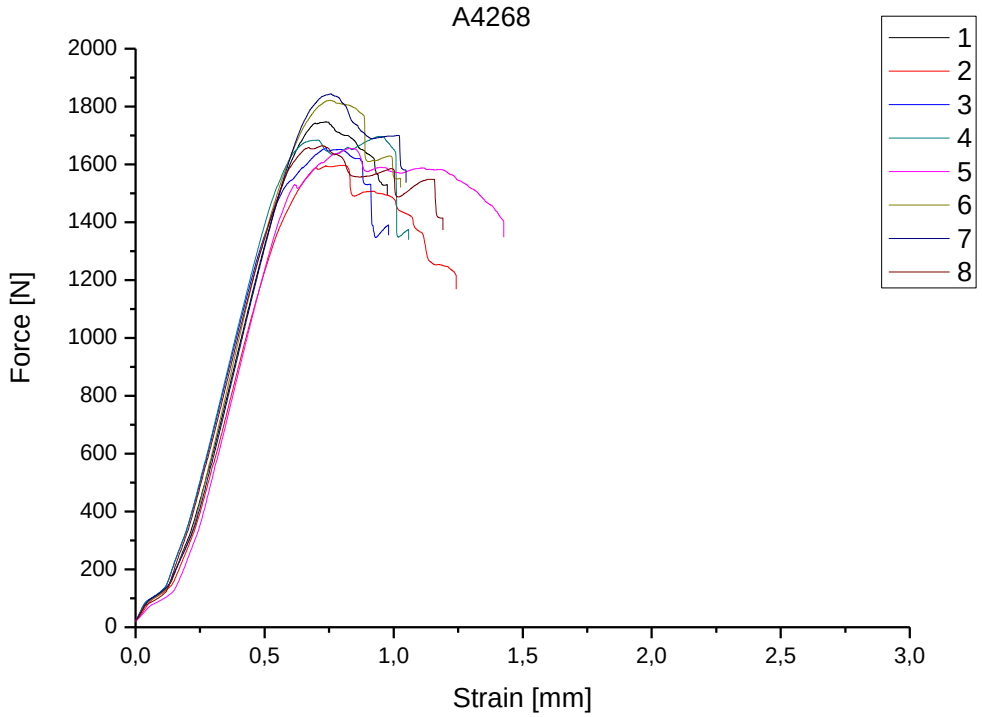

Fig. 4.22: Force-strain curve of plasmochemically treated composites – 42 % O_2 concentration

Table 4.14: Mechanical properties of plasmochemically treated composites – 42 % O_2 concentration

Specimen number	t [mm]	b [mm]	F_{max} [N]	τ_{int} [MPa]
1	2.98	10.06	1747.2	43.7
2	2.86	10.02	1597.0	41.8
3	2.85	10.04	1657.6	43.4
4	2.92	10.01	1696.4	43.5
5	3.02	10.07	1656.0	40.8
6	3.04	10.02	1821.6	44.9
7	2.96	9.98	1843.5	46.8
8	2.89	9.97	1664.7	43.3
	Average :		1710.5	43.5
	σ :		86.5	1.8
	σ_r [%]:		5.1	4.1

Average interlaminar shear strength for plasma treated composites with 42 % O_2 is 43.5 ± 1.8 MPa

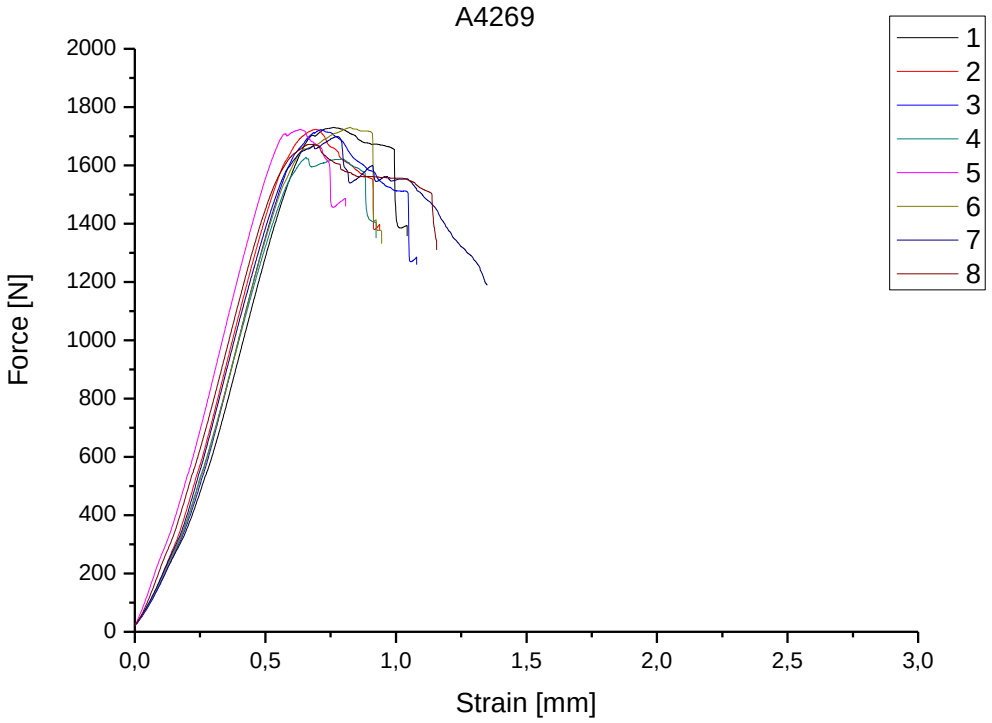

Fig. 4.23: Force-strain curve of plasmochemically treated composites – 52 % O_2 concentration

Table 4.15: Mechanical properties of plasmochemically treated composites – 52 % O_2 concentration

Specimen number	t [mm]	b [mm]	F_{max} [N]	τ_{int} [MPa]
1	2.84	10.10	1730.2	45.2
2	2.85	10.06	1723.6	45.1
3	2.88	10.10	1722.3	44.4
4	2.88	10.11	1627.5	41.9
5	2.88	10.07	1723.5	44.6
6	2.87	10.12	1730.4	44.7
7	2.90	10.19	1698.7	43.1
8	2.92	10.22	1672.5	42.0
	Average :		1703.6	43.9
	σ :		36.5	1.3
	σ_r [%]:		2.1	3.0

Average interlaminar shear strength for plasma treated composites with 52 % O_2 is 43.9 ± 1.3 MPa

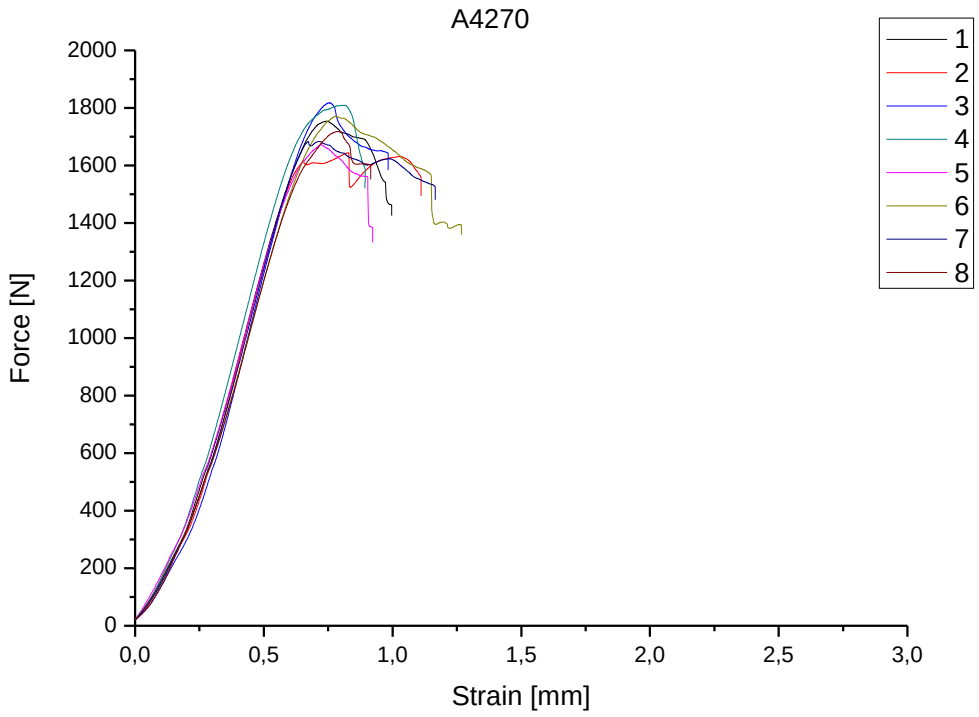

Fig. 4.24: Force-strain curve of plasmochemically treated composites – 61 % O_2 concentration

Table 4.16: Mechanical properties of plasmochemically treated composites – 61 % O_2 concentration

Specimen number	t [mm]	b [mm]	F_{max} [N]	τ_{int} [MPa]
1	2.86	10.18	1754.3	45.2
2	2.86	10.18	1644.2	42.4
3	2.84	10.18	1817.5	47.1
4	2.92	10.16	1809.0	45.7
5	2.90	10.20	1672.2	42.4
6	2.88	10.22	1770.8	45.1
7	2.89	10.30	1683.7	42.4
8	2.92	10.36	1718.1	42.6
	Average :		1733.7	44.1
	σ :		64.4	1.9
	σ_r [%]:		3.7	4.3

Average interlaminar shear strength for plasma treated composites with 61 % O_2 is 44.1±1.9 MPa

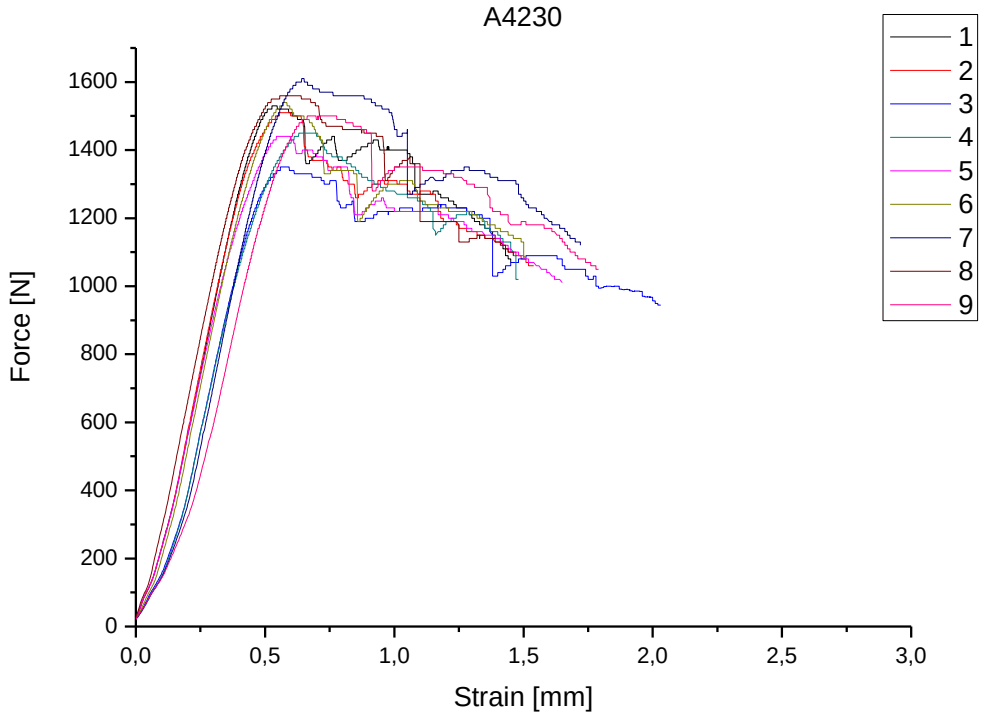

Fig. 4.25: Force-strain curve of plasmochemically treated composites – 71 % O_2 concentration

Table 4.17: Mechanical properties of plasmochemically treated composites – 71 % O_2 concentration

Specimen number	t [mm]	b [mm]	F_{max} [N]	τ_{int} [MPa]
1	2.99	9.75	1531.3	39.4
2	2.96	9.58	1509.0	39.9
3	2.96	9.36	1349.2	36.5
4	2.96	9.32	1453.7	39.5
5	2.93	9.55	1444.4	38.7
6	2.94	9.75	1536.6	40.2
7	2.96	9.79	1605.8	41.6
8	2.92	9.74	1561.8	41.2
9	2.99	9.93	1500.1	37.9
	Average :		1499.1	39.4
	σ :		75.3	1.6
	σ_r [%]:		5.0	4.0

Average interlaminar shear strength for plasma treated composites with 71 % O_2 is 39.4 ± 1.6 MPa. At this concentration, the fiber-matrix adhesion is distinguishingly weakened compared to other tested concentrations. This may be due to oxygen oversaturation and

possible formation of carbonyl and hydroxyl groups in deposited film instead of strengthening the bond between the substrate and the film by forming more covalent bonds.

4.2.5 Result summary

All created composites and their interlaminar shear strength is shown in table 4.18. Samples that underwent only oxygen pre-treatment have their shear strength increased (22.4 MPa) but is still significantly lower than commercial sizing (39.2 MPa).

Table 4.18: Result interlaminar shear strength comparison.

Sample type	τ_{int} [MPa]	σ [MPa]	σ_r [%]
Unsized	15.1	1.0	6.6
Sized	39.2	2.4	6.2
Pre-treated only	22.4	2.6	11.7
A4263 (2 W)	32.0	1.6	5.1
A4272 (5 W)	34.9	1.1	3.2
A4267 (10 W)	34.9	1.9	5.3
A4226 (25 W)	28.1	0.9	3.3
A4264 (100 W)	26.2	1.1	4.1
A4271 (33 % O_2)	44.1	0.9	2.1
A4268 (42 % O_2)	43.5	1.8	4.1
A4269 (52 % O_2)	43.9	1.3	3.0
A4270 (61 % O_2)	44.1	1.9	4.3
A4230 (71 % O_2)	39.4	1.6	4.0

The effect of RF power on interlaminar shear strength and fiber-matrix adhesion is depicted in figure 4.26, having an uphill trend with its maximum at 10 W with 34.9 ± 1.9 MPa. Further increase in power causes the composites to lose shear strength, which is most likely due to decrease in the concentration of vinyl groups, fragmenting it into CH_x groups as shown in acquired FTIR spectra (Fig. 4.8) for given series. While the shear strengths for this series are generally lower than of the commercial sizing, it is a good starting point to implement different settings such as gas mixtures on this effective power range.

The effect of oxygen concentration on interlaminar shear strength is depicted in figure 4.27. We can observe a significant increase in shear strength (averaging 43.9 ± 1.5 MPa) at concentrations 33–61 % compared to samples deposited without the presence of oxygen. This is thanks to the increased number of covalent bonds between the substrate and the matrix confirmed by higher presence of Si–O–Si and Si–O–C groups as shown in figure 4.9. At 71 % concentration, the adhesion weakens because of oxygen oversaturation, creating more C=O groups, thus reducing the number of covalent bonds between the substrate and the matrix as an unwanted side effect.

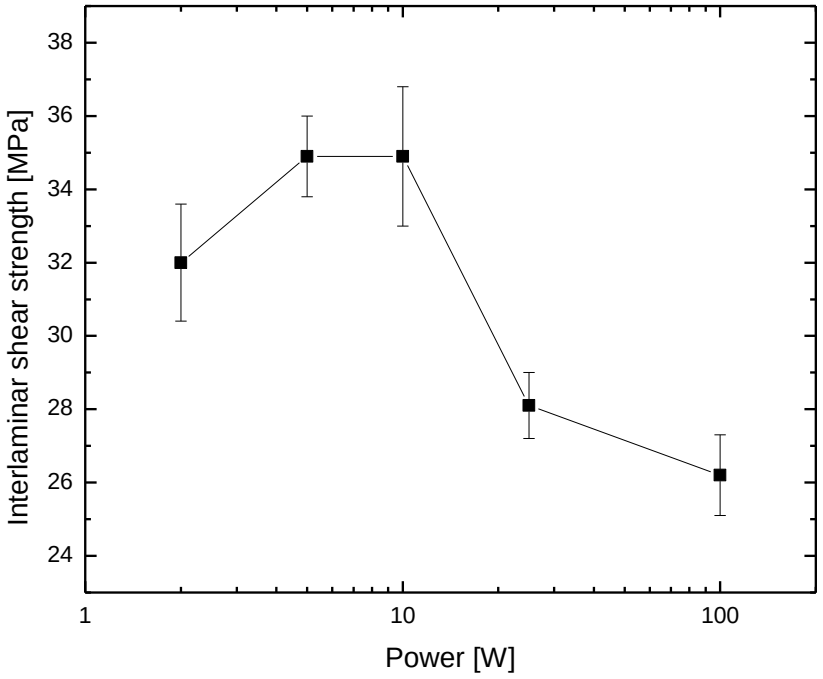

Fig. 4.26: Composite interlaminar shear strength – power series

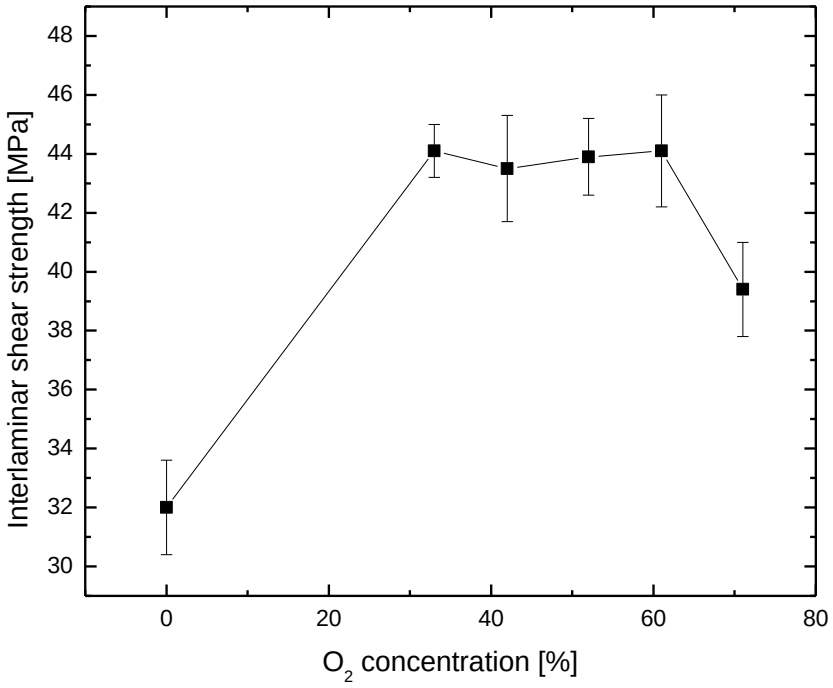

Fig. 4.27: Composite interlaminar shear strength – O_2 concentration series

4.3 SEM

Pictures of already delaminated unsized as well as plasmochemically modified samples were taken using SEM to compare the effect of adhesion on said samples. Figure 4.28 with enhanced detail in figure 4.30 shows the smooth surface of the unsized fibers with only minimal residual matrix fragments attached. This confirms that the adhesion between fibers and matrix is poor compared to figure 4.29, where the matrix is severely damaged after the delamination, creating arrow fletching-like structures in the place of the fracture. These structures confirm good adhesion and the unwillingness to delaminate from the fibers. Figure 4.31 shows the detail of fibers that are still coated with lingering matrix.

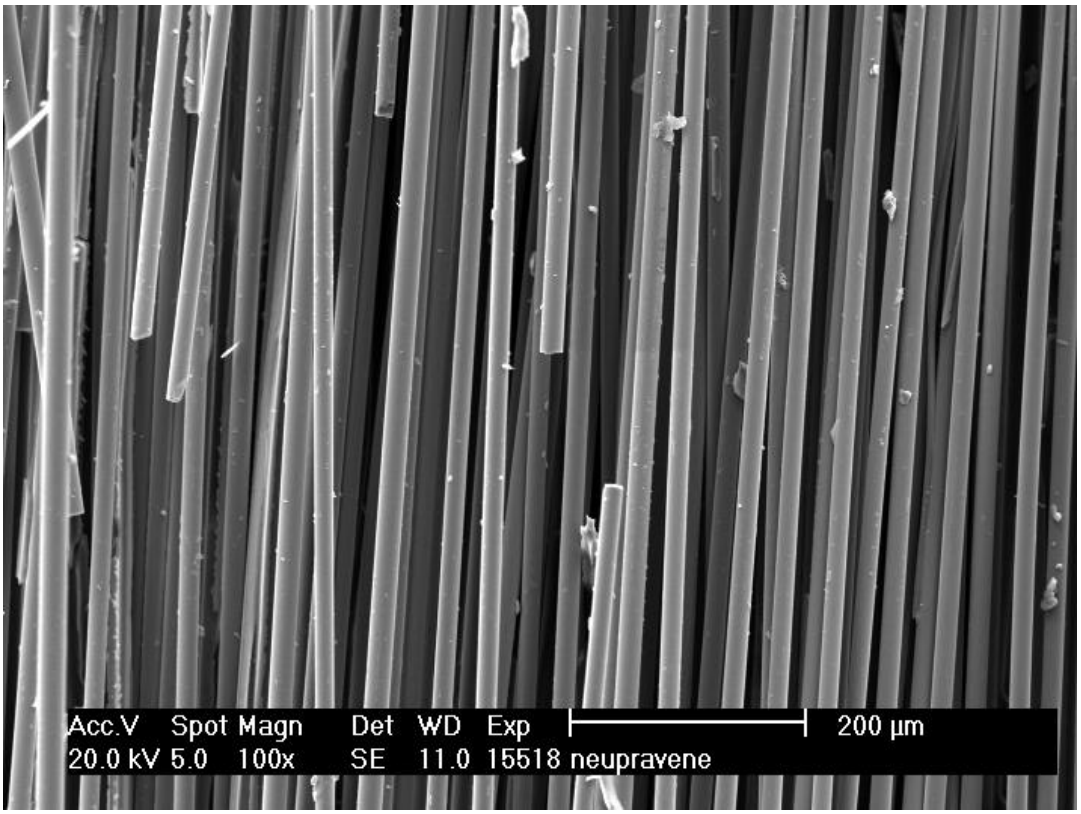

Fig. 4.28: SEM – composite using unsized fibers.

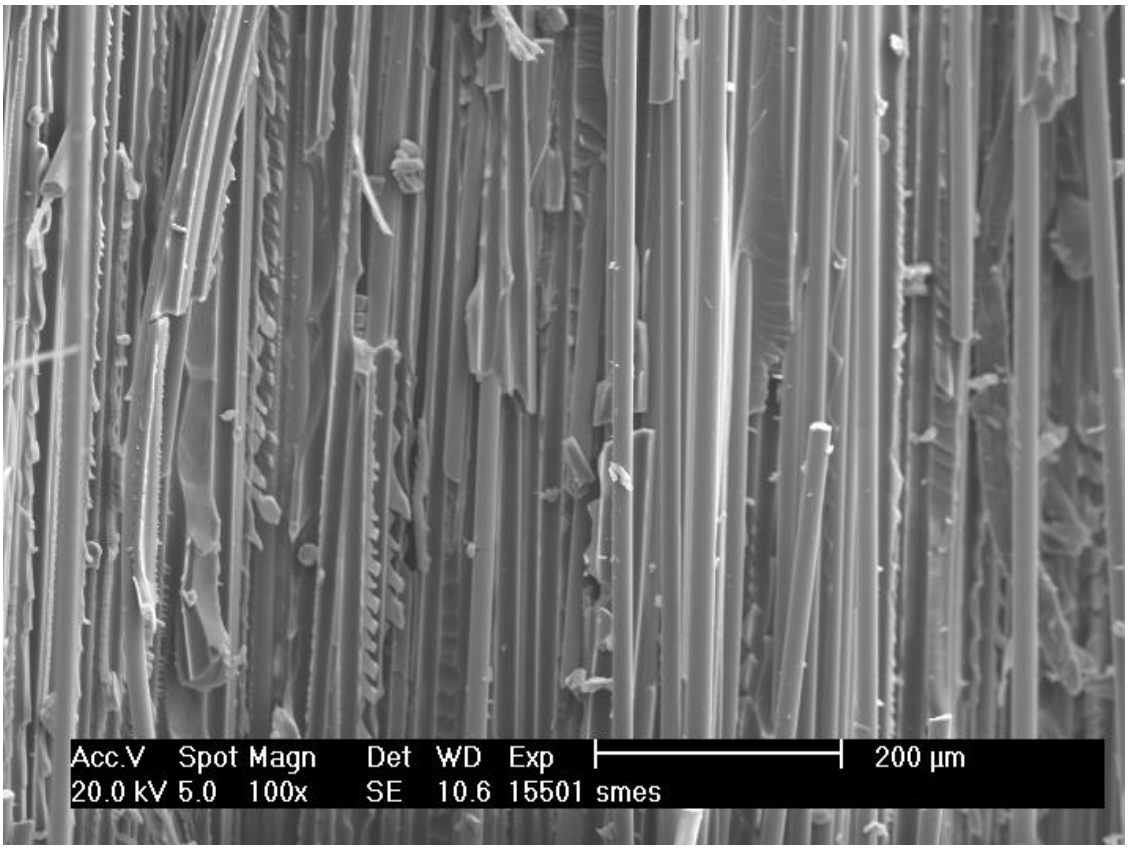

Fig. 4.29: SEM – plasmochemically modified composite, TVS/O_2 (4/10 sccm) gas mixture.

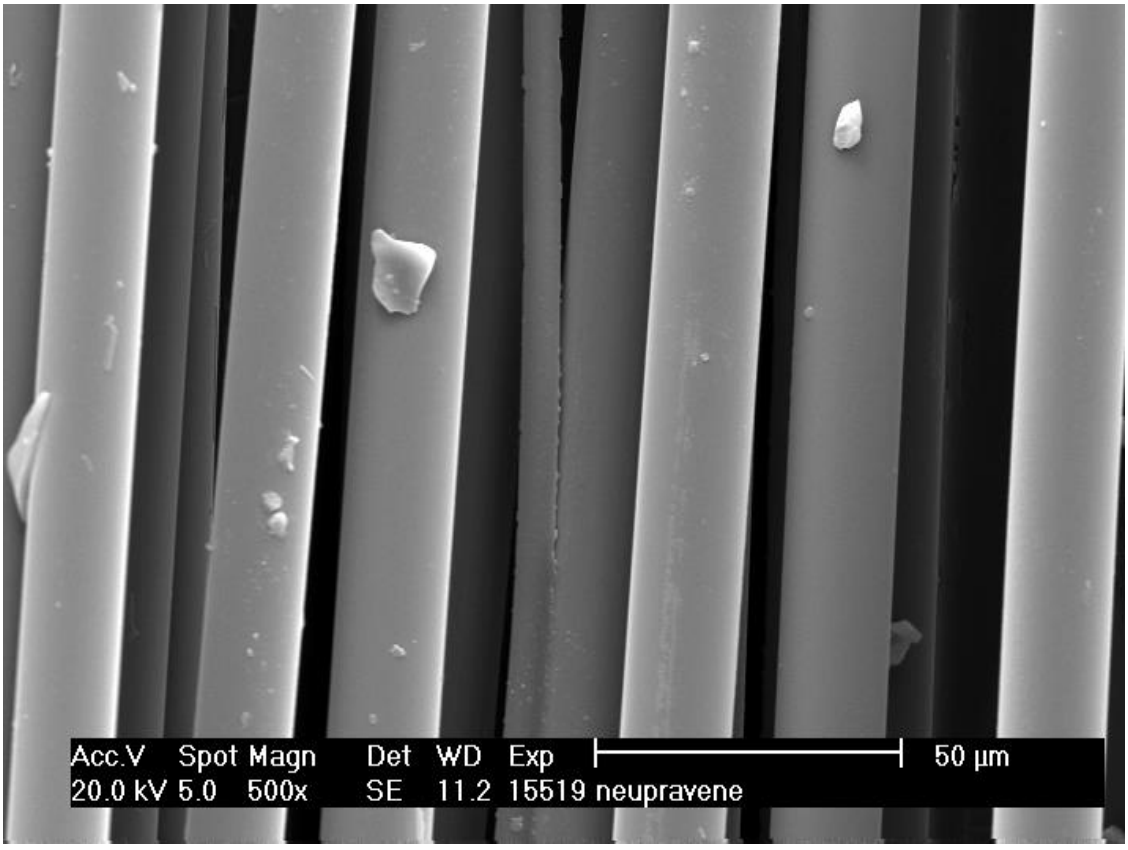

Fig. 4.30: SEM – detail of unsized fiber composite.

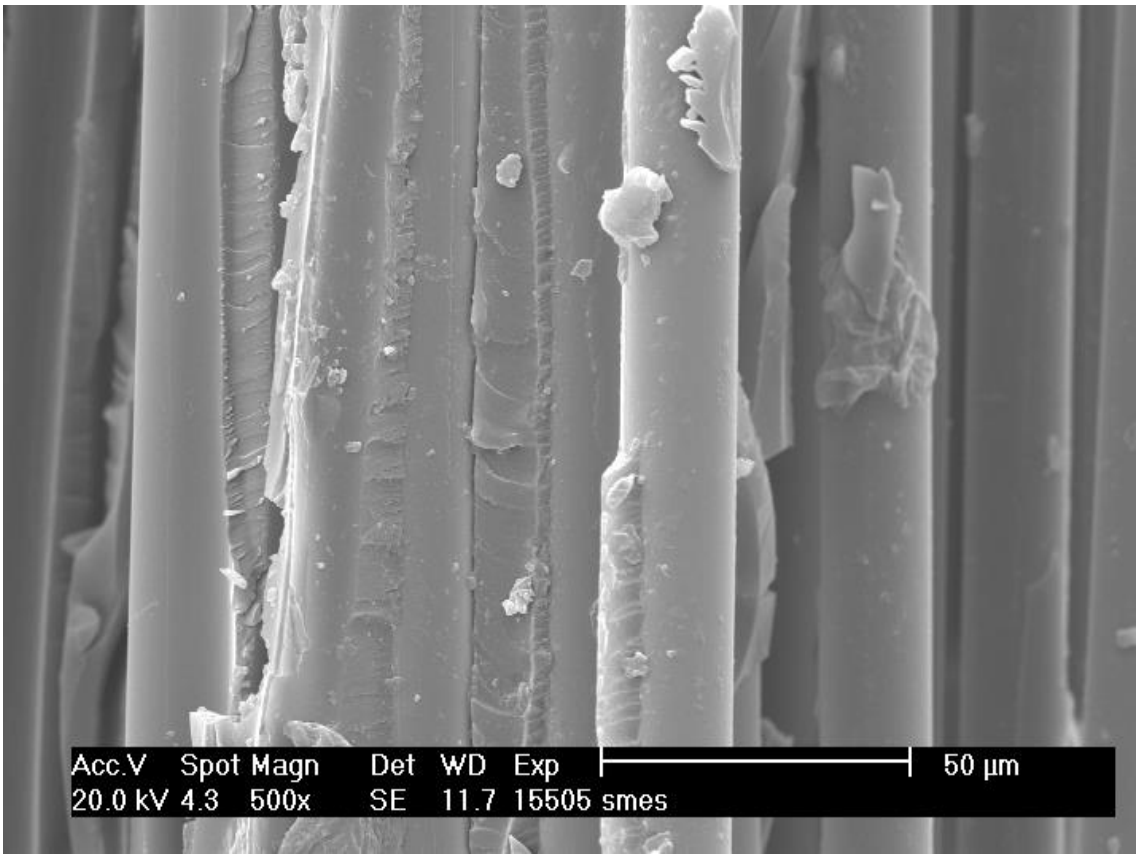

Fig. 4.31: SEM – detail of plasmochemically modified composite, TVS/O_2 (4/10 sccm) gas mixture.

5 CONCLUSION

The aim of the bachelor thesis was to prepare and analyze unsaturated polyester resin based composites with controlled interphase using TVS monomer for PECVD. The first step was to characterise aparature A4 and find optimal deposition conditions. Gas profile was made to observe the behaviour of used gases (Ar, O_2, TVS) with increasing RF power. As the power increased, Ar pressure was at a constant value, while oxygen pressure was increasing due to dissociation, TVS pressure decreased significantly at the early stages because of its fragmentation and subsequent deposition onto the reaction chamber surface.

The second step was to acquire deposition speed for both generator modes using various RF power. Deposition speed in CW mode was increasing in 2–10 W interval (31–144 $nm \cdot min^{-1}$). With further increase in power up to 100 W the deposition speed was relatively constant. Deposition speed in pulsed mode was lower compared to CW mode within range of 32–90 $nm \cdot min^{-1}$. The position of the sample was also important during the deposition because of the uneven distribution of plasma discharge with higher intensity as well as deposition speed at the ends of the reaction chamber. Adding oxygen into the deposition gas mixture generally increased the deposition speed.

Thin films deposited on planar substrates were analyzed using FTIR spectrometer. The result shows that increasing RF power reduces the amount of vinyl and CH_x groups of the samples. Higher oxygen content increases the concentration of Si–O–Si and Si–O–C groups which improve the adhesion between fiber and matrix. Position of the samples have no real effect on the composition.

Performed scratch test confirms the homogeneous conditions within the reaction chamber with constant critical load throughout all positions. Oxygen content slightly decreases the critical load. The effect of RF power on the critical load is negligible.

Composites modified with different deposition conditions were prepared and the effect of used RF power and oxygen content on interlaminar shear strength was observed and compared to composites using unsized (15.1 ± 1.0 MPa) and commercially sized (39.2 ± 2.4 MPa) fibers. Increasing RF power had pleasant effects on the resulting shear strength up to 10 W reaching 34.9 ± 1.9 MPa. Further increase in power lead to lower shear strength due to vinyl fragmentation during higher power output. The implementation of oxygen into the gas mixture had positive effects thanks to the improved covalent bonding between fiber and matrix, with resulting shear average strength 43.9 ± 1.5 MPa except for O_2 concentration of 71%, where the shear strength declined to 39.4 ± 1.6 MPa.

The results of this diploma thesis show the importance of fiber-matrix interphase and its adhesion. While some composite samples yield good shear strength, there is still room for improvement by altering the deposition conditions.

6 REFERENCES

[1] SABU, T., ed. *Polymer Composites*. Weinheim: Wiley-VCH, 2012. ISBN 978-352-7645-213.

[2] QIN, Q., ed. *Toughening mechanisms in composite materials*. Boston, MA: Elsevier, 2015. ISBN 978-1-78242-279-2.

[3] HULL, D. a T. W. CLYNE. *An introduction to composite materials*. 2nd ed. Cambridge: Cambridge University Press, 1996. ISBN 0-521-38855-4.

[4] MLEZIVA, J.; ŠŇUPÁREK, J. *Polymery - výroba, struktura, vlastnosti a použití.* 2. přepr. vyd. Praha: Sobotáles, 2000, 537 s. ISBN 80-85920-72-7.

[5] CECH, V. New Progress in Composite Interphases: A Use of Plasma Technologies. *Proc. FRC 2000*. Newcastle: Woodhead Publ, 2000, 246-252. ISBN 1-85573-550-4.

[6] DWIGHT, D. W. Glass fiber reinforcements. *Comprehensive Composite Materials* (Ed. Kelly A., Zweben C.). Vol. 1. Amsterdam: Elsevier, 2000, pp. 231 – 261. ISBN 0-080437192.

[7] CECH, V., A. KNOB, T. LASOTA, J. LUKES a L.T. DRZAL. Surface modification of glass fibers by oxidized plasma coatings to improve interfacial shear strength in GF/polyester composites. *Polymer Composites*. DOI: 10.1002/pc.24573. ISSN 02728397.

[8] KIM, J. K.; MAI, Y. W. *Engineerd interface in fiber reinforced composites*. 1st ed.Amsterdam: Elsevier, 1998. ISBN 0-08-042695-6.

[9] ČECH, V. Řízená mezifáze v dlouhovláknových polymerních kompozitech. Vyztužené plasty. Karlovy Vary, 1999, str. 98-105.

[10] KIYOTAKA WASA, Makoto Kitabatake. *Thin film materials technology: sputtering of compound materials*. Norwich, NY: William Andrew Pub, 2004. ISBN 08-155-1931-1.

[11] FREUND, L a S SURESH. *Thin film materials: stress, defect formation and surface evolution*. Cambridge: Cambridge University Press, 2003. ISBN 05-218-2281-5.

[12] OHRING, Milton. *Materials Science of Thin Films*. 2nd ed. Burlingtont: Elsevier, 2001. ISBN 978-008-0491-783

[13] JONES, Anthony C. a Michael L. HITCHMAN. *Chemical vapour deposition: precursors, processes and applications*. Cambridge, UK: Royal Society of Chemistry, c2009. ISBN 08-540-4465-5.

[14] INAGAKI, N. *Plasma Surface Modification and Plasma Polymerization.* Lancaster:Technomic Publishing Company, 1996. ISBN 1-56676-337-1.

[15] HIPPLER, R., Pfau, S., Schmidt, M., K.H, Shoenbach, Eds. *Low Temperature Plasma Physics – Fundamentals Aspects and Applications*. Berlin: Wiley-VCH, 2001.

[16] YASUDA, H. *Plasma polymerization*. Academic Press, Inc., New York, 1985. ISBN 0-12-768760-2.

[17] BITTENCOURT, J.A. *Fundamentals of Plasma Physics*. Third Edition. New York, NY: Springer New York, 2004. ISBN 14-757-4030-1.

[18] BIEDERMAN, Hynek. *Plasma polymer films*. London: Imperial College Press, c2004, 386 p. ISBN 1-86094-467-1.

[19] CECH, V, J STUDYNKA, F JANOS a V PERINA. Influence of oxygen on the chemical structure of plasma polymer films deposited from a mixture of tetravinylsilane and oxygen gas. *Plasma Processes and Polymers.* 2007, Vol. 4, pp. S776–S780.

[20] STUDYNKA, J. a V. CECH, Aging of silicon-based dielectric coatings deposited by plasma polymerization. *Thin Solid Films.* 2011, Vol. 519, pp. 2168–2171.

[21] SEGUI, Yvan. Plasma deposition from organosilicon monomers. In: D' AGOSTINO, R. (ed.) *Plasma processing of polymers*. Netherlands: Kluwer Academic Publishers, 1997, 305-319. ISBN 0-7923-4859-1.

[22] SEGUI, Y. a Bui AI. Gas discharge in hexamethyldisiloxane. *Journal of Applied Polymer Science*.**20**(6), 1976, 1611-1618. DOI: 10.1002/app.1976.070200618. ISSN 00218995.

[23] WRÓBEL, A. M., M. R. WERTHEIMER, J. DIB a H. P. SCHREIBER. Polymerization of Organosilicones in Microwave Discharges. *Journal of Macromolecular Science: Part A - Chemistry*. 2006, **14**(3), 321-337. DOI: 10.1080/00222338008056716. ISSN 0022-233x.

[24] TAJIMA, Ichiro a Minoru YAMAMOTO. Spectroscopic study on chemical structure of plasma-polymerized hexamethyldisiloxane. *Journal of Polymer Science: Polymer Chemistry Edition*. 1985, **23**(3), 615-622. DOI: 10.1002/pol.1985.170230303. ISSN 03606376.

[25] AKOVALI, G. a N. HASIRCI. Polymerization of hexamethyldisiloxane by plasma on activated charcoal: Investigation of parameters. *Journal of Applied Polymer Science*. **29**(8), 2617-2625. DOI: 10.1002/app.1984.070290816. ISSN 00218995.

[26] SACHDEV, Krishna G. a Harbans S. SACHDEV. Characterization of plasma-deposited organosilicon thin films. *Thin Solid Films*. 1983, **107**(3), 245-250. DOI: 10.1016/0040-6090(83)90403-0. ISSN 00406090.

[27] MUKHERJEE, S.P. a P.E. EVANS. The deposition of thin films by the decomposition of tetra-ethoxy silane in a radio frequency glow discharge. *Thin Solid Films*. 1972, **14**(1), 105-118. DOI: 10.1016/0040-6090(72)90373-2. ISSN 00406090.

[28] PAI, C. S., J. F. MINER a P. D. FOO. Electron Cyclotron Resonance Microwave Discharge for Oxide Deposition Using Tetraethoxysilane. *Journal of The Electrochemical Society*. 1992, **139**(3), 850-856. DOI: 10.1149/1.2069315. ISSN 00134651.

[29] SELAMOGLU, N., J. A. MUCHA, D.E. IBBOTSON a D.L. FLAMM. Silicon oxide deposition from tetraethoxysilane in a radio frequency downstream reactor: Mechanisms and step coverage.*Journal of Vacuum Science*. 1989, **7**(6), 1345-1351. DOI: 10.1116/1.584536. ISSN 0734211x.

[30] ISHII, Keisuke, Yoshimichi OHKI a Hiroyuki NISHIKAWA. Optical characteristics of SiO2 formed by plasma-enhanced chemical-vapor deposition of tetraethoxysilane. *Journal of Applied Physics*. 1994, **76**(9), 5418-5422. DOI: 10.1063/1.357196. ISSN 00218979.

[31] INAGAKI, N., S. KONDO a T. MURAKAMI. Preparation of siloxane-like films by glow discharge polymerization. *Journal of Applied Polymer Science*. 1984, **29**(11), 3595-3605. DOI: 10.1002/app.1984.070291133. ISSN 00218995.

[32] RAU, C. a W. KULISCH. Mechanisms of plasma polymerization of various silico-organic monomers. *Thin Solid Films*. 1994, **249**(1), 28-37. DOI: 10.1016/0040-6090(94)90081-7. ISSN 00406090.

[33] NGUYEN, V. S., J. UNDERHILL, S. FRIDMANN a P. PAN. Plasma Organosilicon Polymers. *Journal of The Electrochemical Society*. 1985, **132**(8), 1925-1932. DOI: 10.1149/1.2114255. ISSN 00134651.

[34] INAGAKI, N., S. KONDO, M. HIRATA a H. URUSHIBATA. Plasma polymerization of organosilicon compounds. *Journal of Applied Polymer Science*. 1985, **30**(8), 3385-3395. DOI: 10.1002/app.1985.070300821. ISSN 00218995.

[35] CECH, V., J. STUDYNKA, N. CONTE a V. PERINA. Physico-chemical properties of plasma-polymerized tetravinylsilane. *Surface and Coatings Technology*. 2007, **201**(9-11), 5512-5517. DOI: 10.1016/j.surfcoat.2006.07.086. ISSN 02578972.

[36] ADAMS, D. F. Test methods for mechanical properties. *Comprehensive Composite Materials* (Kelly, A., Zuben, C., ed.). Vol. 1. Amsterdam: Elsevier, 2000, pp. 113-148. ISBN 0-08-0429939.

[37] STOKES, R. J. a D. F. EVANS, *Fundamentals of Interfacial Engineering*. New York: J. Wiley, 1997, pp. 380-39.

[38] D 2344/D2344M - 00. *Standard Test Metod for Short-Beam Strength of Polymer Matrix Composite Materials and Treir Laminates*. 00. United States: ASTM, 2000

[39] BRUKER OPTIK GmbH, *VERTEX 80v User Manual*. 1st edition 2006. D-76275

[40] CECH, V., J. STUDYNKA, F. JANOS a V. PERINA. Influence of Oxygen on the Chemical Structure of Plasma Polymer Films Deposited from a Mixture of Tetravinylsilane and Oxygen Gas. *Plasma Processes and Polymers*. 2007, **4**(S1), S776-S780. DOI: 10.1002/ppap.200731903. ISSN 16128850

[41] SEDLÁK, F. *Povrchové úpravy skleněných vláken s využitím plazmové nanotechnologie*. Brno: Vysoké učení technické v Brně, Fakulta chemická, 2017. 62 s. Vedoucí diplomové práce prof. RNDr. Vladimír Čech, Ph.D

[42] KNOB, A. *Povrchové úpravy skleněných vláken pro polymerní kompozity.* Brno: Vysoké učení technické v Brně, Fakulta chemická, 2016. 133 s. Vedoucí dizertační práce prof. RNDr. Vladimír Čech, Ph.D

7 LIST OF USED ABBREVIATIONS AND SYMBOLS

ASTM		American society for testing and materials
BTMSM		bis(trimethylsilyl)methane
DVTMDSO		divinyltetramethyldisiloxane
CVD		chemical vapour deposition
ER		epoxy resin
FRC		fiber-reinforced composites
FT-IR		Fourier transform infrared
HMDS		hexamethyldisilane
HMDSN		hexamethyldisilazane
HMDSO		hexamethyldisiloxane
HTP		high-temperature plasma
IR		infrared
LECVD		laser-enhanced chemical vapour deposition
LPCVD		low-pressure chemical vapour deposition
LTP		low-temperature plasma
MIR		middle infrared
MOCVD		metal-organic chemical vapour deposition
OMCATS		octamethylcyclotetrasiloxane
PAN		polyacrylonitrile
PCS		polycarbosilane
PE		polyethylene
PECVD		plasma enhanced chemical vapour deposition
PEEK		polyether ether ketone
PMMA		poly(methyl methacrylate)
PP		polypropylene
PVD		physical vapour deposition
$R\bullet$		radical
RF		radio frequency
SADT		self-accelerating decomposition temperature
SEM		scanning electron microscopy
sccm		standard cubic centimetre per minute
TEOS		tetraethoxysilane
TMDSO		tetramethyldisiloxane
TMOS		methyltrimethoxysilane
TMS		tetramethylsilane
TVS		tetravinylsilane
UP		unsaturated polyester
VE		vinyl ester
b	[m]	sample width
E	[Pa]	Young's modulus
F	[N]	force
F_{max}	[N]	maximum loading force

k_{ij}		reaction rate constant
Mr	[g·mol^{-1}]	molecular weight
N_D		number of charged particles
n_e		concentration of electrons
P	[W]	power
P_{eff}	[W]	effective power
t	[m]	sample thickness
T_b	[K]	boiling point
T_e	[K]	electron energy
T_i	[K]	ion energy
T_g	[K]	translational kinetic energy of gas
T_m	[K]	melting point
t_{on}	[s]	time with power on
t_{off}	[s]	time with power off
W_A	[J]	thermodynamic work of adhesion
α	[K^{-1}]	thermal expansivity
ρ	[kg·m^{-3}]	density
σ	[Pa]	tensile strength
ϵ_*		tfailure strain
γ_{LV}	[J·m^{-2}]	interfacial free energy
γ_{SL}	[J·m^{-2}]	surface free energy of liquid
γ_{SV}	[J·m^{-2}]	surface free energy of solid
λ_D	[m]	Debye length
θ	[°]	contact angle
σ		standard deviation
σ_r		relative standard deviation
ω	[Hz]	angular frequency of typical plasma oscillation
τ_{int}	[Pa]	interlaminar shear stress

Attachment 1: Sample list.

Nr.	Type	Position	Pre-treatment			Deposition					Layer thickness [nm]
			O2 [sccm]	*P* [W]	*t* [min]	TVS [sccm]	O2 [sccm]	P_{eff} [W]	mode	*t* [s]	
A4081	Si	A	10	30	10	4	-	10	CW	420	1248
A4082	Si	G									852
A4083	Si	N									844
A4084	Si	O									784
A4085	Si	U									790
A4086	Si	AA									1535
A4093	Si	A	10	30	10	4	-	30	CW	420	747
A4094	Si	G									364
A4095	Si	N									901
A4096	Si	O									606
A4097	Si	U									833
A4098	Si	AA									3016
A4105	Si	A	10	30	10	4	-	100	CW	420	414
A4106	Si	G									216
A4107	Si	N									243
A4108	Si	O									429
A4109	Si	U									860
A4110	Si	AA									3990
A4163	Glas	A	10	30	10	4	-	2	pulse t_{on}:t_{off} 1:4	300	276
A4164	Glas	G									118
A4165	Glas	N									137
A4166	Si	O									112
A4167	Glas	U									141
A4168	Glas	AA									179
A4169	Glas	A	10	30	10	4	-	10	pulse t_{on}:t_{off} 1:4	300	806
A4170	Glas	G									139
A4171	Glas	N									125
A4172	Si	O									187
A4173	Glas	U									247
A4174	Glas	AA									831
A4175	Glas	A	10	30	10	4	-	25	pulse t_{on}:t_{off} 1:7	300	468
A4176	Glas	G									173
A4177	Glas	N									200
A4178	Si	O									141
A4179	Glas	U									241
A4180	Glas	AA									373
A4181	Glas	A	10	30	10	4	-	75	pulse t_{on}:t_{off} 1:3	300	247
A4182	Glas	G									124
A4183	Glas	N									435
A4184	Si	O									320
A4185	Glas	U									472
A4186	Glas	AA									440

Nr.	Type	Position	Pre-treatment			Deposition					Layer thickness [nm]
			O_2 [sccm]	P [W]	t [min]	TVS [sccm]	O_2 [sccm]	P_{eff} [W]	mode	t [s]	
A4187	Glas	A	10	30	10	4	-	150	pulse t_{on}:t_{off} 1:1	300	332
A4188	Glas	G									X
A4189	Glas	N									248
A4190	Si	O									263
A4191	Glas	U									585
A4192	Glas	AA									1215
A4201	Glas	A	10	30	10	2	2	2	pulse t_{on}:t_{off} 1:4	600	781
A4202	Glas	G									253
A4203	Glas	N									339
A4204	Glas	O									210
A4205	Glas	U									289
A4206	Glas	AA									735
A4207	Glas	A	10	30	10	4	10	2	pulse t_{on}:t_{off} 1:4	600	807
A4208	Glas	G									472
A4209	Glas	N									253
A4210	Glas	O									326
A4211	Glas	U									498
A4212	Glas	AA									622
A4213	Glas	A	10	30	10	4	-	5	CW	600	2402
A4214	Glas	G									1366
A4215	Glas	N									577
A4216	Glas	O									590
A4217	Glas	U									1117
A4218	Glas	AA									1467
A4219	Glas	A	10	30	10	4	-	2	CW	600	486
A4220	Glas	G									341
A4221	Glas	N									181
A4222	Glas	O									294
A4223	Glas	U									383
A4224	Glas	AA									161
A4226	Glas fibers		10	100	30	4	-	25	pulse t_{on}:t_{off} 1:7	600	-
A4230	Glas fibers		10	100	30	4	10	2	pulse t_{on}:t_{off} 1:4	240	-
A4236	Si	A	10	30	10	4	10	2	pulse (t_{on}:t_{off} 1:4)	75	95
A4237	Si	G								120	102
A4238	Si	N								240	97
A4239	Si	O								180	126
A4240	Si	U								120	101
A4241	Si	AA								120	102

Nr.	Type	Position	Pre-treatment			Deposition					Layer thickness [nm]
			O_2 [sccm]	P [W]	t [min]	TVS [sccm]	O_2 [sccm]	P_{eff} [W]	mode	t [s]	
A4244	Si	O	10	30	10	4	-	2	CW	180	107
A4245	Si	O						5		120	147
A4246	Si	O						10		60	104
A4247	Si	O						30		70	180
A4248	Si	O						100		120	163
A4253	Si	O	10	30	10	4	6.2	2	pulse t_{on}:t_{off} 1:4	180	95
A4254	Si	O					4.3				98
A4255	Si	O					2.9				104
A4256	Si	O					2				93
A4263	Glas fibers		10	100	30	4	-	2	CW	420	-
A4264	Glas fibers		10	100	30	4	-	100	CW	270	-
A4266	Glas fibers		10	100	30	-	-	-	-	-	-
A4267	Glas fibers		10	100	30	4	-	10	CW	180	-
A4268	Glas fibers		10	100	30	4	2.9	2	pulse t_{on}:t_{off} 1:4	420	-
A4269	Glas fibers						4.3				-
A4270	Glas fibers						6.2				-
A4271	Glas fibers						2				-
A4272	Glas fibers		10	100	30	4	-	5	CW	180	-